universität wien

MASTERARBEIT/MASTER'S THESIS

Titel der Masterarbeit / Title of the Master's Thesis

„Synthesis of silaffin-inspired peptides for generating silica nanomaterials“

verfasst von / submitted by

Johannes Strobl, BSc

angestrebter akademischer Grad / in partial fulfilment of the requirements for the degree of

Master of Science (MSc)

Wien, 2020 / Vienna 2020

Studienkennzahl lt. Studienblatt / degree programme code as it appears on the student record sheet:	A 066 862
Studienrichtung lt. Studienblatt / degree programme as it appears on the student record sheet:	Masterstudium Chemie
Betreut von / Supervisor:	Univ.-Prof. Dr. Christian Friedrich Wilhelm Becker

Table of Contents

Acknowledgements

I would like to thank Prof. Christian Becker for the opportunity to perform my master's thesis in his working group. My special thanks go to my co-supervisor Meder Kamalov, BSc PhD, for his support, his many valuable advices and his patience with my work. I would also like to thank all members of the working group for the friendly atmosphere and their extensive helpfulness.

Finally, I would like to express my gratitude to my parents, who have always encouraged me to pursue my goals and stand with me in every moment of my life.

Abstract

Silica nanostructures are widespread in nature and used in several commercial applications because of their low toxicity and tunable morphologies. Since the industrial production of silica nanomaterials is energy-intensive and requires harsh conditions, it is of great importance to further develop alternative methods for silica precipitation. The *in vitro* synthesis of silica nanoparticles under biomimetic conditions has recently gained increased attention due to its promising biotechnological and medical applications. A potential approach is via the use of the silaffin protein-based R5 peptide, which has the ability to precipitate monodisperse silica particles from silicic acid under mild conditions.

Besides several lysine residues within the R5 peptide, the C-terminal RRIL motif appears to play an important role in the synthesis of silica particles by the R5 peptide, mainly due to its ability to facilitate self-assembly. Different RRIL-containing peptides can form various structural assemblies that later serve as templates for precipitation and thus influence the morphology of the resulting nanoparticles.

In this work, the effects of various modifications to peptides containing the RRIL sequence were examined. It could be shown that the central residue of RRIL-containing peptides exerts a considerable influence on self-assembly. With decreasing size of the central residue, a transformation of rod-like particles to spherical silica nanoparticles could be observed. In addition, the variation of the stereochemistry of the *C*- and *N*-terminal RRIL sequences showed a significant effect on the self-assembly mechanism. Finally, the fluorescent dye cyanine-5 was successfully introduced via covalent attachment. As a result, co-precipitation of the Cy5-modified peptide could be confirmed using fluorescence spectroscopy. Simultaneously, it could be proven that the incorporation rate of RRIL peptides into the silica nanoparticles depends strongly on the primary structure and the solubility of the peptide.

This work contributes to elucidating the relationship between peptide primary structure and peptide self-assembly as well as to exploring new avenues of creating biologically relevant nanomaterials.

Zusammenfassung

Silika-Nanomaterialien sind in der Natur weit verbreitet und werden wegen ihrer geringen Toxizität und manipulierbaren Morphologie bereits in einer Vielzahl kommerzieller Anwendungen eingesetzt. Jedoch ist die industrielle Herstellung von Silika-Nanopartikel äußerst energieintensiv und verlangt harsche Bedingungen. Umso wichtiger ist es, zusätzliche alternative Methoden für die Silika-Präzipitation zu entwickeln. In letzter Zeit erhielt die in vitro Synthese von Silika-Nanopartikel unter biomimetischen Bedingungen große Aufmerksamkeit, vor allem wegen seiner vielversprechenden biotechnologischen und medizinischen Anwendungen. Das Silaffin-Protein abgeleitete R5-Peptid erwies sich in zahlreichen Untersuchungen als ein aussichtsreicher Ansatz, nicht zuletzt wegen der Fähigkeit monodisperse Silika-Partikel aus Kieselsäure unter milden Bedingungen zu fällen.

Neben Lysinresten innerhalb des R5-Peptids spielt das *C*-terminale RRIL Motiv eine wichtige Rolle bei der Silika-Präzipitation, hauptsächlich durch die Beschleunigung der Selbstassemblierung. Da das selbstassemblierte R5-Peptid als Vorlage für die aus dem Präzipitationsprozess hervorgehenden Silika-Nanomaterialien dienen, kann durch Variation von RRIL-enthaltenden R5-Analoga die Morphologie der resultierenden Nanopartikel gezielt beeinflusst werden.

In der vorliegenden Arbeit wurden die Auswirkungen der Modifikation unterschiedlicher RRIL basierender Peptide auf die Morphologie der Silika-Partikel untersucht. Es konnte gezeigt werden, dass die zentrale Seitenkette einen erheblichen Einfluss auf die Selbstassemblierung ausübt. Mit abnehmender Länge der zentralen Seitenkette konnte eine Transformation von stäbchenförmigen hin zu sphärischen Silika-Nanopartikel beobachtet werden. Zusätzlich konnte durch die Variation der Stereochemie der *C*- und *N*-terminalen RRIL-Sequenzen ein signifikanter Effekt auf den Selbstassemblierungsmechanismus nachgewiesen werden.

Schlussendlich wurde der fluoreszierende Farbstoff Cyanine-5 erfolgreich über eine kovalente Bindung eingeführt. Somit war es möglich, die Co-Präzipitation eines modifizierten RRIL-Peptids mittels spektroskopischer Untersuchung zu verfolgen. Gleichzeitig konnte ein Zusammenhang zwischen der Löslichkeit der modifizierten RRIL-Peptide und der Inkorporationsrate in die Silica-Nanopartikel beobachtet werden.

Diese Arbeit hilft, die strukturelle Abhängigkeit der Selbstassemblierung von R5-inspirierten Peptiden aufzuklären und leistet in weiterer Folge einen Beitrag, der zu neuen Routen für die Herstellung von biologisch relevanten Nanomaterialien führt.

Abbreviations

ACN	Acetonitrile
AU	Absorption unit
Boc	Tert-butyloxycarbonyl protecting group
Cy5	Cyanine-5
Dap	2,3-Diaminopropionic acid
DCM	Dichloromethane
DDM	N-dodecyl-β-D-maltoside
DIPEA	N,N-Diisopropylethylamine
DMF	N,N-Dimethylformamide
EtOH	Ethanol
Fmoc	Fluorenylmethoxycarbonyl
HATU	O-(7-Azabenzotriazol-1-yl)-N,N,N',N'-tetramethyluronium-hexafluorphosphat
HPLC	High-performance liquid chromatography
Lys	Lysine
MeOH	Methanol
OGP	Octyl-β-D-glucopyranoside
Orn	Ornithine
PA	Peptide amphiphile
Pbf	2,2,4,6,7-Pentamethyldihydrobenzofuran-5-sulfonyl protecting group
PTM	Posttranslational modification
R5	Silaffin Repetitive unit 5
RP-HPLC	Reversed-phase high-performance liquid chromatography
RPM	Revolutions per minute
RT	Room temperature
SEM	Scanning Electron Microscopy
Sil1p	Silaffin precursor protein Sil1p
TFA	Trifluoroacetic acid
TIPS	Triisopropylsilane
TMOS	Tetramethoxysilane
UV-Vis	Ultraviolet-visible
βAla	Beta-Alanine

1. Introduction

1.1 The process of self-assembly

The process of self-assembly is one of the prerequisites for the existence of biological organisms, since it ensures compartmentalization and thus the separation of cellular compartments of single- as well as multi-cell organisms from their harsh environments. Through the formation of stable lipid bilayers via self-assembly during the pre-biological era on earth, it was possible to establish conditions that allow the occurrence of self-replicating systems [4, 5].

In addition to lipids - proteins, sugars and nucleic acids show self-assembling activity and represent indispensable key building blocks of life [3, 6]. The spontaneous and reversible process of self-assembly is triggered by non-covalent inter- and intramolecular interactions, including hydrogen bonding, electrostatic interaction, van der Waals forces and hydrophobic effects such as π-π stacking and can be influenced by varying temperature, pH, ionic strength and concentration. The process of self-assembly is furthermore defined by the balance between attractive and repulsive forces that enables the formation of thermodynamically stable supramolecular structures. Inspired by the stability and diversity of the supramolecular nanostructures resulting from self-assembly, many efforts are devoted to the goal of imitating nature in the synthesis of bionanomaterials [1, 7].

The underlying principle that certain types of molecules organize themselves into nanostructures provides the basis for the *in vitro* production of (bio-)nanomaterials by using self-organizing building blocks. The high biocompatibility of these bionanomaterials allows promising applications in areas such as drug delivery, tissue engineering, bioimaging and biosensors [8, 9]. Particular emphasis has been placed on the use of peptides as building blocks for the production of bionanomaterials, since they allow a large chemical diversity for the establishment of new self-assembled bionanomaterials [10].

Due to electrostatic interactions and the ability to form numerous hydrogen bonds between the backbones, peptides can adopt a variety of different structures during self-assembly. Initially, the molecular interactions described above lead to the formation of secondary structures such as β-sheets, α-helices and turns. These, in turn can continue to assemble and result in supramolecular structures such as micelles, lamellar sheets, vesicles and fibrils [11, 12]. Different structures that peptides can form during self-assembly are shown in Figure 1.

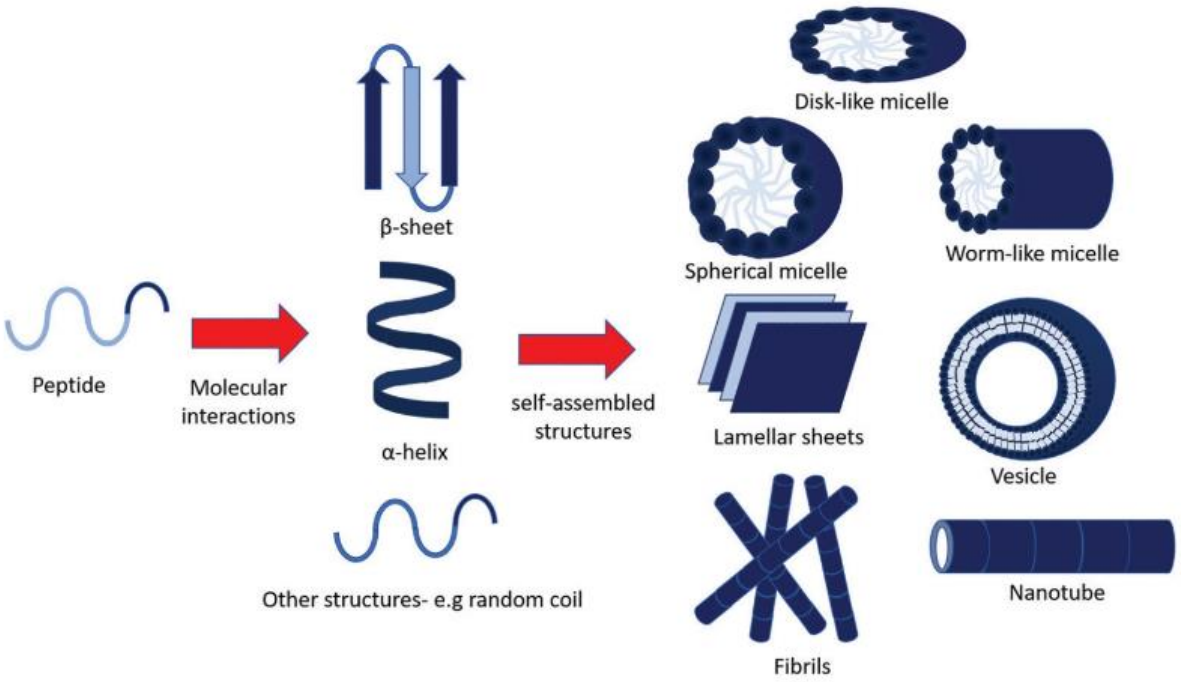

Figure 1: Illustration of how peptides possibly self-assemble via secondary structures such as β-sheets and α-helices into supramolecular structures [1].

Since the 1990s, when Zhang et al discovered the first in vitro self-assembling peptide based on the sequence H-AEAEAKAKAEAKAEAKAK-OH (EAK16-II), numerous other self-organizing peptidic systems have been established [13]. In general, two types of self-assembled peptide types can be distinguished. First, systems based on cyclic peptides and second, systems derived from amphiphilic peptides representing the vast majority of self-assembling peptides. Self-assembling amphiphilic peptides further include pure linear peptides, ionic complementary peptides and long-chain alkylated peptides [3, 14].

1.2 Important players in the world of self-assembling peptides

In aqueous conditions, pure linear peptides or surfactant-like peptides with a hydrophobic tail and a hydrophilic head tend to form structures such as micelles, nanotubes and nanovesicles [3, 15]. Usually the hydrophobic tail consists of six amino acids such as alanine, valine, leucine, isoleucine and phenylalanine, whereas the hydrophilic head mostly consists of only one or two amino acids such as aspartic acid, lysine, glutamic acid, arginine and histidine. For example, pure linear peptides with the sequences A_6D, V_6D and A_6K aggregate to micelles and vesicles in aqueous solutions very similar to phospholipids [15, 16]. This

makes self-assembled linear peptides a good alternative to surfactants such as DDM (*n-dodecyl-β-d-maltoside*) and OGP (*octyl-β-d-glucopyranoside*) for stabilizing membrane proteins [3, 14-18].

In contrast, the primary sequences of ionic complementary peptides differ fundamentally. They consist of alternating hydrophobic and hydrophilic charged amino acids. Figure 2 depicts the three most common types of ionic peptides. The peptide can be either uniformly charged (Figure 2a: positive, b: negative) or consist of alternating positive and negative charged amino acids (C).

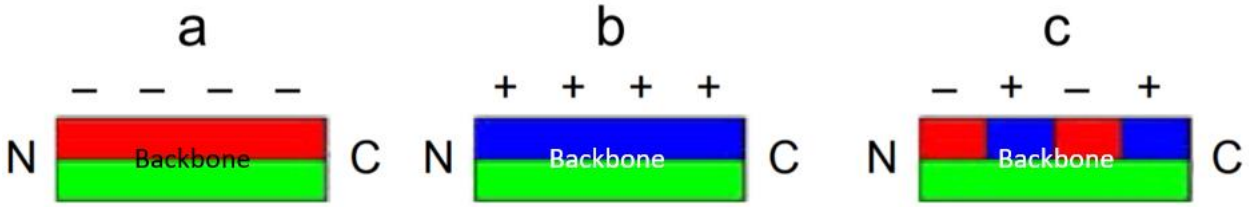

Figure 2: Illustration of the different types of ionic complementary peptides. Red: negative charged amino acids, Blue: positive charged amino acids, Green: hydrophobic amino acid. Modified from [3].

Peptides consisting of charged and hydrophobic amino acids self-organize under aqueous conditions to stable nanostructures. In aqueous solution, charged side chains face the outside and hydrophobic side chains can interact with those of other β-sheets forming double sheets [3]. Due to the ionic and hydrophobic interactions, ionic complementary peptides are extremely robust against broad temperature and pH ranges as well as against high concentrations of denaturing reagents [13, 19]. In addition to the aforementioned synthetic peptide EAK16-II with the sequence H-AEAEAKAKAEAKAEAKAEAKAKAK-OH introduced from Zhang *et al.,* various other self-assembling systems based on ionic complementary peptides have been described, including RADA16 peptide family with members such as RADA16-I (AcN-RADARADARADARADA-CNH_2) and RADA16-II (AcN-RARADADARARADADA-CNH_2). In particular, the capacity to retain water with hydration rates above 99% makes ionic self-assembling peptides promising tools for applications in regenerative medicine, tissue engineering and three-dimensional cell cultivation [20, 21].

The third type of self-assembling amphiphilic peptides comprises long-chain alkylated peptides, often referred to as peptide amphiphiles (PA) [22]. The peculiarity of peptide amphiphiles lies in their dual

Figure 3: Basic structure of a representative peptide amphiphile with the characteristic functional sequences [2].

physicochemical character, which unites the structural attributes of amphiphilic surfactants and bioactive peptides within a single molecule. As the name suggests, PAs consist of a long hydrophobic alkyl chain and a partly hydrophilic peptide domain. In turn, the peptide domain consists of a hydrogen bridge-forming, a charged and a functional epitope sequence [2]. The basic structure of a PA is illustrated in Figure 3.

Hydrophobic interactions in the *N*-terminal alkyl chain are one of the major forces for self-assembly of PAs under aqueous conditions. This effect is enhanced by the β-sheet-forming peptide segment, which accelerates peptide aggregation due to numerous intermolecular hydrogen bonds. To ensure solubility in water, a region with charged amino acids is often required. Asparagine and glutamic acid are well suited and often used for this purpose. Controlled variation of pH and salt concentration allows precise variation of the charge state and furthermore manipulating the dynamics of self-assembly and the formation of nanostructures [23].

Epitopes are usually bioactive peptide sequences which are involved in cell signal transduction and cell adhesion in biological organisms. For instance, the laminin-derived IKVAV pentapeptide, depicted in Figure 4, is specifically used as an epitope for PAs in neurological applications because of its important role in cell attachment, migration, differentiation and neurite outgrowth in neural tissue [22, 24, 25].

Scanning electron microscopy and computer simulations have shown that molecular forces such as hydrophobic interactions, hydrogen bonding and charge repulsion lead to supramolecular cylindrical nanofibers under aquatic conditions [2, 26]. Since the hydrophobic tail and the β-sheet forming segment represent the main forces for self-assembly, the bioactive peptide epitope is inevitably located on the surface of the nanofibers [2]. This is illustrated in Figure 4, where the epitope pentapeptide with the sequence IKVAV continuously covers the surface of the nanostructure.

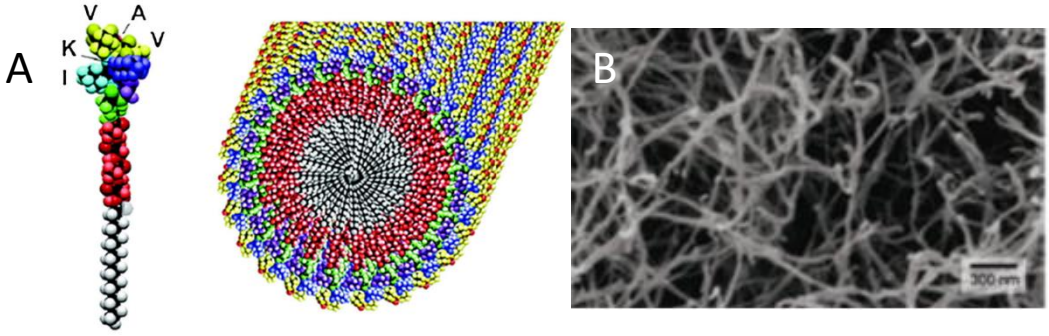

Figure 4: A: Illustration of a self-assembled nanofiber composed of PA molecules with an IKVAV epitope. B: Scanning electron microscopy image of the corresponding nanofiber network [2].

Based on the wide range of possibilities for designing PAs, *in vivo* applications range from regenerative medicine to treatment of ischaemic disease and therapeutic drug delivery solutions. In addition, the

potential benefits of systems incorporating PAs have already been demonstrated in numerous other fields such as tissue engineering, gene delivery and biomineralization [2, 22, 27].

Especially in the domain of biological inspired precipitation of nanomaterials in different morphologies, self-assembled peptides have been used as templates and catalysts for several decades and are promising candidates for exploring new avenues to create bionanomaterials [28].

1.3 Self-assembly and its role in biomineralization

The interaction between self-assembled peptides and inorganic molecules enables a large number of living organisms to form complex inorganic structures in an orderly manner. Among others, such structures include bones, dental structures, silica skeletons, shells and well-ordered magnetic nanoparticle chains [28]. The role of self-assembled peptides and proteins during the formation of functional nanostructures within organisms is to accumulate, transport and precipitate inorganic molecules. Although the artificial production of such structures is far more energy-intensive, less reproducible and often takes place under harsh conditions, the properties of biologically produced bionanomaterials exceed those of their synthetic equivalents in most cases [28-30].

Examples of organisms catalyzing biomineralization via self-assembled peptides include crayfish, Chinese soft-shelled turtle (*Pelodiscus sinensis*) and marine diatoms (*Cylindrotheca fusiformis*). Crayfish use the calcification-associated peptide (CAP-1) to produce robust exoskeletons from dissolved calcium carbonate molecules. Similarly, soft-shelled turtles catalyze the formation of egg shells via the glycine-rich peptide pelovaterin using calcium carbonate as inorganic building block. In contrast, diatoms such as *Cylindrotheca fusiformis* use silicic acid to generate complex silica nanostructures. Through polyamines and peptides such as silacidins and silaffins, diatoms are able to carry out biosilification under mild aquatic conditions [28, 31-33].

Biological systems, such as those mentioned above, serve as platforms for scientists to establish novel biomimetic methods for the efficient production of inorganic nanomaterials. The peptides associated with biomineralization are often isolated from organisms like diatoms and investigated *in vitro* under varying conditions. Although diatoms are in fact only one of many organisms capable of biosilicification, the diversity, size range and morphology of their silica structures are outstanding, which is why they have become the focus of many efforts to mimic biomineralization processes [34].

1.4 Mimicking the biomineralization process of diatoms with R5

Diatoms are unicellular organisms with a size of 10-200 µm predominately living in marine environments, waterways and soils. By using silicic acid, which is ubiquitous in aquatic environments, diatoms are able to biomineralize extremely complex and robust cell wall structures consisting of silica [35]. These types of diatom cell walls are also known as frustules and are shown in Figure 5 [36]. With the help of specific transporter proteins, diatoms are able to enrich the silicon required from their environment in the form of silicic acid. Despite relatively low silicic acid concentrations of 10-70 µM, they reach intracellular concentrations in the range of several hundred millimolar through progressive accumulation [35, 37, 38].

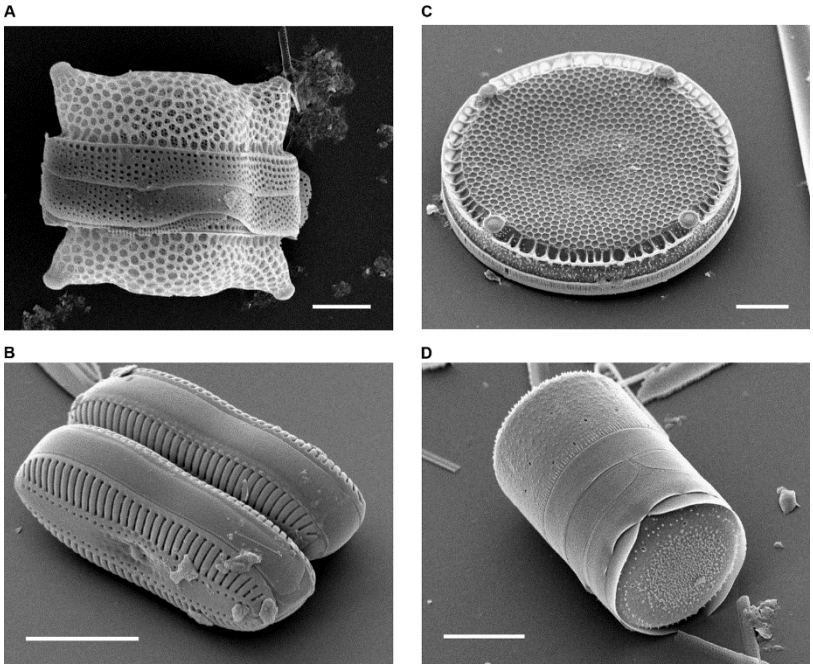

Figure 5: SEM-images of different diatoms. A: Biddulphia reticulata, B: Diploneis splendida, C: Eupodiscus radiatus, D: Melosira varians. scale bar = 10 µm [39].

Studies of silicious cell walls of the diatom species *C. fusiformis* revealed several classes of biomolecules, including polyamines, polysaccharides and proteins such as frustulins, pleuralins and silaffins [40]. Apart from polyamines, silaffin proteins have been shown to play a key role in the biosilicification process of *C. fusiformis*. Interestingly, all silaffin proteins are derived from one precursor protein named Sil1p. Usually the silaffin proteins are classified as Silaffin-1A, Silaffin-1B and Silaffin-2 [41]. The amino acid sequence of the precursor protein Sil1p is shown in Figure 6, highlighting the repetitive units R1-R7. Silaffin-1A is

composed of repetitive units R2-R7 and is further subdivided into silaffin-$1A_1$ (R3-R7) and silaffin-$1A_2$ (R2), whereas silaffin-1B is derived from peptide fragment R1.

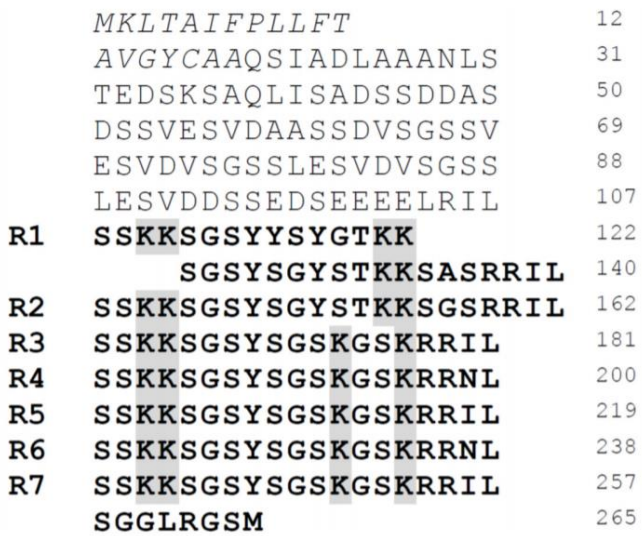

Figure 6: Amino acid sequence of the silaffin precursor protein Sil1p. The repetitive units R1-R7 are shown in bold. Lysine clusters are highlighted by a grey shade [35].

In addition to the primary structure, posttranslational modifications are essential for the biomineralization process. The numerous lysines within the repetitive units of Sil1p show modifications at ε-amino groups, for example, methylations and polyamine residues. Of further importance are phosphorylation, sulfation and glycosylation of hydroxyl amino acids. *In vitro* experiments have shown that the absence of only a few modifications is sufficient to inhibit the silica precipitation process completely [35, 42].

Alongside native silaffins, a synthetic peptide based on the repetitive unit R5 with the sequence SSKKSGSGSGSGSKGSKRRIL but lacking any posttranslational modifications shows the ability to precipitate silica particles from silicic acid under mild aquatic conditions. This is particularly remarkable as the industrial process for the production of silica nanoparticles requires harsh temperature and pH conditions [40]. However, polyamines show similar silica precipitation activity under mild conditions, but with the difference that peptides like silaffins can be modified more precisely [43, 44].

Interestingly, *in vitro* precipitation using R5 does not only work with silicon-based compounds. If silicic acid is replaced by titanium(IV)bis(ammonium lactate)dihydroxide, spherical titanium phosphate particles with diameters ranging from 700 nm to 10 µm are formed [45].

Depending on the chemical and physical reaction environment during precipitation process with R5 peptide, the morphology of the nanoparticles can be specifically manipulated. The spectrum of

morphologies that could be obtained ranges from typical spherical nanoparticles to arch-shaped structures and fibrils [46].

Although not completely clarified, it is suspected that silica precipitation is induced by self-assembly of the R5 peptide and catalyzed by an acid-base condensation reaction via lysine residues. Abstraction of a proton of a silicic acid molecule by deprotonated amino groups leads to the formation of reactive silanolates, which in the next step add to a second silicic acid molecule (see Figure 7) [35].

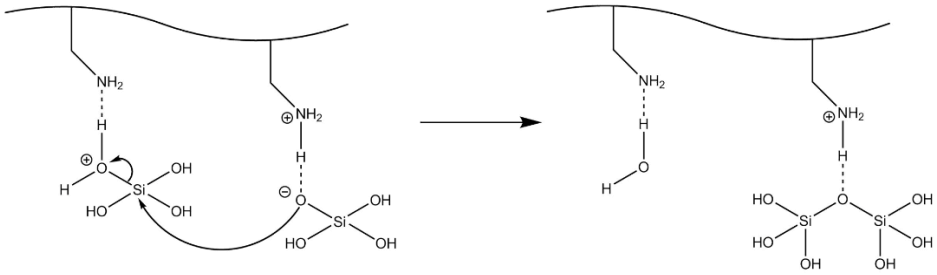

Figure 7: Postulated mechanism of amino group catalyzed polycondensation of silicic acid.

With progressive polycondensation of silicic acid monomers, co-precipitation of silaffin-derived peptides occurs. Through covalent binding of a target molecule to R5 peptides, it is possible to encapsulate fragile biologically active molecules in a stable silica matrix. Potential applications of the resulting material include vaccine adjuvants, drug delivery and enzyme immobilization [47-49].

Sequence function analyses with R5 have revealed that in addition to lysines, the *C*-terminal tetrapeptide RRIL plays a crucial role in silica precipitation. Modified R5 derived peptides with a lack of the RRIL sequence in the primary structure no longer show silicification activity *in vitro*. Less important for the precipitation of silica particles is the position of the RRIL sequence within the primary structure. The replacement of the *C*-terminal by an *N*-terminal RRIL sequence did not lead to a loss of precipitation activity. It is suggested that salt bridges between positively charged guanidine groups of arginine and negatively charged phosphate anions as well as negatively charged silicate monomers facilitate self-assembly of R5 and subsequently the silicification process [50]. However, synthetic KXXK-based peptides show precipitation activity even in the absence of RRIL. Instead, self-assembly is induced by polycationic lysine residues carrying typical posttranslational modifications of native silaffins (e.g. methylation and polyamine modification) [51]. In contrast, unmodified peptides require a RRIL motif for self-assembly, even though the presence of RRIL is not sufficient for silica precipitation activity. Experiments with the tetrapeptide RRIL showed no silica precipitation activity [50]. As soon as an additional lysine was coupled via the *N*-terminus, silica precipitation could be observed again. Nevertheless, silica precipitation activity

was only fractional compared to full length R5. Furthermore a strong shift in morphology away from spherical to amorphous particles was evident [50]. The decrease in silica precipitation activity and the shift in morphology were explained by a reduced self-assembly tendency of the KRRIL pentapeptide compared to R5 [50].

With these findings in mind, Becker and co-workers synthesized KRRIL-based peptide analogues with an additional RRIL sequence attached to the *N*-terminus [52]. They were able to show that a peptide with the sequence RRILKRRIL produces spherical silica particles similar to those of full length R5. From this, they concluded that the additional RRIL sequence greatly enhances self-assembly and silica precipitation activity [52]. Furthermore, they were able to show that the distance between the two RRIL sequences of RRILKRRIL based peptides as well as the introduction of D- instead of L- amino acids of the *N*-terminal RRIL sequence had minimal effect on silica particle morphology (see Figure 8, A-D). After an unintentional introduction of an additional D-leucine or D-isoleucine in the form of the sequence rri(i/l)lK*RRIL (K* denotes isopeptide bond with lysine ε-amine), a dramatic change in morphology towards rod-like silica structures was observed, as can be seen in figure 8, E-H [52].

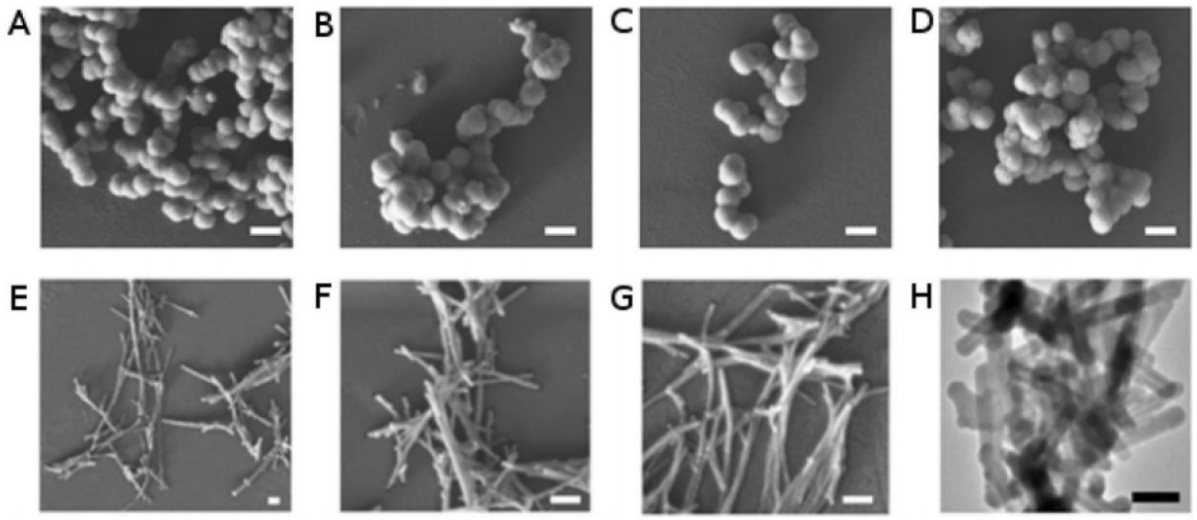

*Figure 8: SEM images of silica particles obtained with different KRRIL-based peptides, A: RRILKRRIL, B:RRILK*RRIL, C: rrilKRRIL, D:rrilK*RRIL, E: unintentional batch with rril(i/l)K*RRIL, F: rrillK*RRIL, G: rriilK*RRIL, H:TEM image of silica particles of rrillK*RRIL, K* denotes side chain elongation, (scale bar: 500 nm) [52].*

The authors not only demonstrated that an additional hydrophobic amino acid within the *N*-terminal motif had dramatic effects on the morphology of precipitated silica particles, but also confirmed that peptide assembly served as a template for silica precipitation. In order to obtain rod-like silica instead of spherical particles, two conditions were crucial: first the introduction of another hydrophobic amino acid

(leucine or isoleucine) to the N-terminal RRIL motif and second, the use of D- instead of L-amino acids for the N-terminal RRIL sequence [52]. Although self-assembly mechanism of this KRRIL derived systems could not yet be elucidated, parallels with respect to the molecular dynamics during self-organization process can be observed by comparison with other self-assembling peptides.

1.5 How chirality affects peptide self-assembly

Homochirality of amino acids within peptides and proteins is universally present in practically all biological organisms. With the exception of glycine, all amino acids occur in L-configuration. Chirality guided interactions are one of the main driving forces for correct folding of peptides and proteins into secondary, tertiary and quaternary structures. Even the smallest deviations or errors in protein folding usually lead to a significant loss of protein activity. It is believed that this is a decisive factor for the lack of racemic biological systems in nature [53].

Peptides and proteins consisting of L-amino acids usually form right-handed α-helices and right-handed twisted β-strands structures [54]. Self-assembly of right-handed twisted β-strands usually results in left-handed β-sheets and subsequently in fibrils with a left-handed twist. At the same time studies show that peptides composed of D-amino acids form fibrils with right-handed twists [55, 56]. Nevertheless, it is difficult to predict the supramolecular structure of peptides and proteins on the basis of the primary sequence and chirality, as most studies were carried out *in vitro* under specific conditions. Minimal changes in pH or temperature can lead to substantial shifts in the configuration of supramolecular structures [55].

In recent years, heterochiral peptides, such as the KRRIL derived systems mentioned above, have received special attention. Responsible for this are highly divergent self-organizing properties compared to their homochiral counterparts. For instance, heterochiral tripeptides with the sequence $^{D}F^{L}F^{L}V$/ $^{L}F^{D}F^{D}V$ assemble via β-sheets to fibrils under physiological conditions, whereas the homochiral equivalent with the sequence FFV did not show ordered structures [57]. In addition, no signs of self-organization could be observed in tripeptides in the form of $^{D}F^{D}F^{L}V$/ $^{L}F^{L}F^{D}V$ and $^{L}F^{D}F^{L}V$/ $^{D}F^{L}F^{D}V$ indicating that the *N*-terminal position of the amino acid with diverging stereochemistry is the main driving force for aberrant self-assembling behavior [57]. Another example is a tripeptide with the sequence $^{L}F^{D}L^{L}F$, which aggregated under physiological conditions to amphiphilic superstructures and through this to self-supportive hydrogels [58].

However, self-assembly behavior depends strongly on the primary sequence of the peptide and has to be investigated on a case-by-case basis. While homochiral peptides based on the tripeptide EAK have a tendency to self-assemble, their heterochiral counterparts show little to no self-organizing properties. Thus, exactly the opposite characteristic compared to the tripeptides FFV and FLF is evident [59]. Another different case is that of a peptide amphiphile consisting of two alanines and an additional hydrophobic C18 alkyl chain at the *N*-terminus ($C_{18}H_{35}O$-AA). Neither homo- nor heterochirality of this peptide amphiphile were the determining criteria for the handedness of the self-assembled structures, but rather the chirality of the *C*-terminal amino acid [60]. Wang *et al.* obtained a similar result with different stereoisomers of the tetrapeptide I_3K, where the handedness of self-assembling nanofibrils was exclusively controlled by the chirality of lysine [55]. Analogously, the chirality of lysine residues incorporated into peptide nucleic acids (PNAs) also showed major structural and functional consequences [61].

To summarize, further research needs to be carried out to elucidate the impact of chirality on self-assembly and the handedness of resulting supramolecular structures.

1.6 Arginine as a driver of self-assembly

Charged side chains are known to play a key role in self-assembly of short peptides [17]. The amino acid arginine with its basic side chain has the ability to form bidentate hydrogen bonds via the delocalized positive charge of the guanidine group. The influence of positively charged arginine residues is particularly evident in the case of RRIL peptides. The arginine residues within the primary sequence enable the formation of salt bridges between positively charged guanidine groups and negatively charged phosphate anions. It is assumed that this process initiates the self-assembly of RRIL-based peptides [50]. Beside RRIL peptides, there are many other peptidic systems whose properties are based among others on the electrostatic interaction of arginine residues.

For example, the interaction of arginine residues with head groups of lipid bilayers allows the permeation of cell membranes [62]. As a result, short antibiotic peptides containing arginine receive increased attention. Many of the approaches are based on peptides with self-assembling properties. Among them are surfactant-like peptides such as A_9R, A_6R, capA_6R and A_6RGD, which self-assemble to a multitude of structures ranging from vesicles, fibrils and nanotubes to nanosheets. A microbial activity against common pathogens such as *E. coli, S. aureus* and *L. monocytogenes* has already been demonstrated [63, 64].

Arginines are also frequently used for the production of peptide bola-amphiphiles, where a charged residue is present at both ends of the peptide molecule. The peptide bola-amphiphile RA_3R, for example, forms polyproline II secondary structures and interacts strongly with anionic lipid molecules [65]. The relatively good water solubility of the RA_3R peptide hinders self-assembly and therefore the hydrophobic alanine sequence has been extended in recent studies. Similar to the RA_3R peptide, RA_6R showed no signs of self-assembly in water, whereas the RA_9R peptide aggregates to well-ordered nanofibers above a critical concentration [66]. Another remarkable investigation revealed that the peptide $A_{12}R_2$ aggregates to ultra-thin amyloid fibrils with a width in the order of a molecule length [67].

In addition to surfactant-like peptides and peptide bola-amphiphiles, arginine-rich hydrogels are used as promising antibiotics. In 2012 Veiga *et al*. produced a novel optimized hydrogel based on the PEP8R peptide [68]. They were able to show that the arginine-rich peptide with the sequence $VRVRVRVRV^{D}PPTRVRVRVRV\text{-}NH_2$ formed amphiphilic β-hairpins in aqueous NaCl solution. In water at neutral pH, arginine residues of PEP8R are positively charged and peptide folding is prevented because of repulsion of guanidine groups. By shielding the positive charges with negatively charged chloride anions, self-organization of the PEP8R peptides into hairpins is triggered, comparable to R5 and KRRIL-based self-assembly facilitated through phosphate anions (see section 1.4). Self-assembly of the PEP8R hairpins then leads to fibrillar networks rich in β-sheets and subsequently to the formation of a hydrogel, illustrated in Figure 9 [68].

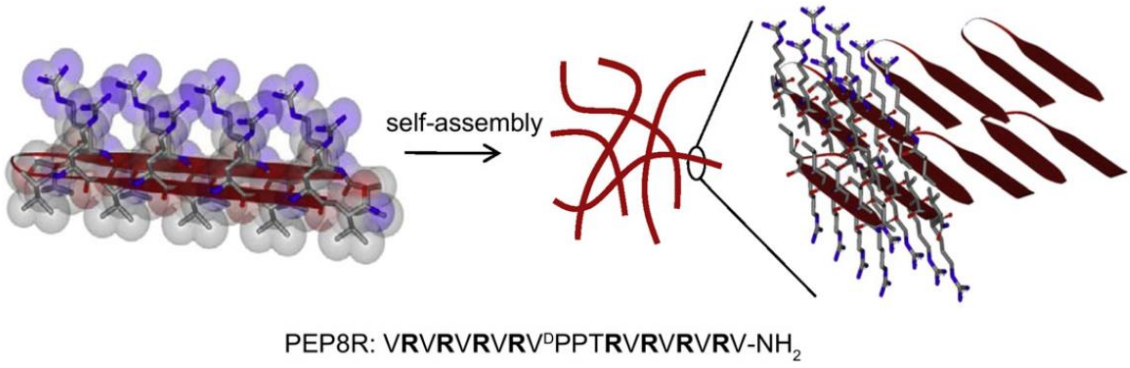

Figure 9: Self-assembly mechanism of PEP8R b-hairpins to b-sheet rich networks that form the characteristic hydrogel [68].

The authors assume that hydrogen bonds and hydrophobic effects caused by valine residues are the driving forces for the formation of the fibrillar network. In the same way as with amphiphilic peptides, they believe that this leads to shielding of the hydrophobic site from aqueous environments and simultaneously to solvent-exposed arginine residues. As a consequence, intermolecular hydrogen bonds

via arginine residues of individual fibrils are formed, triggering the formation of stable fibrillary networks [68, 69].

In 2015, Decandio *et al.* investigated the self-assembling properties of a novel artificial octapeptide consisting of an alternating sequence of hydrophobic and hydrophilic residues. As hydrophilic amino acids, they used arginine because of the guanidine side chain. Paired with phenylalanine, which establishes strong π-π interactions through its aromatic side chain, they produced the ionic complementary octapeptide $[Arg\text{-}Phe]_4$. After reaching the critical aggregation concentration, oligomeric and b-sheet rich structures were formed in the shape of both spheroidal species and ordered fibrils with diameters ranging from 4 nm up to 40 nm [70].

The selection of short peptides presented here intends to illustrate the enormous range that the use of arginine as a molecular tool for promoting self-assembly and generating a variety of supramolecular nanostructures entails. Self-assembling peptides containing arginine residues promise many potential biotechnological and medical applications ranging from novel antiobiotics to deciphering the causes of numerous diseases such as Parkinson's and Alzheimer's [63, 70].

1.7 Leucin and isoleucine in peptide self-assembly

Branched-side chain amino acids such as leucine and isoleucine are key components of many self-assembling peptides. Although leucine and isoleucine are constitutional isomers that differ only in the position of a methyl group, they show different conformational preferences. Small changes in the dihedral angle at the molecular level can have enormous effects on the self-assembly of peptides [71].

As already discussed in section 1.4, the exchange of isoleucine with leucine and *vice versa* in R5 derived peptide variants caused a significant change in self-assembly behavior, thus also impacting the morphology of resulting silica particles. For example, changing the position of a single methyl group resulted in a shift from rod-like particles to silica-sheets. Even more dramatic were the effects of the addition of a single leucine or isoleucine residue within the primary sequence. The addition of a single amino acid led to a transition from spherical to rod-like particles. The underlying mechanism of the dramatic consequences on self-assembly and silica precipitation associated with the variation of individual leucine and isoleucine residues has not yet been clarified [52].

Nevertheless, recent investigations exhibited interesting insights into the role of isoleucine and leucine in peptide conformation and self-assembly. In 2016, Zhou *et al.* investigated the conformational propensity of single leucine and isoleucine residues via the host-guest method, as single amino acids are known to

have unique conformational preferences [72]. For this purpose, they used a host peptide with the sequence GGXGG. In the Ramachandran plot, isoleucine (GGIGG) showed an increased β/extended distribution compared to leucine (GGLGG), as shown in figure 10. The Ramachandran map also reveals an α_L-helical distribution of leucine [72].

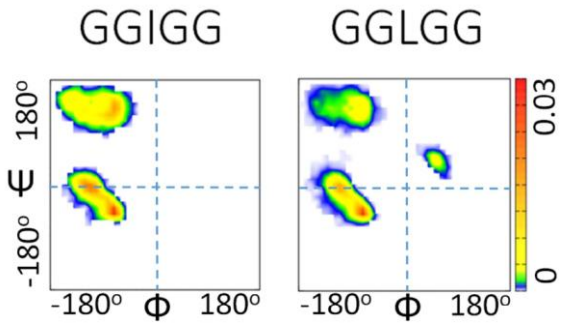

Figure 10: Ramachandran plots of the model peptides GGIGG and GGLGG [72].

Both leucine and isoleucine show α_R-helical conformations in some ways, although their dihedral angle distribution is not completely equal due to different side chain sizes [73]. It should also be noted that the dihedral angle distributions of D- and L- amino acids are similar, except that the Ramachandran plots of the isomers mirror each other [74]. It is obvious that the conformation of individual amino acids simulations strongly depends on the adjacent amino acids or the host framework and differs from that in protein simulations [71]. For instance, leucine showed a stronger α-helix conformation within a host-model with the sequence GXG [75].

In addition, host-guest peptides usually do not show well-defined secondary structure and do not tend to self-aggregate due to their high water solubility. On the contrary, self-assembled short peptides show well-ordered secondary structures leading to a fundamental change of conformational propensities of single amino acids like leucine and isoleucine caused by intra- and intermolecular interactions [71]. Two isomeric self-assembling peptides I_3K and L_3K, for example, showed a stronger β/extended conformation of isoleucine and a higher α-helix distribution of leucine compared to their host-guest-equivalents GGIGG and GGLGG [72]. Therefore, the authors conclude that isoleucine and leucine residues may enhance the conformational propensity of their neighbouring equals. In another experiment, they replaced L-lysine with the D-version and examined the conformational impact on the neighbouring amino acids. Interestingly, the enantiomeric exchange led to some variations in the conformational propensity of adjacent Ile3 and Ile2 residues of $^{L}I_3{}^{D}K$, although D- and L-lysine showed the same conformational distribution compared to those of their host-guest equivalents $GG^{L}KGG$ and $GG^{D}KGG$ [72].

It is obvious that changes in the conformation of individual amino acids within a peptide sequence strongly influence molecular structure. The first step of peptide self-assembly is the adoption of the main chain geometry, followed by intermolecular aligning and building block packing. Even the smallest variation of conformational preferences of individual amino acids can therefore have a large effect on supramolecular structures [71].It seems reasonable to draw conclusions from these findings for self-assembly activity of peptides such as the R5-based RRIL-systems, especially considering that the hydrophobic amino acids leucine and isoleucine make up exactly half of the residues within the primary sequence of RRILLKRRIL peptides and variations of the hydrophobic parts of the primary sequence led to dramatic changes in silica particle morphology [52].

Understanding the underlying mechanisms of self-assembly is an integral part for the production of silaffin-inspired bionanomaterials. This inevitably includes the impact of chirality on self-assembly as well as the roles of the amino acids arginine, leucine and isoleucine for the molecular alignment of RRIL-derived peptides. The elucidation of these aspects will allow a more precise manipulation of self-assembling silaffin-derived peptides and thus lead to specific modification of the morphology of silica nanomaterials.

1.8 Aims of the project

The aim of the present work was to investigate the influence of different modifications of R5-derived RRIL peptides on self-assembly and subsequently on the morphology of resulting silica nanoparticles. On the basis of the sequence-function analysis by Lechner *et al.* and structure-activity relationship study by Kamalov *et al.*, described in section 1.4, the first goal was to elucidate the influence of different central residues (linkers) and thus the distance between two RRIL(L) sequences within a RRILLKRRIL derived peptide. For this purpose, the four amino acids lysine, β-alanine, diaminopropionic acid and ornithine, each in the D and L versions, were used as central residues between two RRIL motifs. In addition, the stereochemistry of the two RRIL motifs was varied in order to investigate its effect on the morphology of the silica particles in more detail.

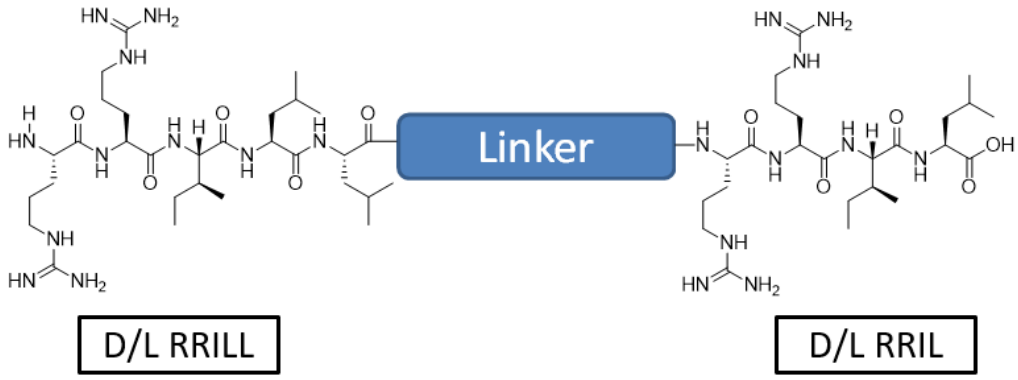

Figure 11: Structure of the initial peptide with the primary sequence RRILL-Linker-RRIL.

The variation of the central residue and the stereochemistry of the N- and C-terminal RRIL sequences results in a total of 14 peptides (β-alanine does not have a stereocenter). After synthesis and purification of the peptide variants, the morphology of the particles resulting from silica precipitation was investigated via SE-microscopy. The comparison of morphologies allowed insights into the underlying self-assembly mechanism of the peptides. Another objective is to test whether the variation of the central residue and/or the stereochemistry is suitable as a tool for precise manipulation of silica nanostructures.

After successfully synthesizing the peptide variants, the second goal was to investigate the influence of functionalization on the silica particle morphology. Since silica nanoparticles are expected to be used in applications such as vaccine adjuvants and drug delivery systems, it is essential to estimate the effect of a covalently bound functionalization on self-assembly and silica structure morphology.

For this reason, the fluorescent dye Cyanine-5 (Cy5) was attached via a second linker molecule such as β-alanine and their influence on self-assembly and silica particle morphology was investigated.

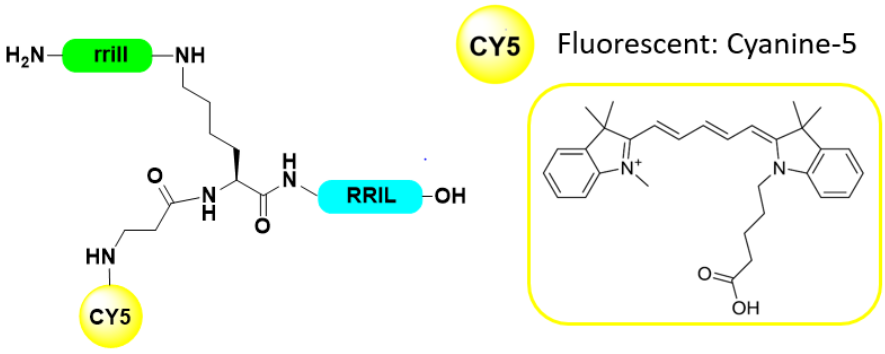

Figure 12: Structure of the peptide rrill-K(βAla(Cy5)RRIl and the structure of the fluorescent cyanine-5.*

Functionalization with Cyanine-5 offers the advantage of making the incorporation of the peptide into the silica nanoparticles spectroscopically observable. Simultaneously, a similar peptide was synthesized with beta-alanine as additional linker that does not have any functionalization, in order to examine its influence on self-assembly in detail. Furthermore, the incorporation rate of these peptides into the silica nanoparticles was monitored using HPLC analyses.

2. Materials and Methods

2.1 General chemicals

Fmoc-Leu-Wang resin, Fmoc-Ile-OH, Fmoc-D-Ile-OH, Fmoc-Leu-OH, Fmoc-D-Leu-OH, Fmoc-Arg(Pbf)-OH, Fmoc-Lys(Boc)-OH, Fmoc-β-Ala-OH and (1-[Bis(dimethylamino)methylene]-1H-1,2,3-triazolo-[4,5-b]-pyridinium 3-oxide hexafluorophosphate (HATU) were purchased from Novabiochem (Nottingham, United Kingdom).

Fmoc-D-Leu-Wang resin, Fmoc-D-Arg(Pbf)-OH, Boc-L-Dap(Fmoc)-OH, Boc-D-Dap(Fmoc)-OH, Boc-L-Orn(Fmoc)-OH and Boc-D-Orn(Fmoc)-OH were obtained from Iris Biotech GmbH (Marktredwitz, Germany), Boc-Lys(Fmoc)-OH from Orpegen Peptide Chemicals GmbH (Heidelberg, Germany), Boc-D-Lys(Fmoc)-OH from Bachem Holding (Bubendorf, Schweiz). Acetonitrile (ACN) was purchased from Biosolve (Valkenswaard, the Netherlands), TFA and DCM from VWR International (Radnor, Pennsylvania USA). All other chemicals used were obtained from Sigma-Aldrich (Taufkirchen, Germany).

2.2 Solid phase peptide synthesis

All peptide syntheses described below were performed according to the Fmoc strategy using Wang-resins as a solid phase [76]. The synthesis steps were carried out on a 0.01 mmol scale and at room temperature, unless otherwise stated. The washing steps were carried out with approximately 1 ml DMF per 25 mg resin.

First, the Wang-resin was weighed in a syringe with frit and swollen with DMF for 45 minutes. The Fmoc deprotection was then performed with 20 % piperidine in DMF solution with first 3 min and second 7 min reaction time (1 ml/25 mg resin). Afterwards the resin was washed 5 times with 1 ml DMF. For the coupling of native amino acids 5 eq of Fmoc-protected amino acid were dissolved in 4.2 eq HATU (0.5M HATU solution in DMF), 10 eq DIPEA were added and the mixture was activated for 3 min at RT. The coupling solution was then transferred to the resin with a reaction time of 30 min. After that, the resin was filtered and washed 10x with 1 ml DMF. The cycle started again with Fmoc deprotection. For overnight storage, the resin was kept in DMF.

2.3 N-Acetylation of β-Alanine

To acetylate the Fmoc-deprotected beta-alanine, the resin was incubated for 30 min with 1 ml of an acetylation solution consisting of acetic anhydride/DIPEA/DMF (1:1:3). This process was repeated again, but with an incubation time of 24 hours. The solution was then discarded and the resin was washed 3 times with 1 ml DMF. After acetylation, selective Boc-deprotection was performed as described in section 2.5.

2.4 Coupling of the fluorescent dye Cyanine-5

After Fmoc-deprotection with 20 % piperidine in DMF, 4 eq Cy5 (0.04 mmol, 18.8 mg) were dissolved in a solution of 3.5 eq HATU in DMF (0.035 mmol HATU, 0.5 M solution of HATU in DMF) and 10 eq DIPEA (0.1 mmol, 17 µl) were added to the mixture before it was diluted to 1 ml with DMF and added to the resin for 18 hours. The resin was then washed 10 times with 1 ml DMF and 3 times with 1 ml DCM. After the coupling of Cy5, the resin was dried via desiccator in the absence of light.

2.5 Selective Boc-deprotection

First, the resin was swollen in 1,4-dioxane for 45 minutes at RT. The resin was then mixed with 0.5 ml of Boc-deprotection solution (10 % H_2SO_4 in 1,4-dioxane), shaken at 8°C for 2.5 hours in the absence of light. The Boc-deprotection solution was replaced every 30 minutes. After the incubation, the resin was washed 5x with 1 ml 1,4-dioxane, 3x with 1 ml of 10 % DIPEA in DMF solution and 3x with 1 ml DMF. Finally, the resin was swollen in DMF for 45 minutes so that the peptide synthesis via SPPS (section 2.2) could be continued.

2.6 Final cleavage and lyophilization

After completion of the peptide synthesis, final Fmoc-deprotection was performed using 1 ml of 20 % piperidine in DMF. The resin was then washed with DMF as well as DCM and dried over vacuum for at least 3 hours. The dry resin was mixed with 0.5 mL cleavage cocktail (92.5 % TFA, 5.0 % TIPS, 2.5 % H_2O) per 25 mg dry resin and rotated for 3 hours, in the absence of light and at RT. The peptide was then precipitated using 5 times the volume of ice-cold diethyl ether based on the volume of cleavage solution. After precipitation (10 min, -18°C), centrifugation was performed (4°C, 5 min, 5400 rpm). The resulting pellet was washed twice with 5x cold diethylether and centrifuged (4°C, 5 min, 5400 rpm). The supernatant was then removed and the pellet dried under argon. Finally, the dried pellet was dissolved in 5 ml ACN/H_2O 1:1 and lyophilized overnight.

2.7 Purification via HPLC

Before purification, a HPLC-MS run of the crude product was performed on an analytical Kromasil C4 RP-HPLC column using a gradient from 5 %- 45 % buffer B (ACN with 0.08 % TFA) in buffer A (H_2O with 0.1 % TFA) over 20 minutes at a flow rate of 1 ml/min. The crude peptide was then dissolved in 8 ml deionized water and injected for purification on Waters Prep 150 System on a Kromasyl C4 semi-preparative RP-HPLC column using a gradient from 5 % - 45 % buffer B in buffer A over 30 minutes at a flow rate of 10 ml/min. The fractions of all UV peaks with an absorption above 100 mAU were collected automatically. Subsequently, 20 µl of each fraction were directly injected into Thermo Fisher HPLC-MS system to identify product peaks based on mass spectra. The fractions in which a product peak without impurities was identified were combined and lyophilized overnight.

2.8 Final analysis

For the final analysis via RP-HPLC a small amount of the purified peptide was dissolved in buffer A, injected into a Dionex Ultimate 3000 HPLC system and separated by an analytical Kromasil C4 RP-HPLC column using a gradient from 5 % - 65 % buffer B in buffer A over 30 minutes at a flow rate of 1 ml/min. In a further step, a small amount of peptide was dissolved in water and directly injected into a Thermo Fisher HPLC-MS system.

2.9 Silica precipitation

First, a 4 mg/ml solution of purified peptide (~3 mM) in deionized water was prepared. Then the peptide solution was diluted 1:1 with 100 mM potassium phosphate buffer (pH 7), so that the final peptide concentration was 2 mg/ml. The solution was then incubated for 24 hours at RT. Sometimes a precipitate occurred after incubation with phosphate buffer which, unless otherwise stated, was not separated.

Next day, silicic acid was freshly prepared by adding 40 µl (270 µmol) tetramethoxysilane to 960 µl 1 mM HCl, vortexing for 3 seconds and incubating for 4 minutes at RT. Then 10 µl from the resulting silicic acid solution were added to 100 µl of the 2 mg/ml peptide solution in potassium phosphate buffer, so that the final concentration of silicic acid was 25 mM. The solution was then vortexed and incubated for 30 min at RT to initiate silica precipitation. After precipitation the suspension was centrifuged (RT, 5 min, 14 000 rpm) and the precipitate was washed twice with 100 µl H_2O each. Finally, the precipitate was resuspended in 1 ml of H_2O for the preparation of SEM samples.

2.10 Scanning electron microscopy (SEM)

2.10.1 SEM-imaging of peptide precipitates after incubation in phosphate buffer

The precipitate that formed upon incubation of peptide in phosphate buffer (section 2.9) was spinned off, separated and resuspended with 1 ml 50 mmol phosphate buffer (pH 7). 3 µl of the resulting suspension were applied to a Thermanox™ coverslip and air-dried. The sample applied to the coverslip was then washed 3 times with 3 µl H_2O and dried. A layer of gold was subsequently applied to all samples by sputter coating under high vacuum (Bal-Tec SCD 005) and SEM imaging was performed with a Zeiss SEM supra 55 VP at 20 kV.

2.10.2 SEM-imaging of silica particles

10 µl of the silica particles suspension from section 2.9 were applied onto Thermanox™ coverslips and dried on air. A layer of gold was subsequently applied to all samples by sputter coating in high vacuum (Bal-Tec SCD 005) and SEM imaging was performed with a Zeiss SEM supra 55 VP at 20 kV.

2.11 Determination of peptide concentration using RP-HPLC

In order to determine the peptide concentration, a volume of 10 µl of a given peptide solution with a concentration of 4 mg/ml (~3 mM) were taken and 50 µl of buffer A were added. From this solution, 50 µl were injected into a Dionex Ultimate 3000 HPLC system and separated by an analytical Kromasil C4 RP-HPLC column using a gradient from 5 % - 65 % buffer B in buffer A over 30 minutes at a flow rate of 1 ml/min. Subsequently, the area under the curve was calculated from the UV peak at a wavelength of 214 nm in order to verify whether a correlation can be established between the concentration of the various peptide analogues and their peak areas.

2.12 Determination of peptide incorporation rate during silica precipitation

In order to determine the degree of peptide incorporation during the silica precipitation process, 10 µl from the peptide sample solution before and after silica precipitation were taken and mixed with 50 µl buffer A. If a precipitate occurred during incubation in phosphate buffer, the sample was vortexed and the suspension was used for diluting with 50 µL buffer A. After dilution, the precipitation dissolved almost completely. If there was still precipitation, the sample was spinned and filtered before injection into the HPLC system. 50 µl were injected into a Dionex Ultimate 3000 HPLC system and separated by an analytical Kromasil C4 RP-HPLC column as described in section 2.11. By comparing the peak areas, it is possible to estimate the degree of incorporation of peptide into the silica particles.

2.13 Fluorescence imaging via IncuCyte® ZOOM analysis system

From the silica particle suspension resulting from section 2.9, 3 µl were initially applied to a 96 well plate. Then 30 µl deionized water were added to cover the surface of the 96 well plate with liquid. The sample was then dried overnight in the absence of light.

The fluorescence images were performed using an IncuCyte® ZOOM analysis system 20x zoom with a resolution of 0.61 µm/pixel with a green and a red channel. The wavelengths of excitation and emission of the green and red channel were in the following ranges:

Table 1: Wavelength range of absorption and emission.

Channel	Excitation	Emission
Green	440–480 nm	504-544 nm
Red	565–605 nm	625-705 nm

The analysis of the data was done using the software of the manufacturer.

3. Results

3.1 Results of the synthesis, purification & silica precipitation of KRRIL derived peptides

In the following two sections, the results of the synthesis, purification and silica precipitation of a total of 16 different peptides are shown. The first section summarizes the data of the peptides with varying stereochemistry and different central residues. In section 3.1.2, the results of the Cy5-functionalized peptide and an analog without Cy5 modification are presented.

Table 2: Overview of the 16 synthesized peptides including sequence and structure. The star at the central residue in the primary sequence indicates that the N-terminal RRILL sequence was coupled via the amine of the amino acid side chain. Lower case letters correspond to the D-version and upper case letters to the L-version of the amino acids. Dap = 2,3-Diaminopropionic acid, bAla = β-alanine, Orn = Ornithine, k/K = D/L-Lysine.

Peptide No.	Sequence	Structure
1	rrill-LDap*-RRIL	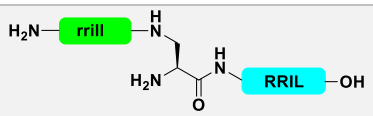
2	rrill-DDap*-RRIL	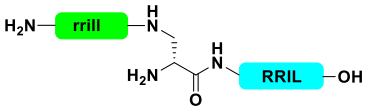
3	RRILL-LDap*-rril	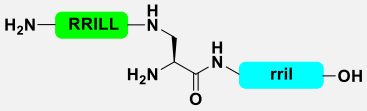
4	RRILL-DDap*-rril	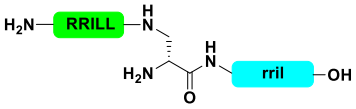
5	rrill-bAla-RRIL	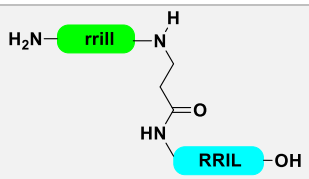
6	RRILL-bAla-rril	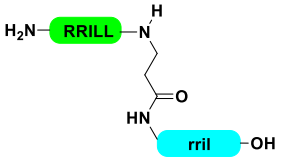
7	rrill-LOrn*-RRIL	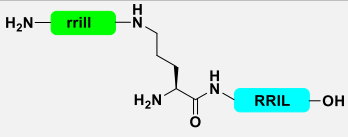

8	rrill-DOrn*-RRIL	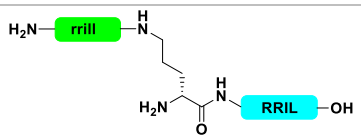
9	RRILL-LOrn*-rril	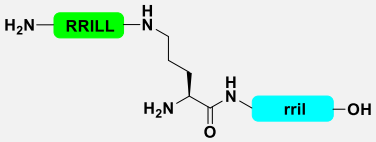
10	RRILL-DOrn*-rril	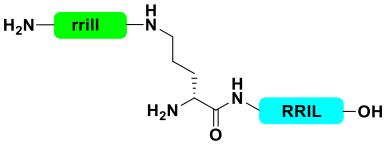
11	rrill-K*-RRIL	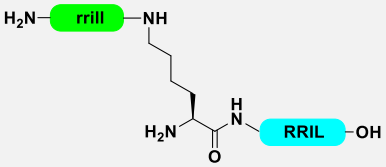
12	rrill-k*-RRIL	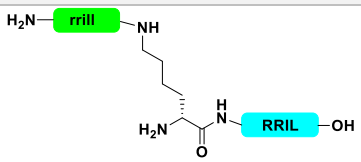
13	RRILL-K*-rril	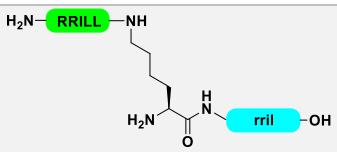
14	RRILL-k*-rril	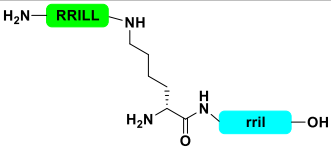
15	rrill-K*(βAla(Ac))-RRIL	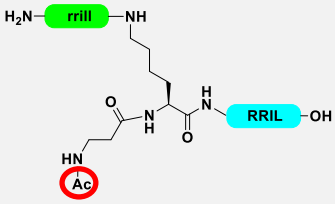
16	rrill-K*(βAla(Cy5))-RRIL	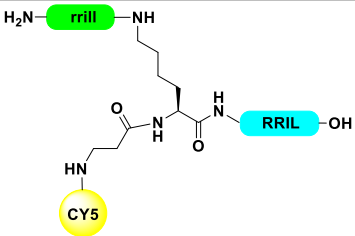

3.1.1 RRIL-peptides with different central residues and varying stereochemistry

Peptides 1-14 shown in this section were synthesized via SPPS as described in section 2.2. After final cleavage (see section 2.6), purification was performed using RP-HPLC according to section 2.7. The purity of the resulting products was determined via HPLC and direct injection mass spectrometry (see section 2.8). After purification, silica precipitation and SEM-imaging were performed, as described in Section 2.9 and 2.10. In the following, the data obtained from the above steps are presented separately for each peptide.

3.1.1.1 Results of the synthesis, purification and silica precipitation of peptide 1

The yield of peptide 1 with the sequence *rrill-LDap*-RRIL* after RP-HPLC purification was 11.6 mg (90 % of the theoretical yield of 12.9 mg for 0.01 mmol synthesis scale).

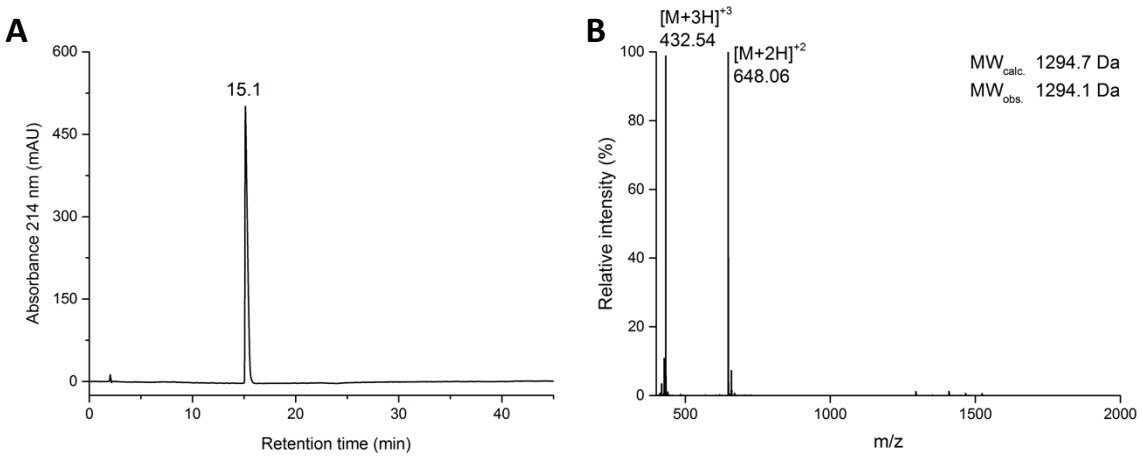

Figure 13: A: HPLC chromatogram of purified peptide 1. B: Mass spectrum obtained from a direct injection of purified peptide 1 on a Thermo Fisher HPLC-MS system.

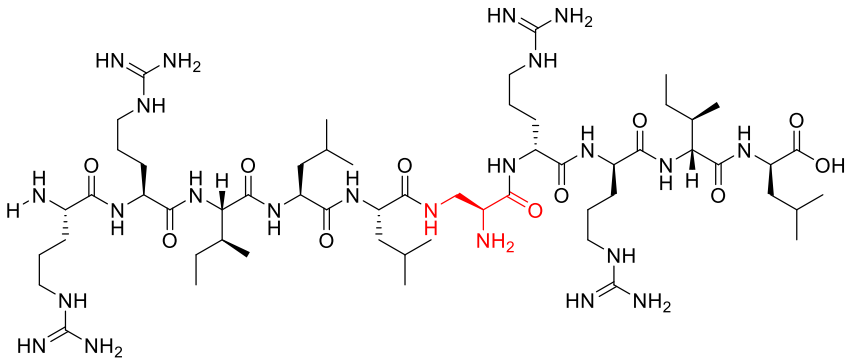

Figure 14: Structure of peptide 1 with L-Dap as central residue.

Figure 13A depicts the chromatogram (214 nm absorbance wavelength) from the RP-HPLC analysis of purified peptide 1 (structure shown in Figure 14) and the corresponding mass spectrum is visualized in Figure 13B, which shows peaks corresponding to an observed mass of 1294.1 Da, which is in good agreement with the expected mass of 1294.7 for peptide 1. Based on the data shown, it can be concluded that the purification of peptide 1 was successful.

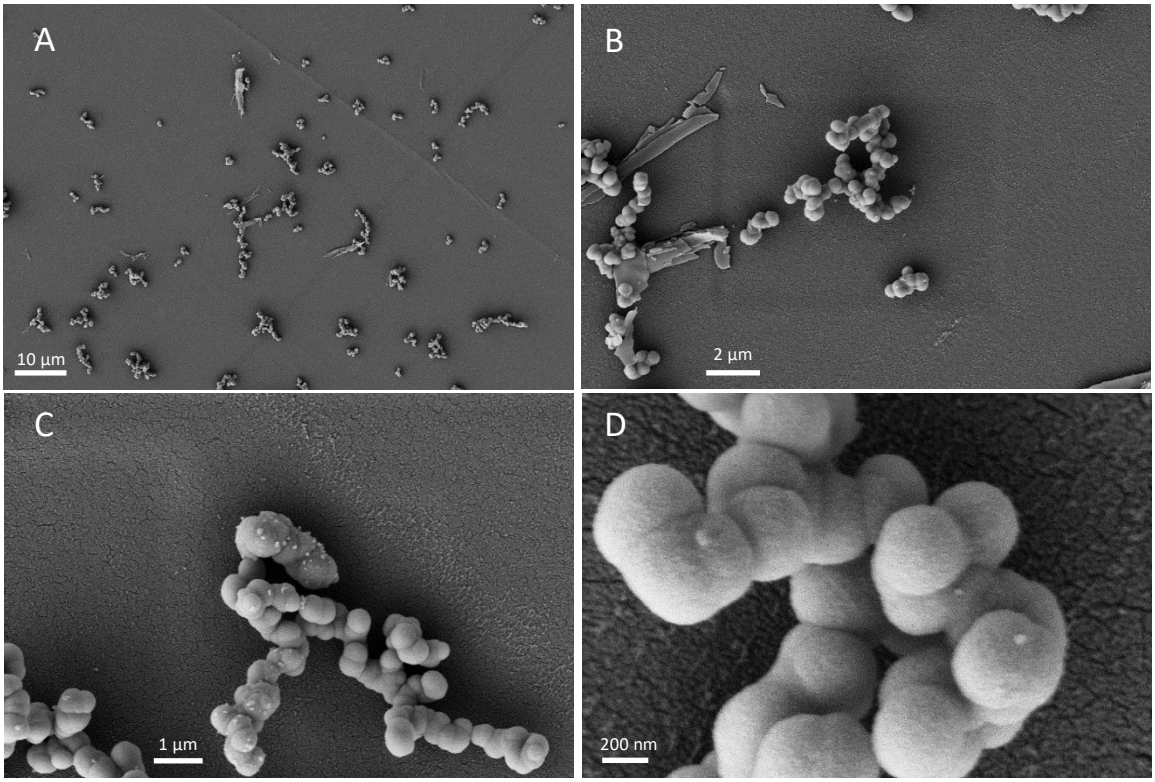

Figure 15: SEM images of particles obtained after silica precipitation according to section 2.9 with peptide 1.

Figure 15 shows the particles obtained during silica precipitation with peptide 1 in different scales. As can be seen from the images A and B, the majority of the particles show a spherical morphology. Most of the particles have a diameter of 300-400 nm. By increasing the scale (images C and D), it is noticeable that the majority of spherical particles have a relatively smooth surface. However, single particle surfaces with small irregularities can also be recognized (image C and D).

3.1.1.2 Results of the synthesis, purification and silica precipitation of peptide 2

The yield of peptide 2 with the sequence *rrill-DDap*-RRIL* after RP-HPLC purification was 7.9 mg (61 % of the theoretical yield of 12.9 mg for 0.01 mmol synthesis scale).

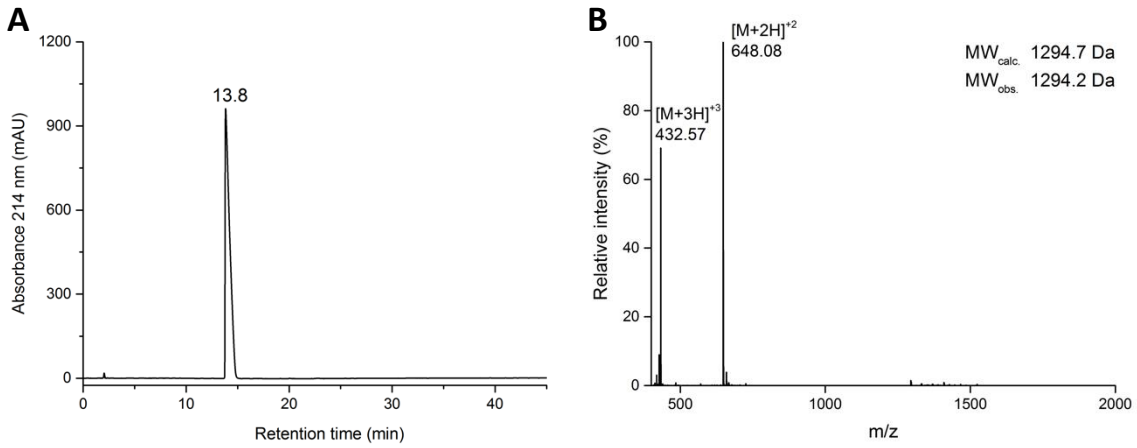

Figure 16: A: HPLC chromatogram of purified peptide 2. B: Mass spectrum obtained from a direct injection of purified peptide 2 on a Thermo Fisher HPLC-MS system.

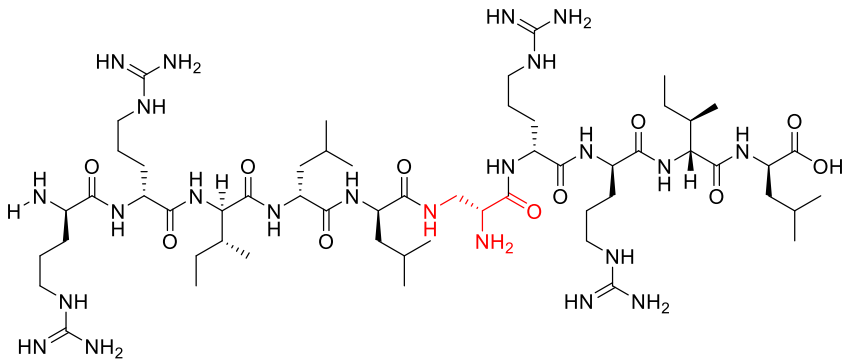

Figure 17: Structure of peptide 2 with D-Dap as central residue.

The HPLC chromatogram of purified peptide 2 is presented in Figure 16A and demonstrates the elution of the peptide after 13.8 min. The corresponding mass spectrum in figure 16B shows a charge pattern corresponding to an observed mass of 1294.2 Da, which is in good agreement with the expected mass of 1294.7.3 Da. Since neither the HPLC chromatogram nor the mass spectra show significant additional peaks, it can be concluded that peptide 2 purification was successful.

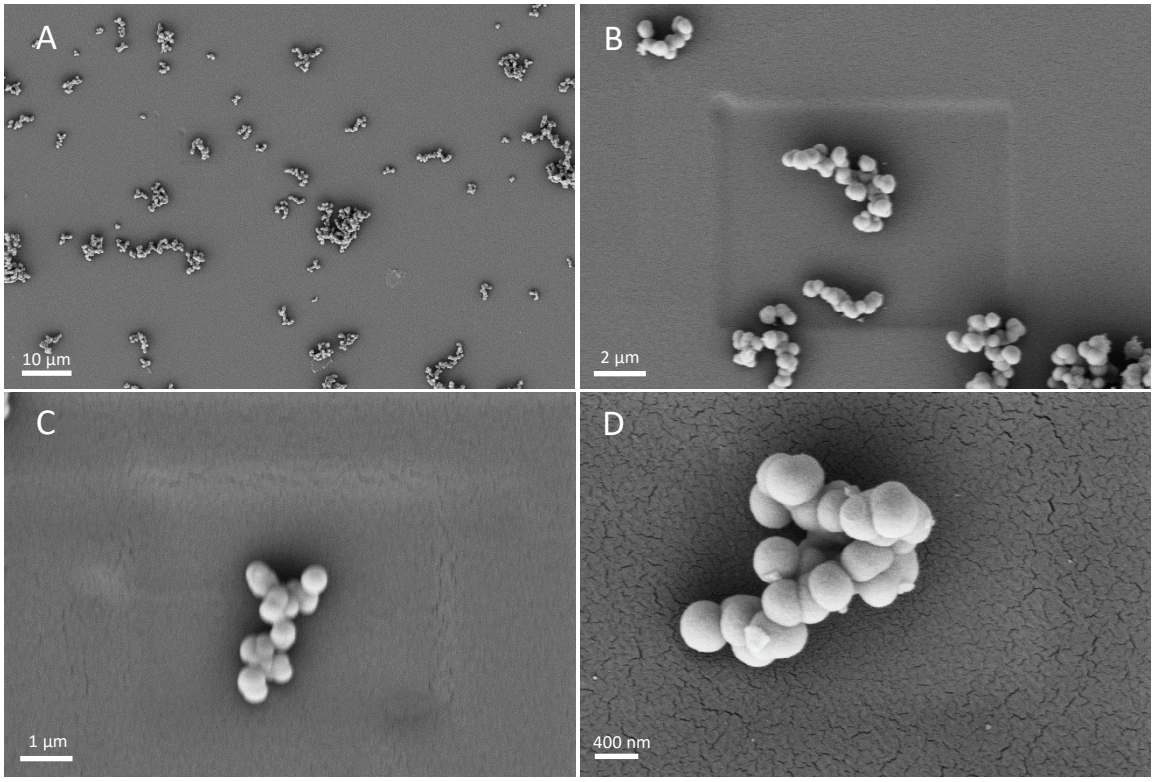

Figure 18: SEM images of particles obtained after silica precipitation according to section 2.9 with peptide 2.

Figure 18 depicts the SEM images of the silica particles resulting from silica precipitation with peptide 2, as described in section 2.9. The images A and B clearly indicate that the majority of the particles have a spherical morphology. In addition, the images C and D show that the particles have a consistently smooth surface with a diameter of about 300-400 nm.

3.1.1.3 Results of the synthesis, purification and silica precipitation of peptide 3

The yield of peptide 3 with the sequence *RRILL-LDap*-rril* after RP-HPLC purification was 9.0 mg (70 % of the theoretical yield of 12.9 mg for 0.01 mmol synthesis scale).

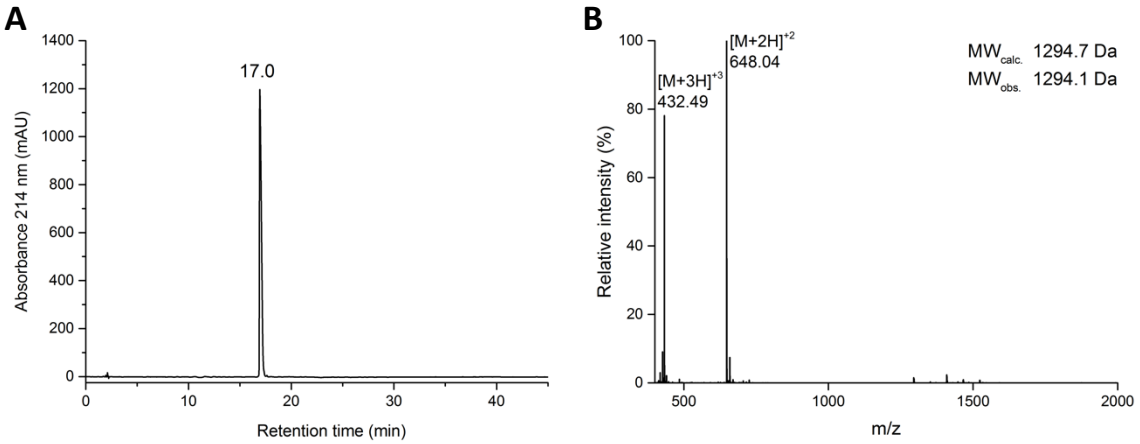

Figure 19: A: HPLC chromatogram of purified peptide 3. B: Mass spectrum obtained from a direct injection of purified peptide 3 on a Thermo Fisher HPLC-MS system.

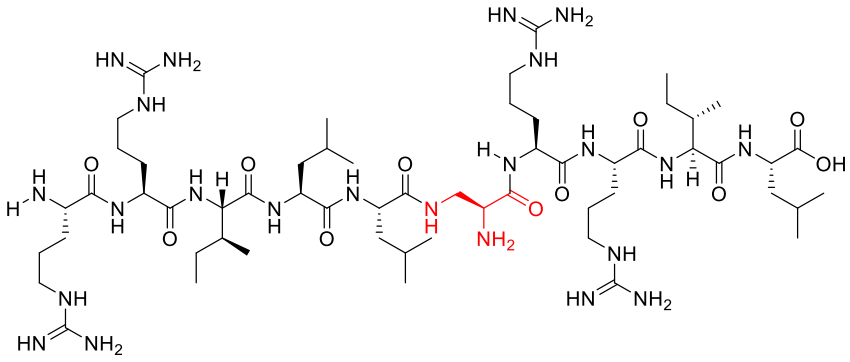

Figure 20: Structure of peptide 3 with L-Dap as central residue.

The HPLC chromatogram (A) and the corresponding mass spectrum (B) in Figure 19 show that peptide 3 could be isolated pure. The charge patterns also exhibit an observed mass of 1294.1 Da, which agrees well with the calculated mass of the peptide of 1294.7 Da.

However, the retention time of peptide 3 (17.0 min, Figure 19A) does not correspond to that of peptide 2 (13.8 min, Figure 16), which would not have been expected due to the fact that the two molecules are a pair of enantiomers. Therefore, a co-injection of peptides 2 and 3 on an analytical HPLC column (see

section 2.8) was initiated and resulted in both compounds eluting as one peak. The previously observed differences in retention time were probably due to an accidental change in HPLC conditions.

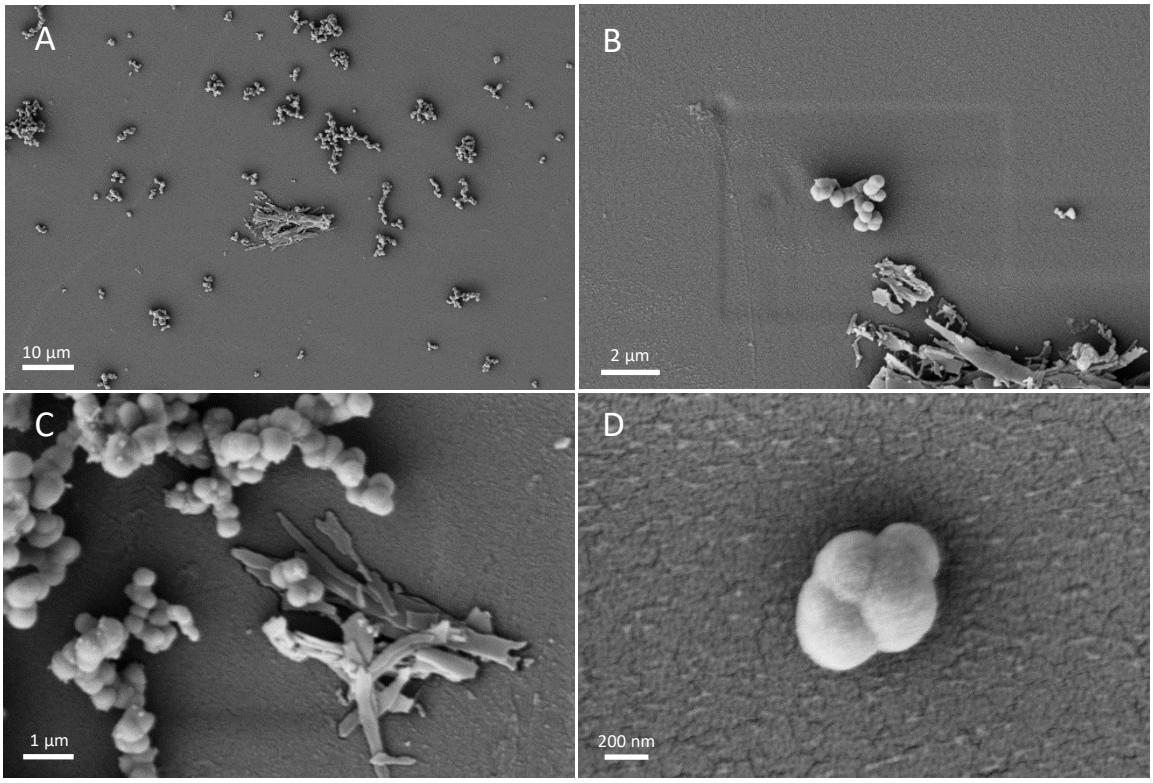

Figure 21: SEM images of particles obtained after silica precipitation according to section 2.9 with peptide 3.

Figure 21 shows the SEM images of the particles formed by silica precipitation with peptide 3. Although the majority of the particles have a spherical morphology (see Image A), some sheet structures can be identified. Nevertheless, most of the particles are spherical and have a smooth surface, as shown in Figure D, even though some rough surfaces are visible (Figure C). Similar to the silica particles from section 3.1.1.1 and 3.1.1.2, the spherical particles have a diameter of 300-400 nm.

3.1.1.4 Results of the synthesis, purification and silica precipitation of peptide 4

The yield of peptide 4 with the sequence *RRILL-DDap*-rril* after RP-HPLC purification was 10.5 mg (81 % of the theoretical yield of 12.9 mg for 0.01 mmol synthesis scale).

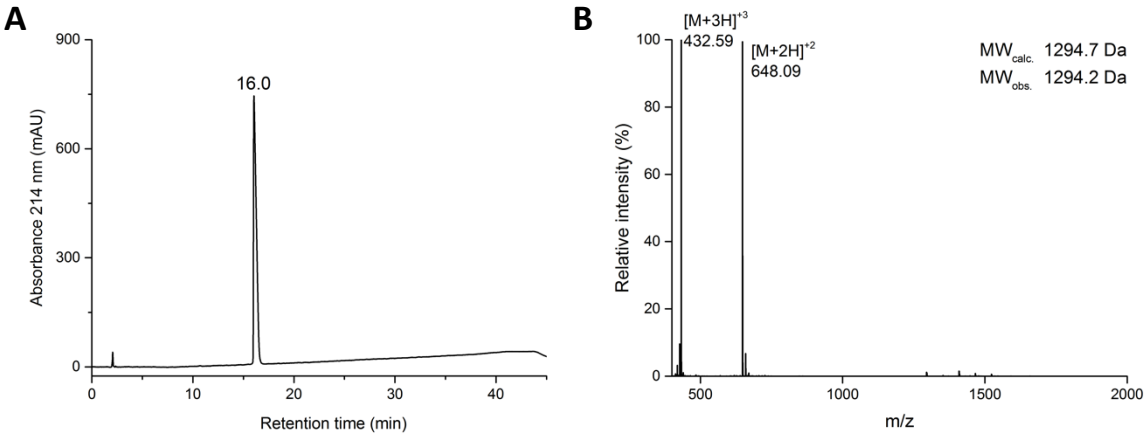

Figure 22: A: HPLC chromatogram of purified peptide 4. B: Mass spectrum obtained after direct injection of purified peptide 4 on a Thermo Fisher HPLC-MS system.

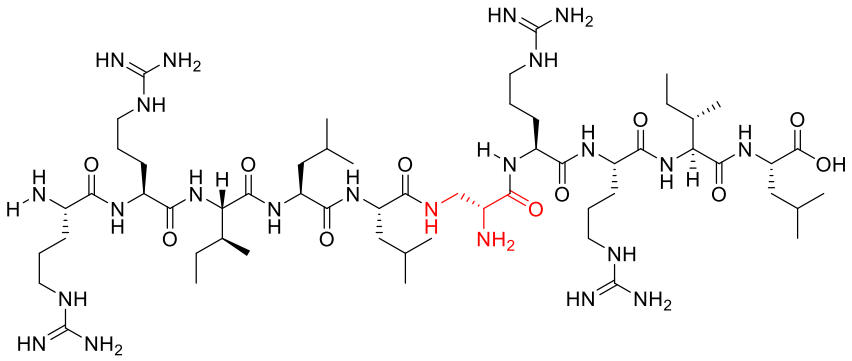

Figure 23: Structure of peptide 3 with D-Dap as central residue.

As can be seen from the chromatogram in Figure 22A, no impurities could be detected and peptide 4 could therefore be purified well. The corresponding mass spectrum (Figure 7B) shows an observed mass of 1294.2 Da, which matches the calculated mass of peptide 4 of 1294.7 Da quite well.

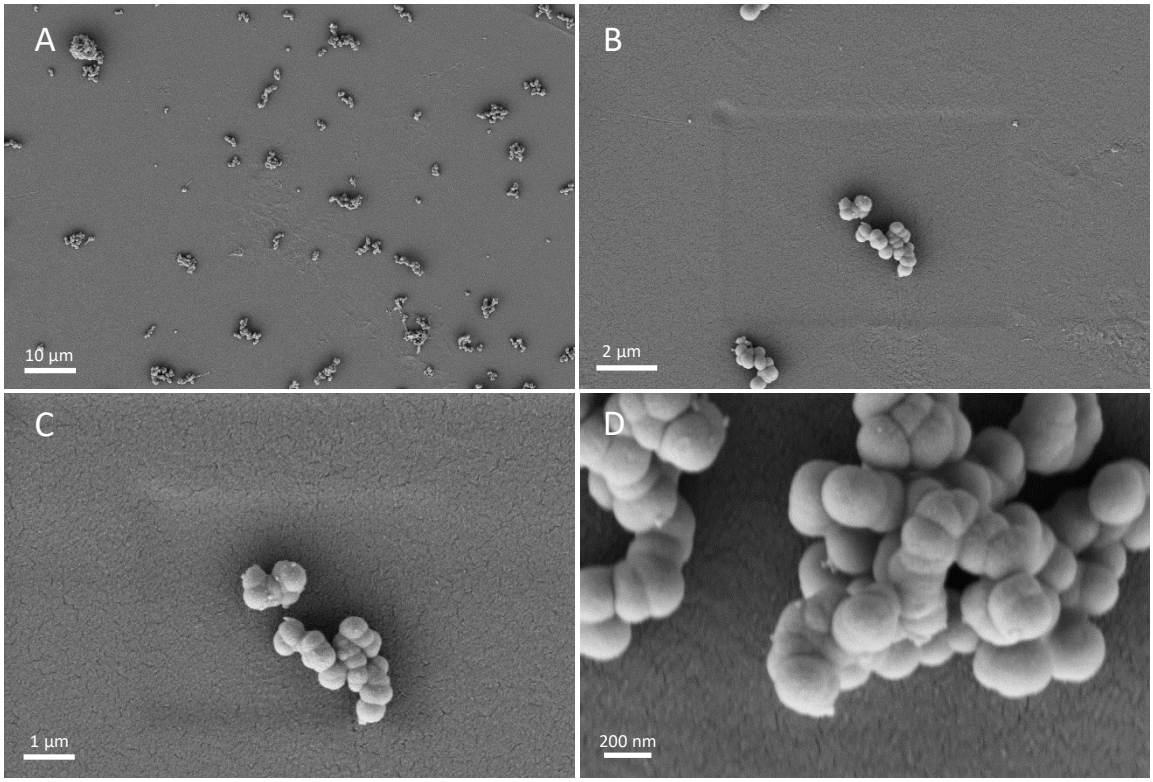

Figure 24: SEM images of particles obtained after silica precipitation according to section 2.9 with peptide 4.

The SEM images of the particles obtained through silica precipitation with peptide 4 are shown in different scales in Figure 24. It is apparent that the vast majority of the particles has a spherical structure. In addition, the particles have a consistently smooth surface with only a few rough exceptions, as can be seen in Figures C and D. The diameter of 200-300 nm of the particles resulting from peptide 4 seems to be slightly smaller compared to the particles resulting from peptides 1-3.

3.1.1.5 Results of the synthesis, purification and silica precipitation of peptide 5

The yield of peptide 5 with the sequence *rrill-ßAla-RRIL* after RP-HPLC purification was 3.8 mg (30 % of the theoretical yield of 12.8 mg for 0.01 mmol synthesis scale).

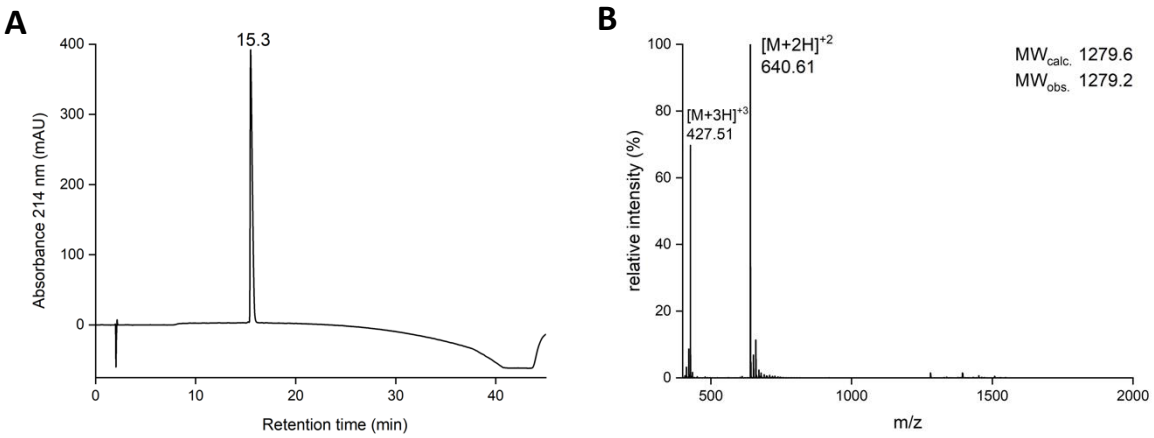

Figure 25: A: HPLC chromatogram of purified peptide 5. B: Mass spectrum obtained from direct injection of purified peptide 5 on a Thermo Fisher HPLC-MS system.

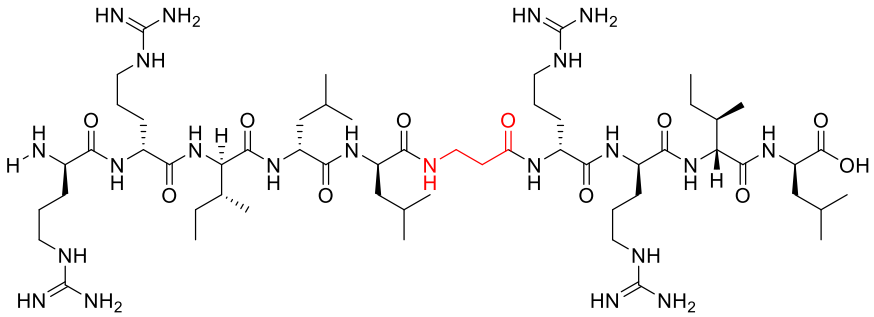

Figure 26: Structure of peptide 5 with β-Alanine as a central residue.

Figure 25A depicts the chromatogram (214 nm absorbance wavelength) from the RP-HPLC analysis of purified peptide 5 (structure shown in Figure 26) and the corresponding mass spectrum is visualized in Figure 25B, which shows peaks corresponding to an observed mass of 1279.2 Da. This is in good agreement with the expected mass of 1279.6 Da. The data shown indicate that the synthesis and purification of peptide 5 were successful.

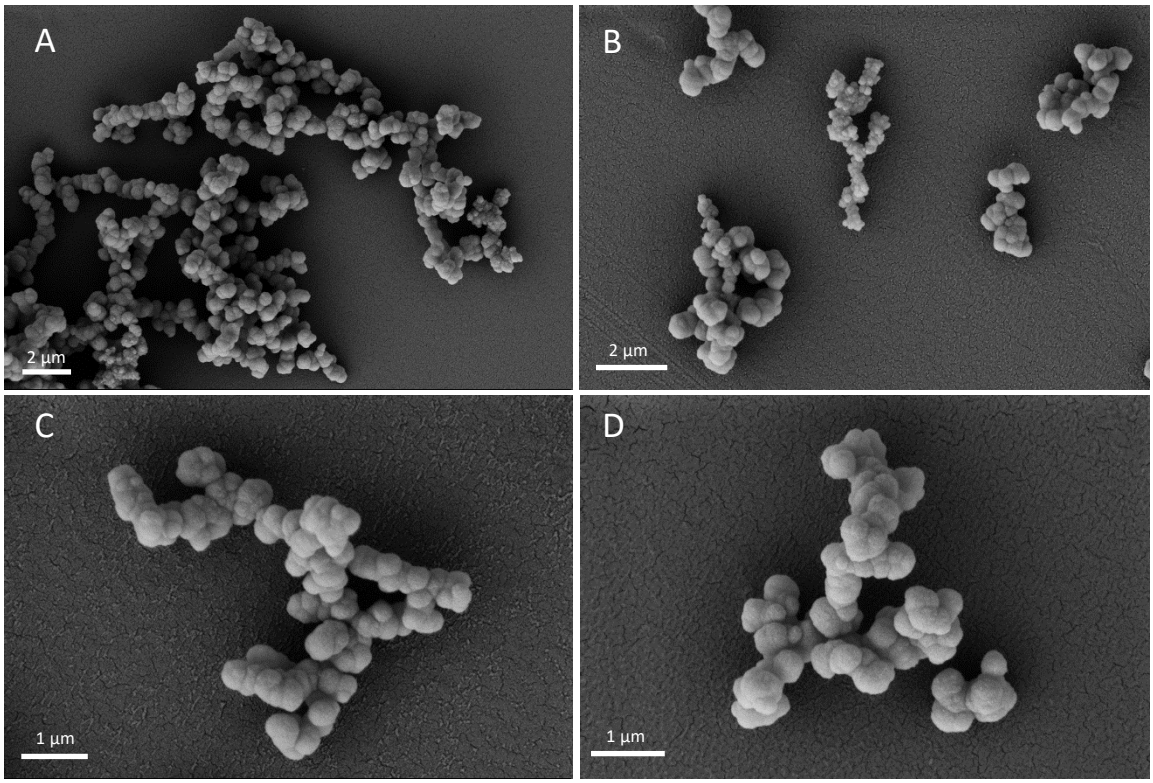

Figure 27: SEM images of particles obtained after silica precipitation according to section 2.9 with peptide 5.

Figure 27 clearly shows that the silica particles obtained after silica precipitation with peptide 5 have a predominantly spherical morphology with a smooth surface. However, there is a partially large variation in particle size and surface composition. This is most obvious in Image B, where relatively small silica structures are attached to larger spherical particles. The diameter varies in a range of 200-500 nm, which is clearly different from peptide 1-4.

3.1.1.6 Results of the synthesis, purification and silica precipitation of peptide 6

The yield of peptide 6 with the sequence *RRILL-ϐAla-rril* after RP-HPLC purification was 4.9 mg (38 % of the theoretical yield of 12.8 mg for 0.01 mmol synthesis scale).

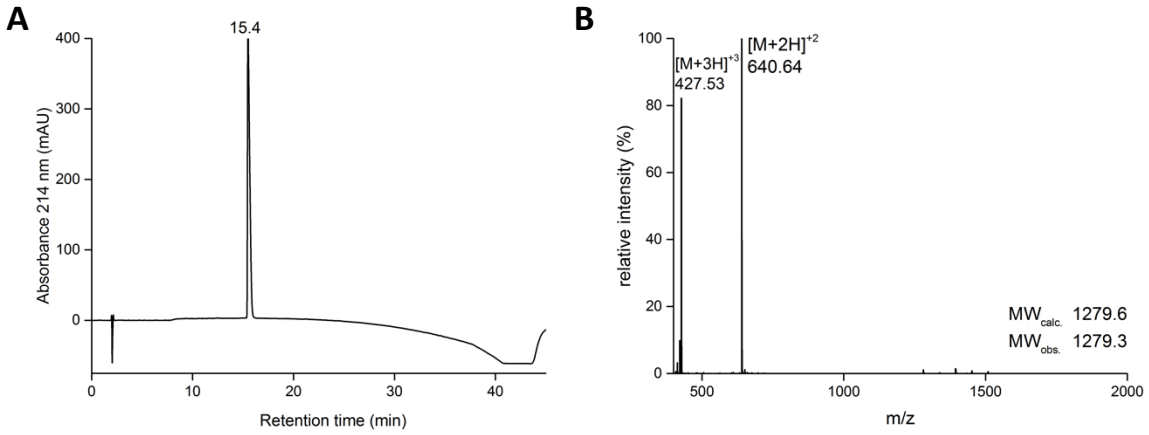

Figure 28: A: HPLC chromatogram of purified peptide 6. B: Mass spectrum obtained from a direct injection of purified peptide 6 on a Thermo Fisher HPLC-MS system.

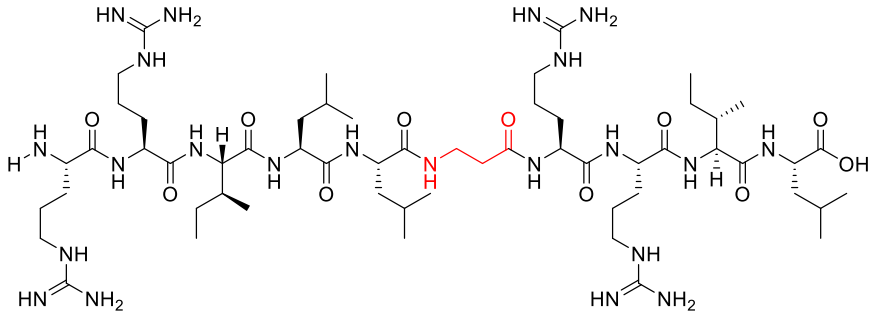

Figure 29: Structure of peptide 6 with β-Alanine as a central residue.

The HPLC chromatogram of purified peptide 6 (shown in Figure 28 A) exhibits an elution peak of the peptide after 13.8 minutes. The corresponding mass spectrum in figure 28 B shows a charge pattern corresponding to an observed mass of 1279.3 Da, which is in good agreement with the expected mass of 1279.6 Da. Since neither the HPLC chromatogram nor the mass spectra show significant additional peaks, it can be concluded that the purification of peptide 6 was successful.

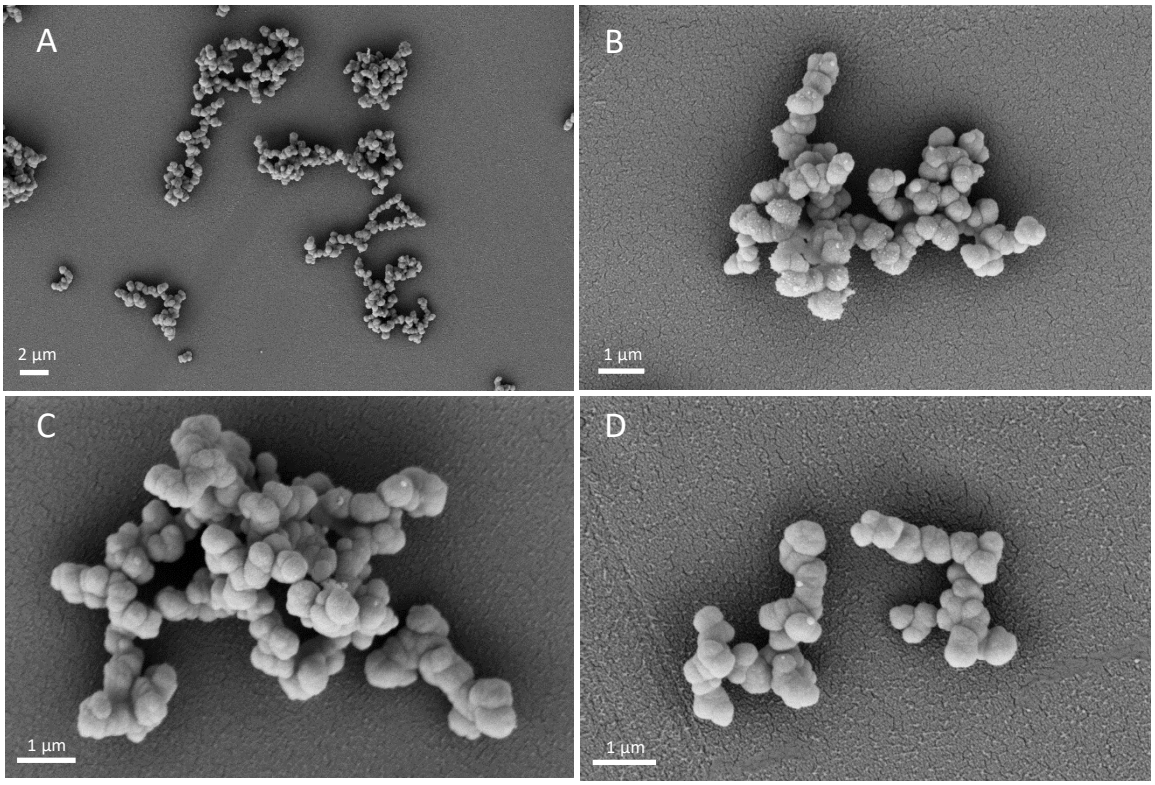

Figure 30: SEM images of particles obtained after silica precipitation according to section 2.9 with peptide 6.

Figure 30 illustrates SEM images of the nanoparticles resulting from silica precipitation with peptide 6. Similar to section 3.1.1.5 (peptide 5), the silica particles show a spherical morphology with a predominantly smooth surface. However, there are a few rough structures on the surfaces of some particles, as can be seen in images B and D. The diameter of the particles is in a similar range to that of the particles obtained with peptide 5 (200-500 nm).

3.1.1.7 Results of the synthesis, purification and silica precipitation of peptide 7

The yield of peptide 7 with the sequence *rrill-LOrn*-RRIL* after RP-HPLC purification was 10.9 mg (83 % of the theoretical yield of 13.2 mg for 0.01 mmol synthesis scale).

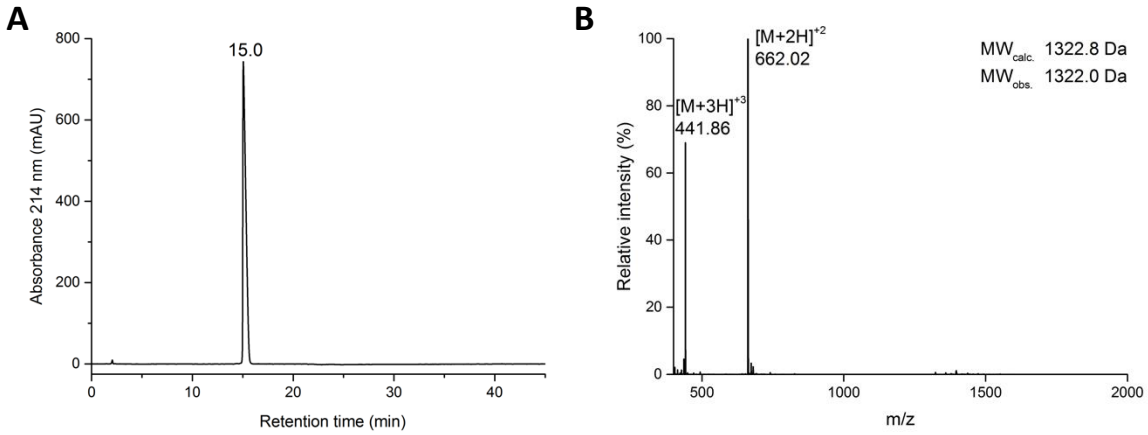

Figure 31: A: HPLC chromatogram of purified peptide 7. B: Mass spectrum obtained after direct injection of purified peptide 7 on a Thermo Fisher HPLC-MS system.

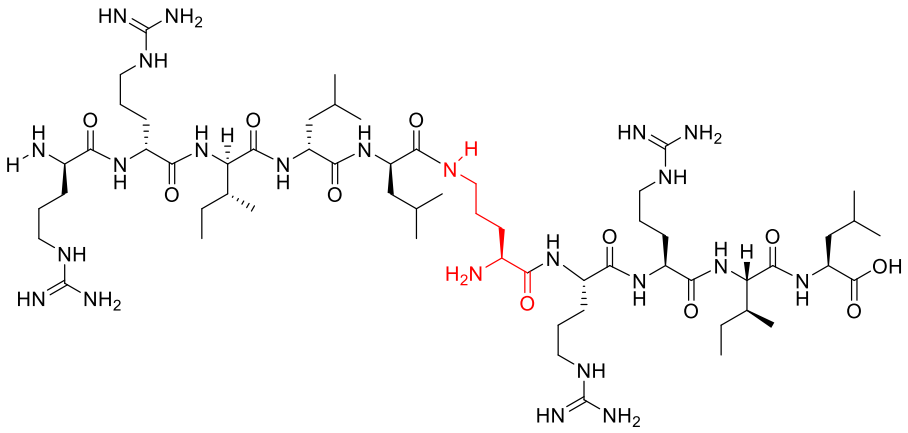

Figure 32: Structure of peptide 7 with L-Ornithine as a central residue.

The chromatogram in Figure 31 A shows a single peak after 15 min at a wavelength of 214 nm without any additional peaks. In addition, the observed and calculated masses of the mass spectra in Figure 31 B are almost identical as a result of direct injection. From these two facts it can be concluded that the synthesis and purification of peptide 7 was successful.

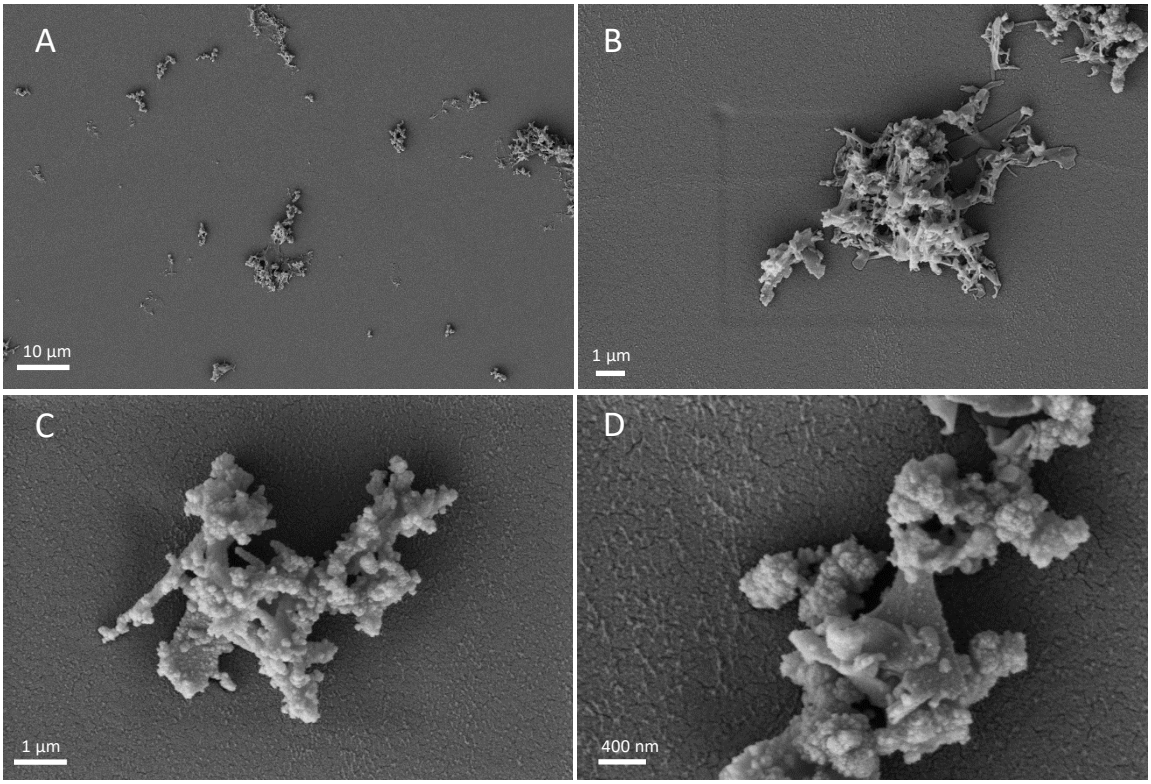

Figure 33: SEM images of particles obtained after silica precipitation according to section 2.9 with peptide 7.

Figure 33 shows SEM microscopy images of silica particles derived from peptide 7. In contrast to the particles from section 3.1.1, no uniform morphology can be identified in the present case. Instead, morphologies with a partial sheet character (B and D) or reminiscent of rods (C) can be identified. Also the surfaces of the particles are inconsistent, from smooth spots to rough surfaces. The diameter of the particles cannot be determined due to the non-uniformity of the structures. It seems that the two additional methyl groups of L-ornithine (peptide 7) compared to L-Dap (peptide 1) result in a different self-assembly mechanism and thus in a different function as a template for silica precipitation.

Another difference compared to peptides 1-6 was observed during incubation with phosphate buffer in preparation for silica precipitation, as a visible precipitate formed after a few minutes of incubation time. This peptide precipitate was investigated via SEM-microscopy (see section 2.10.1) in order to depict possible similarities with the morphology of the particles in Figure 33.

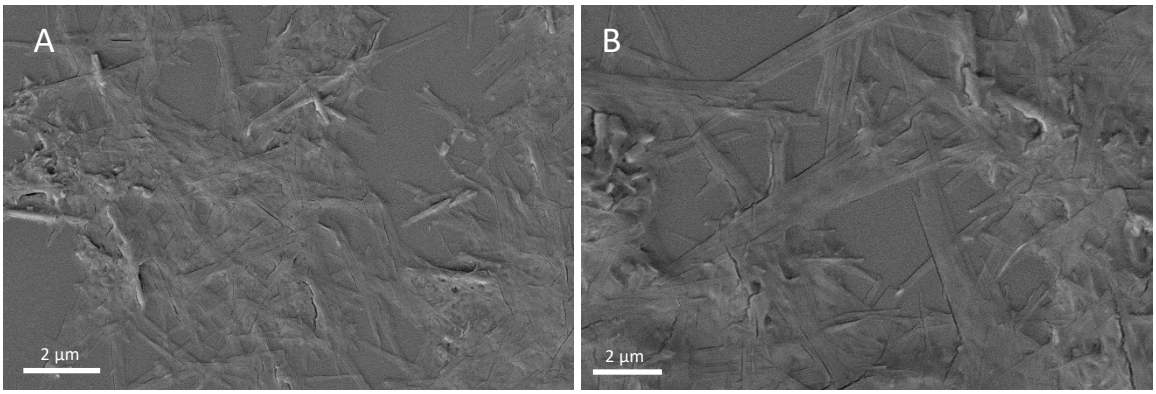

Figure 34: SEM images of peptide 7 precipitate obtained during incubation with phosphate buffer according to the protocol in section 2.9.

Figure 34 shows sheet and rod like peptide structures and occasionally larger amorphous structures. It appears that these structures serve as a template for the precipitation of some silica particles. However, considerable differences in morphology can also be observed. Despite the fact that the majority of the peptides in figure 34 show similar board-shaped structures, the particles in figure 33 are significantly more heterogeneous.

3.1.1.8 Results of the synthesis, purification and silica precipitation of peptide 8

The yield of peptide 8 with the sequence *rrill-DOrn*-RRIL* after RP-HPLC purification was 8.4 mg (64 % of the theoretical yield of 13.2 mg for 0.01 mmol synthesis scale).

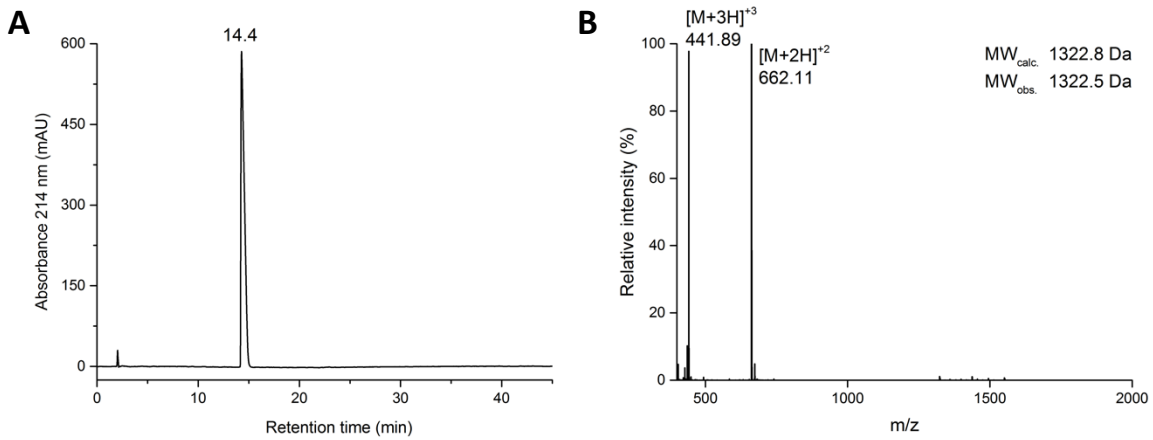

Figure 35: A: HPLC chromatogram of purified peptide 8. B: Mass spectrum obtained from direct injection of purified peptide 8 on a Thermo Fisher HPLC-MS system.

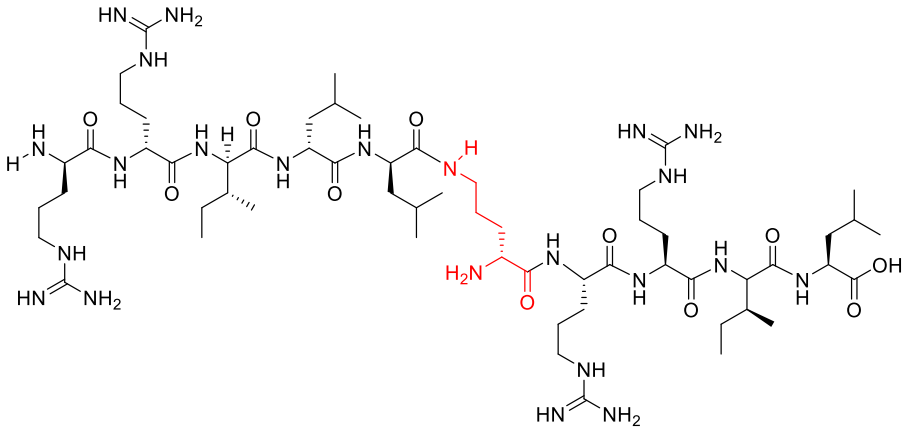

Figure 36: Structure of peptide 8 with D-Ornithine as a central residue.

Figure 35 A shows the chromatogram from the RP-HPLC analysis with a single peak of purified peptide 8 at a wavelength of 214 nm and the mass spectrum is presented in Figure 35 B, which shows peaks corresponding to an observed mass of 1322.5 Da. This is in good agreement with the expected mass of 1322.8, indicating that peptide 8 could be purified quite well.

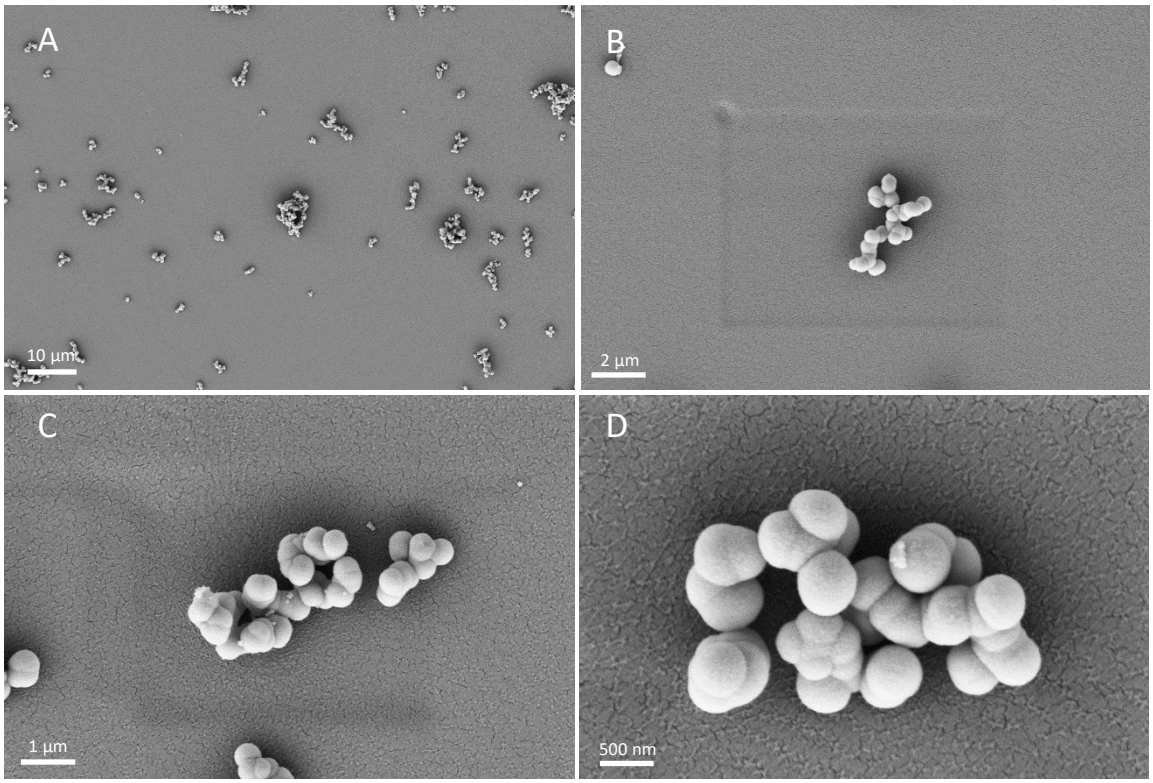

Figure 37: SEM images of particles obtained after silica precipitation according to section 2.9 with peptide 8.

Unlike peptide 7, the silica particles derived from peptide 8 show a uniform spherical morphology, as shown in Figure 37. In addition, no precipitate formed during incubation in phosphate buffer (see section 2.9), which is in contrast to peptide 7. The particles obtained from silica precipitation process peptide 8 (images B-D) have a smooth surface and a diameter in the range of 300-500 nm. It should be noted that the differences to peptide 7 derived silica particles are caused solely by the stereochemical configuration of the central residue ornithine (see structure in Figure 36).

3.1.1.9 Results of the synthesis, purification and silica precipitation of peptide 9

The yield of peptide 9 with the sequence *RRILL-LOrn*-rril* after RP-HPLC purification was 8.9 mg (67 % of the theoretical yield of 13.2 mg for 0.01 mmol synthesis scale).

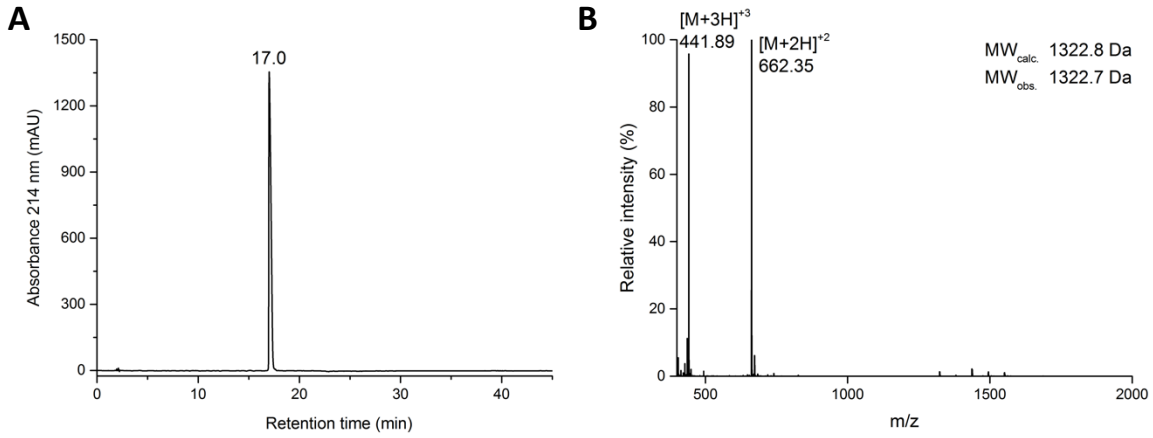

Figure 38: A: HPLC chromatogram of purified peptide 9. B: Mass spectrum obtained from direct injection of purified peptide 9 on a Thermo Fisher HPLC-MS system.

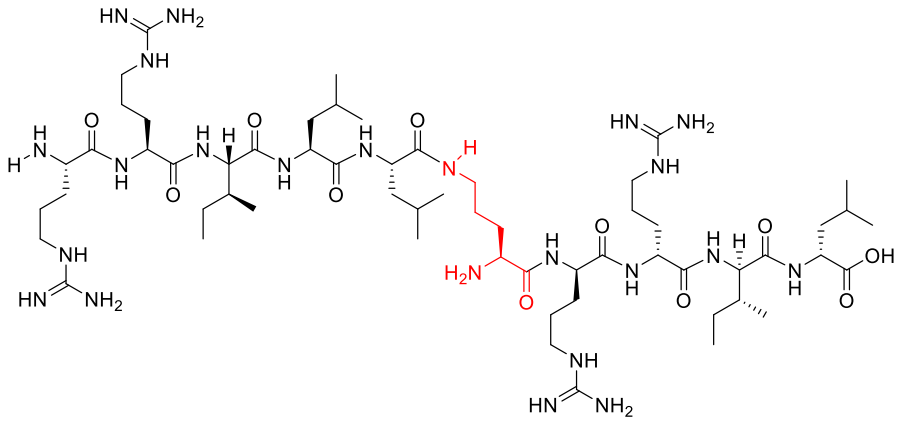

Figure 39: Structure of peptide 9 with L-Ornithine as a central residue.

Figure 38A shows the chromatogram of the final analysis after purification of peptide 9 at a wavelength of 214 nm. As expected, a single peak can be detected without any additional peaks. However, the elution time of 17 min significantly differs from the enantiomer peptide 8 (14.4 min), which was not expected. Therefore, a co-injection of peptides 8 and 9 on an analytical HPLC column (see section 2.8) was initiated and resulted in both compounds eluting as one peak. The previously observed differences in retention time were probably due to an accidental change in HPLC conditions. The mass spectrum in Figure 38B

shows a charge pattern corresponding to an observed mass of 1322.7 Da, which is in good agreement with the expected mass of 1322.8 Da. From this it can be concluded that the synthesis and purification of peptide 9 (structure shown in Figure 39) were successful.

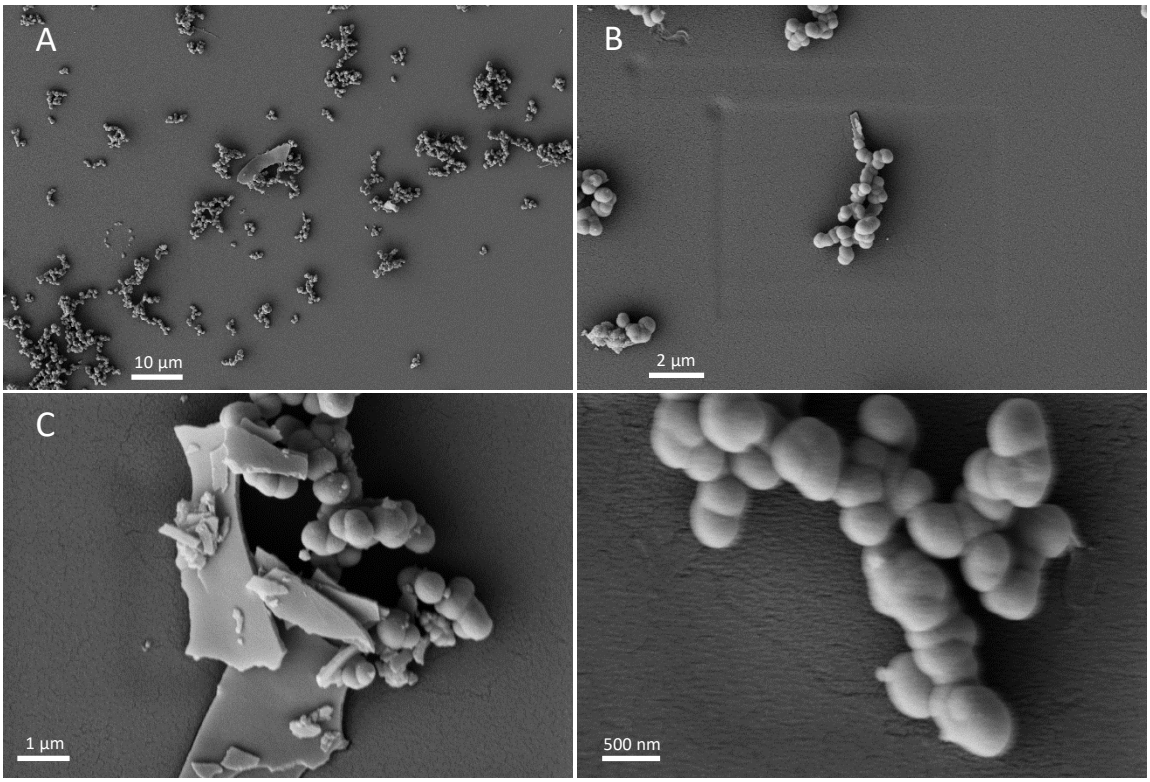

Figure 40: SEM images of particles obtained after silica precipitation according to section 2.9 with peptide 9.

Figure 40 shows SEM images of the silica particles obtained via peptide 9. The particles generally show a spherical morphology with a relatively smooth surface, as expected by the fact that peptide 9 is the stereochemical mirror peptide of peptide 8. However, sheet like structures can be detected in some cases, as can be seen in image A and C. Nevertheless, the vast majority of the particles show a spherical pattern with a diameter in the range of 300-400 nm (images A, B, D).

3.1.1.10 Results of the synthesis, purification and silica precipitation of peptide 10

The yield of peptide 10 with the sequence *RRILL-DOrn*-rril* after RP-HPLC purification was 10.1 mg (77 % of the theoretical yield of 13.2 mg for 0.01 mmol synthesis scale).

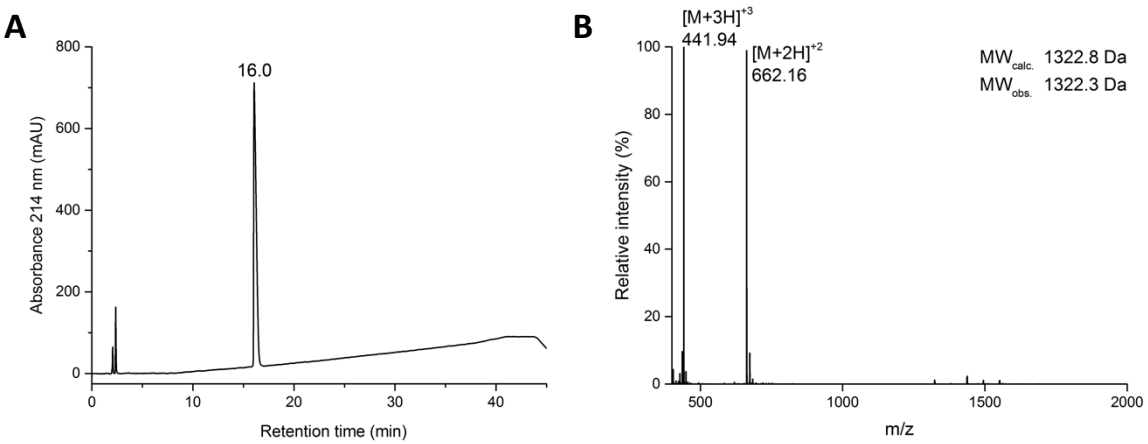

Figure 41: A: HPLC chromatogram of purified peptide 10. B: Mass spectrum obtained after direct injection of purified peptide 10 on a Thermo Fisher HPLC-MS system.

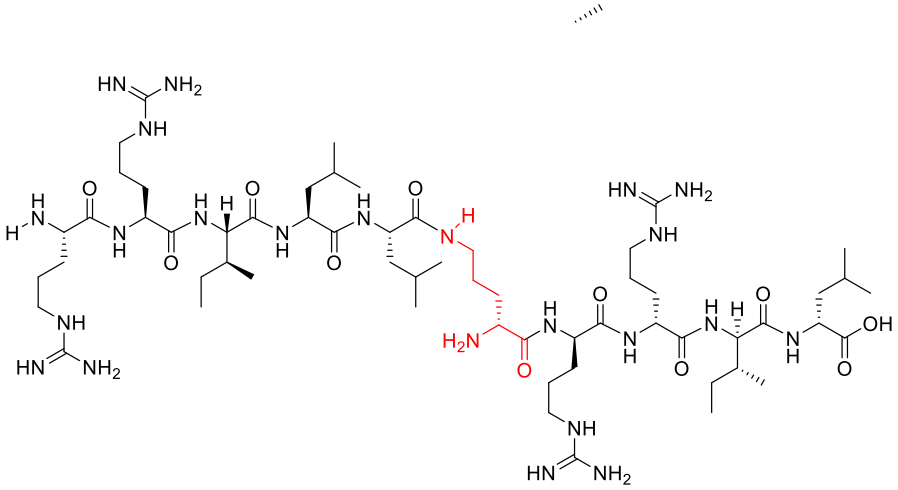

Figure 42: Structure of peptide 10 with D-Ornithine as a central residue.

The chromatogram in Figure 41 A shows a single peak indicating that the purification was successful. The corresponding mass spectrum in Figure 41 B confirms this assumption, since there are no peaks other than the expected charge patterns for peptide 10. In addition, the observed mass of 1322.3 Da agrees well with the calculated mass of 1322.8 Da.

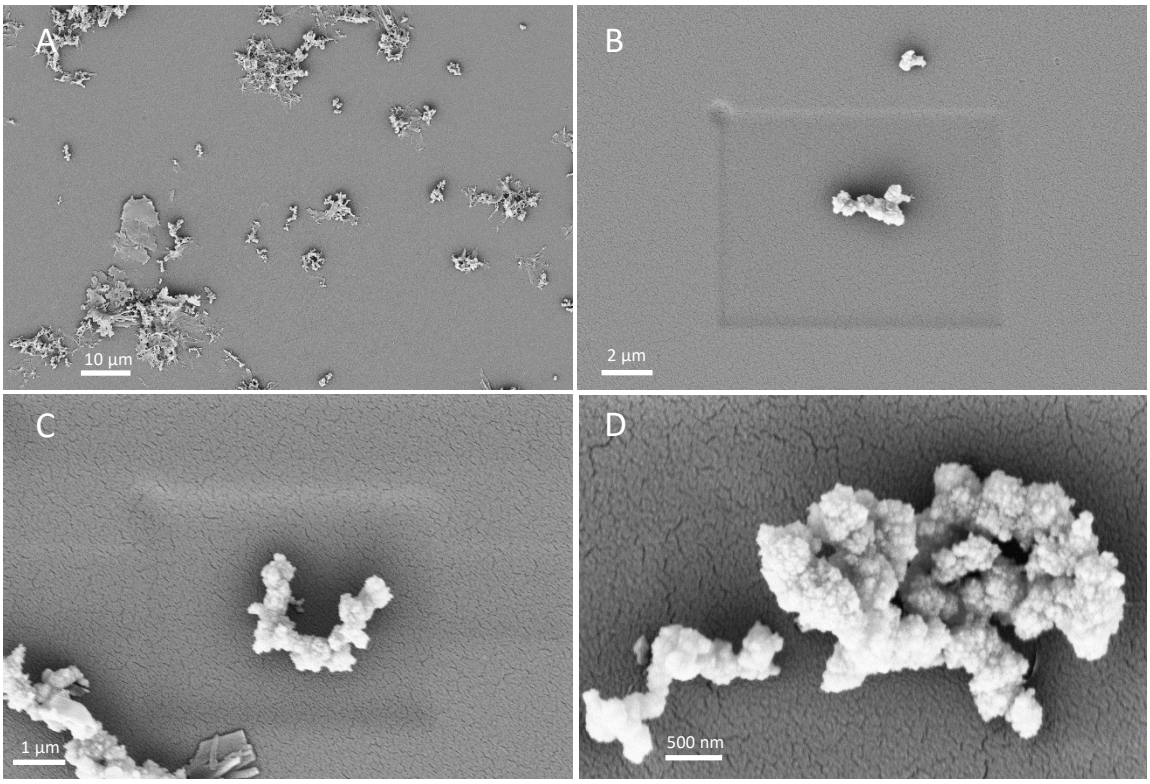

Figure 43: SEM images of particles obtained after silica precipitation according to section 2.9 with peptide 10.

Figure 43 displays the SEM images of the silica particles obtained from peptide 10. The images show that particles with inconsistent morphology were formed during silica precipitation. Rather, structures reminiscent of sheets, sticks and amorphous spherical structures with a rough surface can be observed. The result was expected due to the fact that peptide 10 is the enantiomer of peptide 7, which similarly produce silica particles with mixed morphology.

In accordance with peptide 7, a visible precipitate formed during incubation in phosphate buffer (see section 2.9). Therefore, the precipitate was investigated via SEM microscopy (see section 2.10.1).

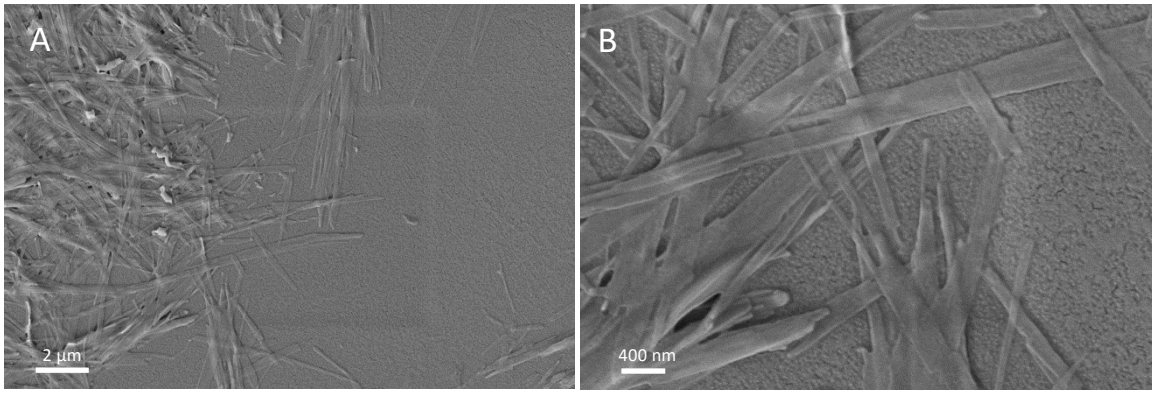

Figure 44: SEM images of peptide 10 precipitate obtained during incubation with phosphate buffer according to section 2.9.

Similar to the precipitation of peptide 7, peptide 10 formed board-shaped and partially heterogeneous amorphous structures. The size of the board-shaped peptide particles extends over several µm in length. Since the morphology and the size of the peptide precipitate in figure 44 differs significantly from that of the silica particles in figure 43, it is hard to imagine that these structures serve as templates for silica precipitation.

3.1.1.11 Results of the synthesis, purification and silica precipitation of peptide 11

The yield of peptide 11 with the sequence rrill-*K*-RRIL* after RP-HPLC purification was 12.2 mg (91 % of the theoretical yield of 13.4 mg for 0.01 mmol synthesis scale).

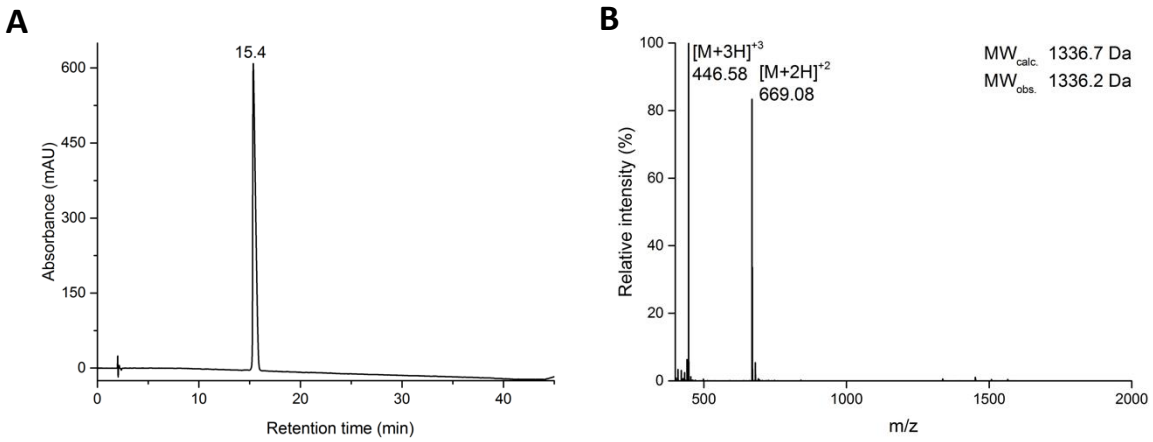

Figure 45: A: HPLC chromatogram of purified peptide 11. B: Mass spectrum obtained from a direct injection of purified peptide 11 on a Thermo Fisher HPLC-MS system.

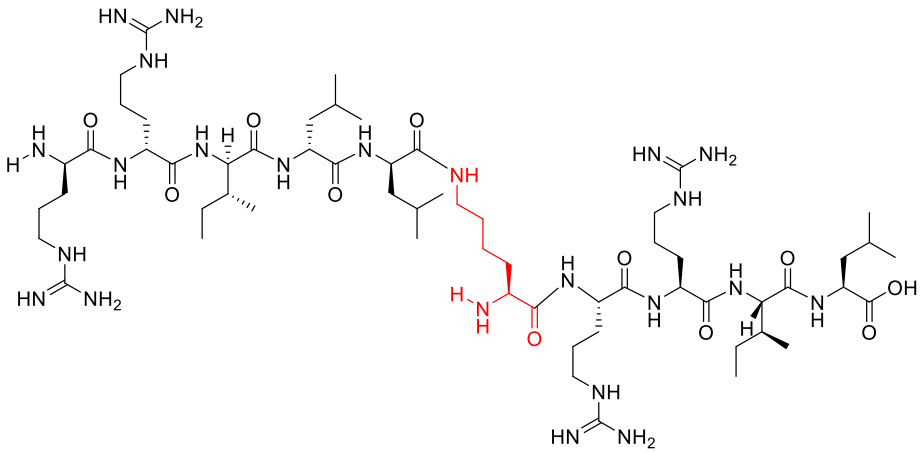

Figure 46: Structure of peptide 11 with L-Lysine as a central residue.

The chromatogram in figure 45A shows a single peak after a retention time of 15.4 min, indicating successful purification of peptide 11. This is confirmed by the mass spectrum in figure 45B, showing a charge pattern corresponding to an observed mass of 1336.2 Da. This is in good agreement with an expected mass of 1336.7 Da. Apart from the characteristic charge peaks of the mass spectrum, no other significant peaks can be detected.

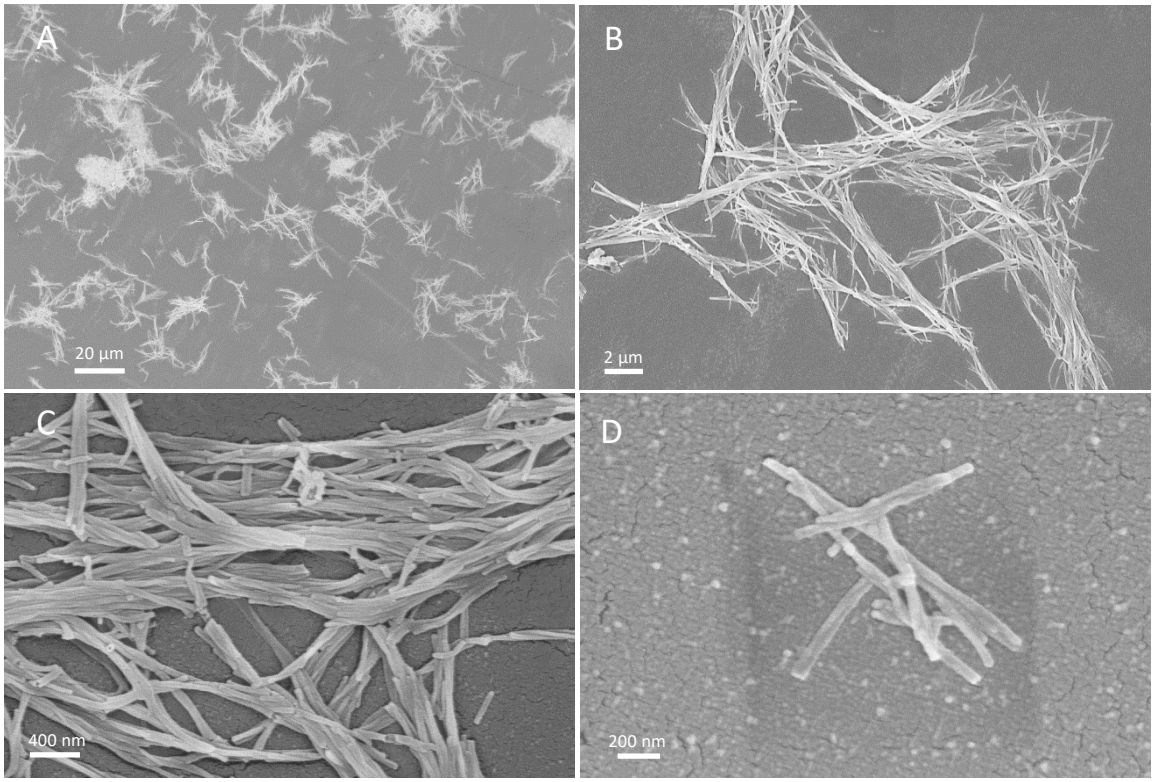

Figure 47: SEM images of particles obtained after silica precipitation according to section 2.9 with peptide 11.

Figure 47 shows the silica particles obtained during silica precipitation with peptide 11 according to section 2.9. As can be seen, the rod like morphology of the particles differs fundamentally from the results of peptides 1-10. This was expected since the same phenomenon has already been described in previous works (see section 1.4).

It should be emphasized that the additional CH_2 group of the lysine residue seems to be the cause of a different silica formation process compared to peptide 7. In addition to a smooth surface, a relatively inhomogeneous distribution of the length of the sticks in the range of 400 nm to several µm can be observed.

Similar to peptide 7 and 10, a visible precipitate formed during incubation in phosphate buffer (see section 2.9). A sample of the precipitate was examined via SEM-microscopy according to section 2.10.1.

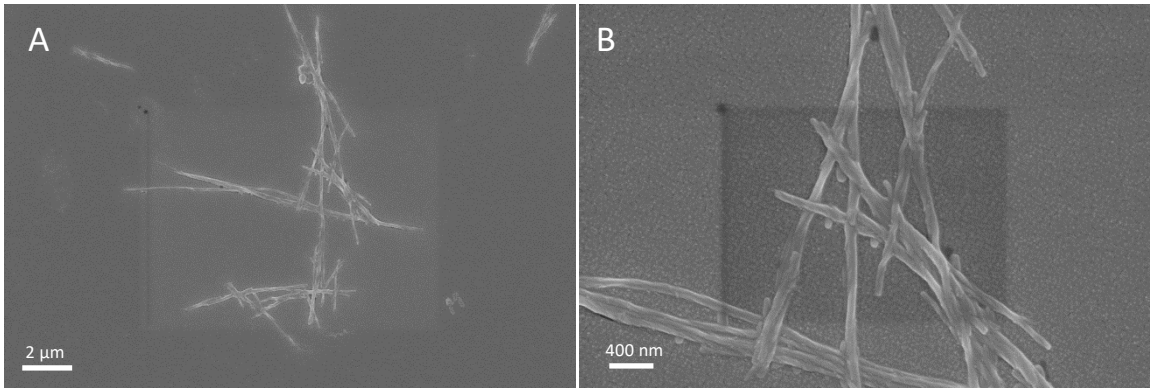

Figure 48: SEM images from the precipitate obtained during phosphate buffer incubation with peptide 11 according to section 2.9.

Figure 48 shows that the rod-like morphology of the assembled peptide 11 precipitate is somewhat similar to the morphology of the silica particles in Figure 47. In addition, it can be seen that the size of the particles is comparable to their silica equivalents in Figure 47. Based on these results, it can be assumed that the peptide precipitate shown in the images A and B of Figure 48 serves as a template for the silicification process.

Based on the fact that a peptide precipitate was formed during incubation in phosphate buffer, the question arises to what extent the morphology of the silica particles would change if the supernatant was separated from the precipitate for silica precipitation. Thus a further silica precipitation was carried out according to the protocol in section 2.9 using the supernatant only.

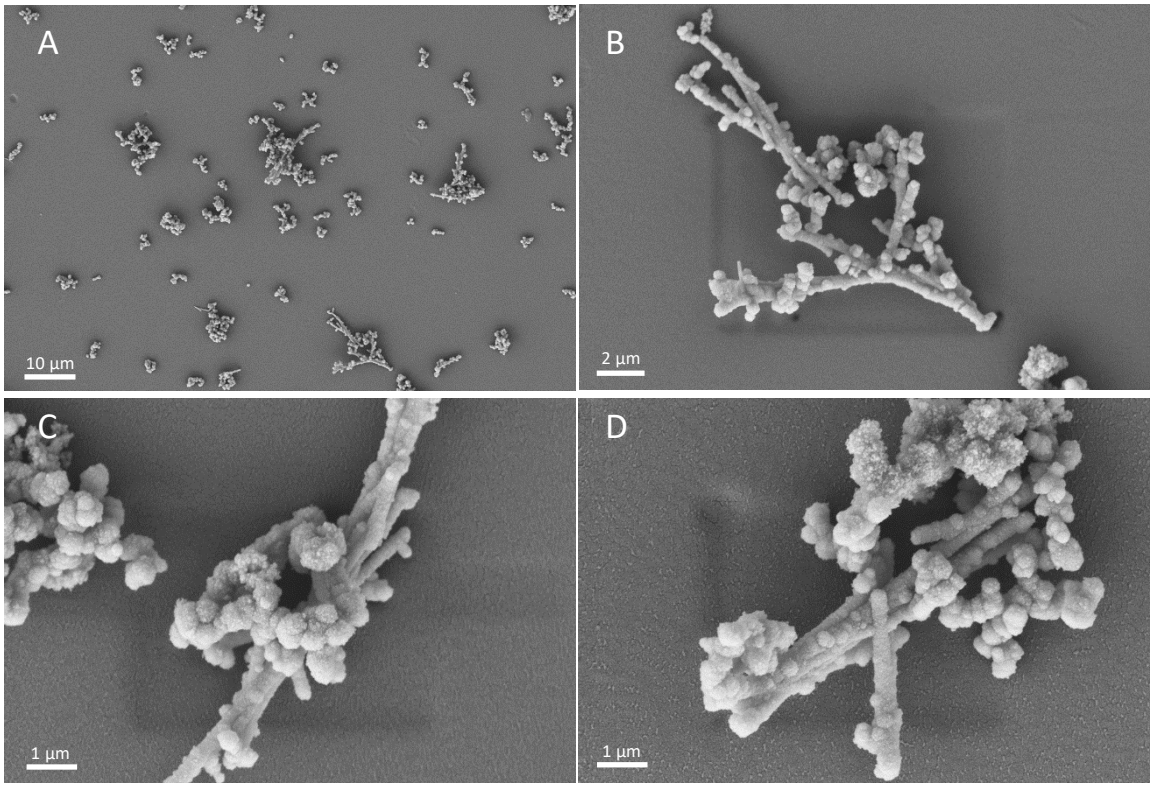

Figure 49: SEM images of the particles obtained using the supernatant after incubation in phosphate buffer for silica precipitation with peptide 11 according to section 2.9.

As can be seen from Figure 49, the morphology of the particles, resulting from the supernatant after incubation in phosphate buffer, differs substantially from that of the silica particles in Figure 47. Although rod like particles can be observed, they show spherical irregularities on their surfaces. In addition, small spherical structures can be identified. It can be concluded that the supernatant of peptide 11 serves as a different type of template for silica precipitation than a suspension consisting of peptide 11 precipitate and supernatant.

3.1.1.12 Results of the synthesis, purification and silica precipitation of peptide 12

The yield of peptide 12 with the sequence *rrill-k*-RRIL* after RP-HPLC purification was 12.3 mg (92 % of the theoretical yield of 13.4 mg for 0.01 mmol synthesis scale).

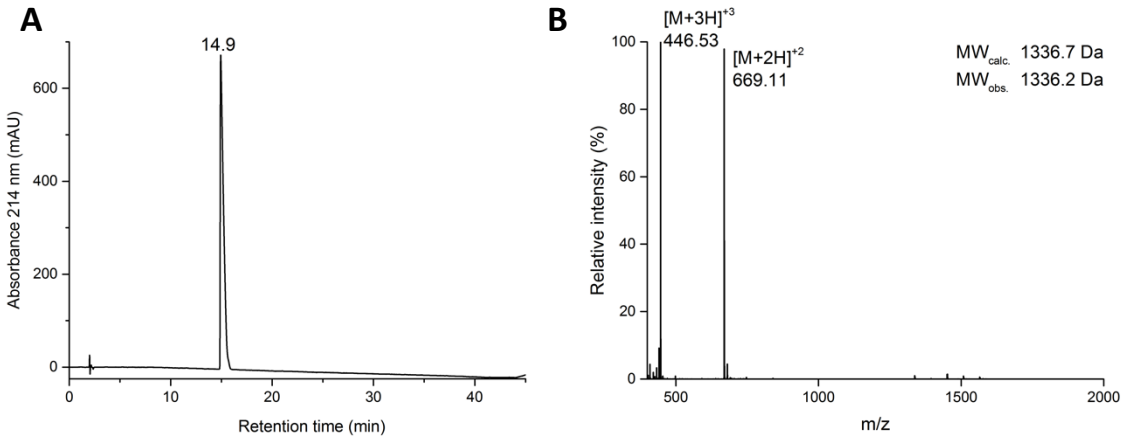

Figure 50: A: HPLC chromatogram of purified peptide 12. B: Mass spectrum obtained from a direct injection of purified peptide 12 on a Thermo Fisher HPLC-MS system.

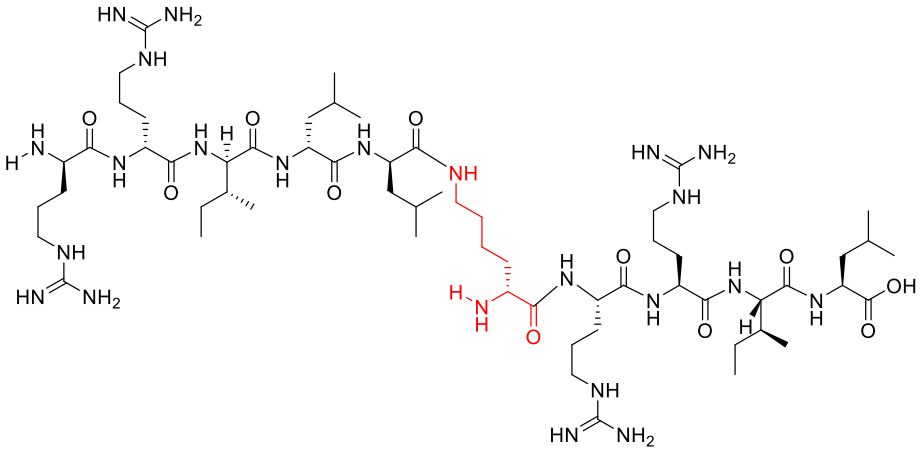

Figure 51: Structure of peptide 12 with D-Lysine as a central residue.

Figure 50 depicts the chromatogram (A) and the mass spectrum (B) of peptide 12 (structure shown in Figure 51) after purification via HPLC. The chromatogram shows a single peak after 14.9 min retention time, indicating that the purification was successful. The mass spectrum in figure 50B depicts a charge pattern corresponding to an observed mass of 1336.2 Da, which is in good agreement with the calculated mass of 1336.7.3 Da.

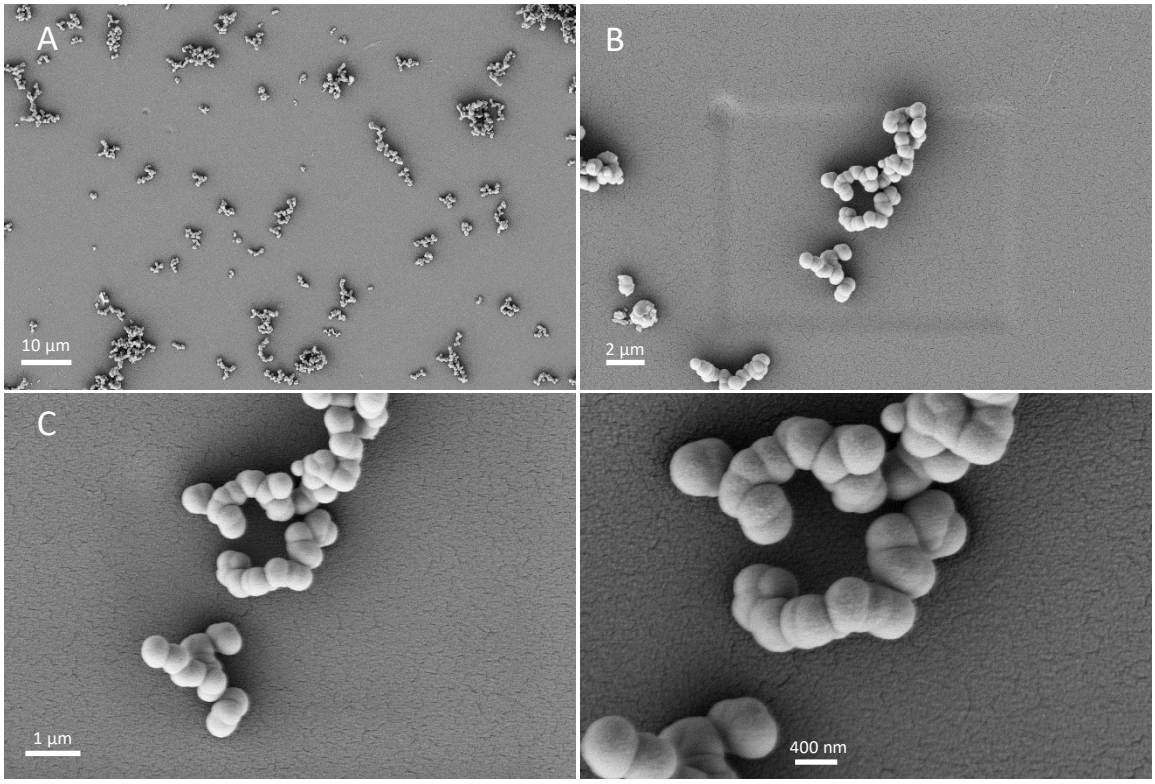

Figure 52: SEM images of particles obtained after silica precipitation according to section 2.9 with peptide 12.

Unlike peptide 11, the SEM images in Figure 52 show a spherical morphology instead of rod like silica particles. The shift in morphology of the particles is caused by the stereochemical modification of the lysine residue (see structure of peptide 12 in Figure 51). In addition to a relatively smooth surface, images C and D in Figure 52 show that the size of the particles is in a range of 300-500 nm, which is similar to the spherical silica particles obtained from previous peptides.

3.1.1.13 Results of the synthesis, purification and silica precipitation of peptide 13

The yield of peptide 13 with the sequence *RRILL-K*-rril* after RP-HPLC purification was 5.2 mg (39 % of the theoretical yield of 13.4 mg for 0.01 mmol synthesis scale).

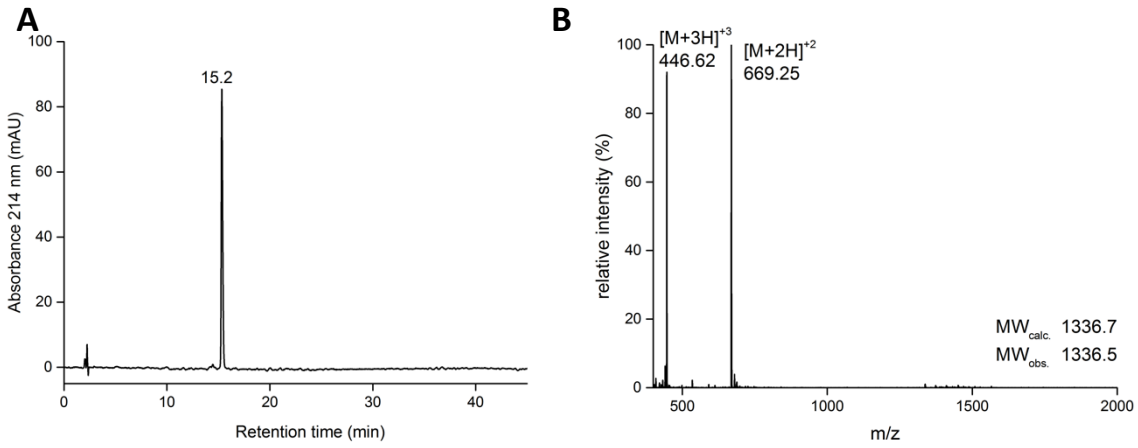

Figure 53: A: HPLC chromatogram of purified peptide 13. B: Mass spectrum obtained from a direct injection of purified peptide 13 on a Thermo Fisher HPLC-MS system.

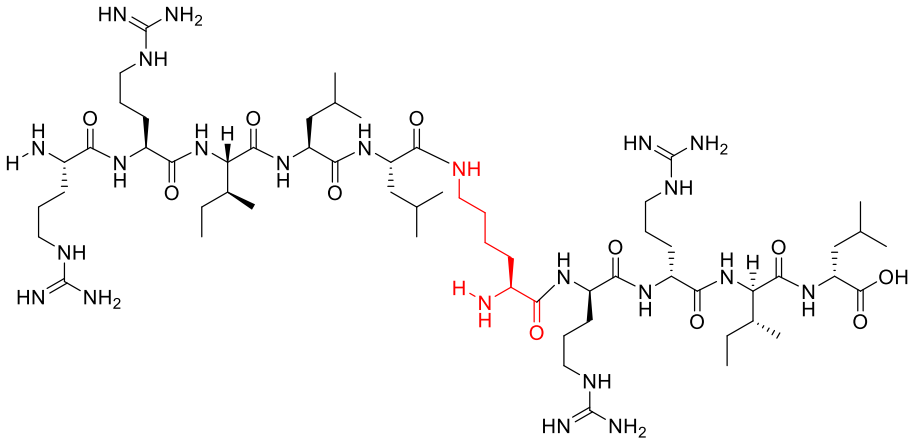

Figure 54: Structure of peptide 13 with L-Lysine as a central residue.

The HPLC chromatogram of purified peptide 13 (shown in Figure 53 A) exhibits the elution of the peptide after 15.2 minutes, comparable to the enantiomer peptide 12 (14.9 minutes). The side peak after 14 minutes can probably be explained by the scaling of the y-axis. The mass spectrum in Figure 53 B shows a charge pattern corresponding to an observed mass of 1336.5 Da, which is in good agreement with the

expected mass of 1336.5 Da. Furthermore, no significant additional peaks can be observed in the mass spectrum. Thus, it can be concluded that the purification of peptide 13 was successful.

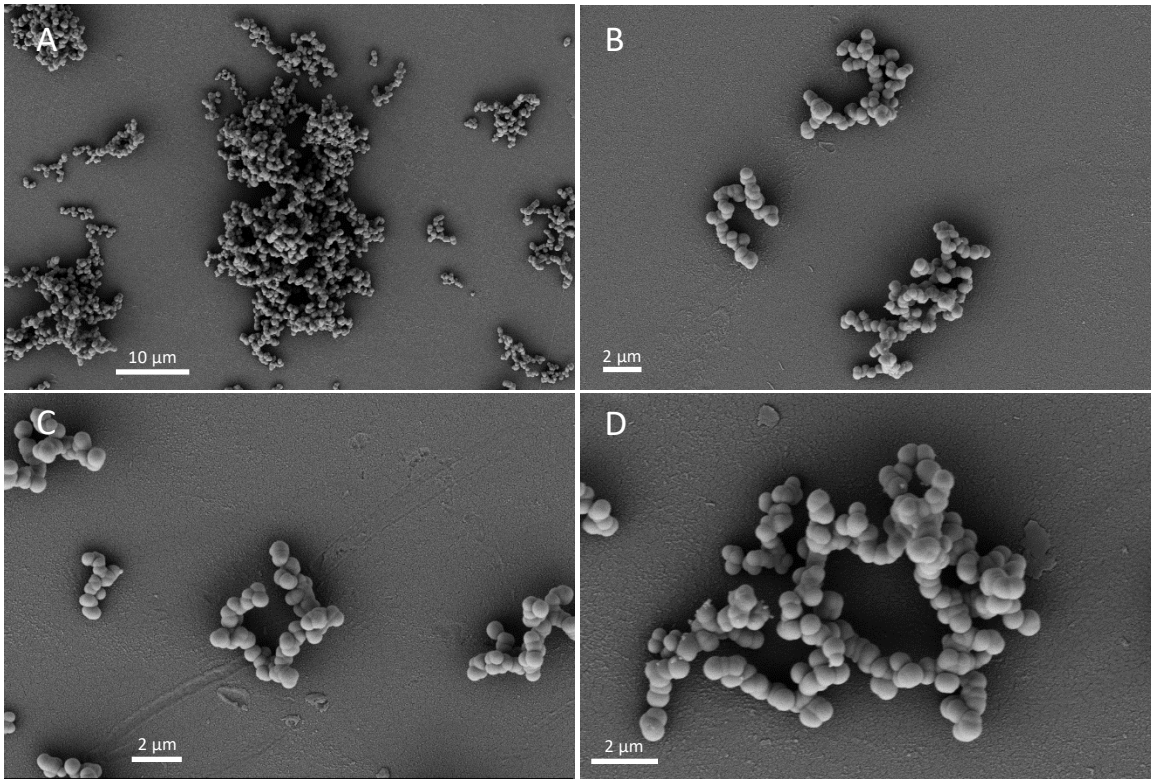

Figure 55: SEM images of particles obtained after silica precipitation according to section 2.9 with peptide 13.

The SEM images of the silica particles derived from peptide 13 are shown in Figure 55. Image A and B show that the particles have a uniform spherical morphology, similar to the particles derived from peptide 12. This was expected considering the fact that peptides 12 and 13 represent a pair of enantiomers. Like peptide 12, a smooth surface of the particles and a particle diameter in the range of about 300-500 nm can be observed.

3.1.1.14 Results of the synthesis, purification and silica precipitation of peptide 14

The yield of peptide 14 with the sequence *RRILL-k*-rril* after RP-HPLC purification was 8.2 mg (62 % of the theoretical yield of 13.4 mg for 0.01 mmol synthesis scale).

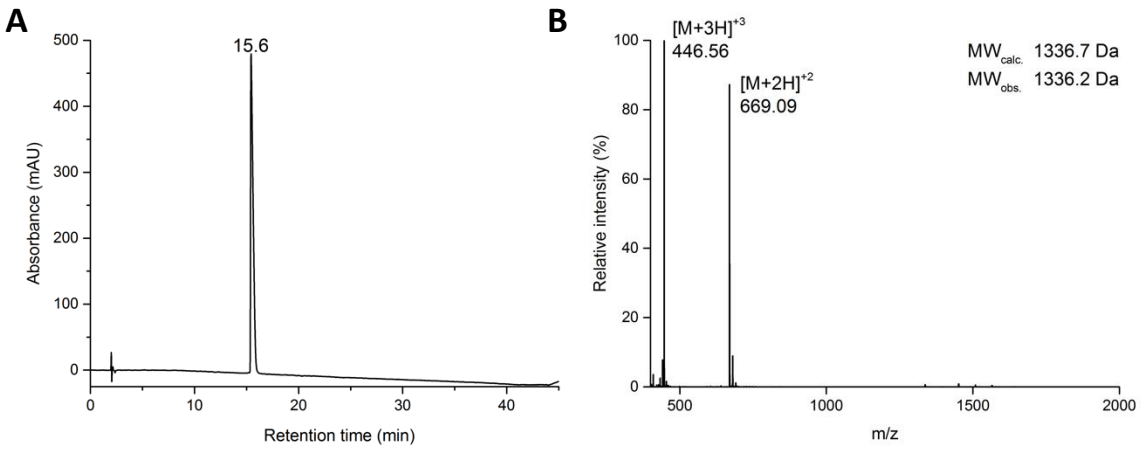

Figure 56: HPLC chromatogram of purified peptide 14. B: Mass spectrum obtained from a direct injection of purified peptide 14 on a Thermo Fisher HPLC-MS system.

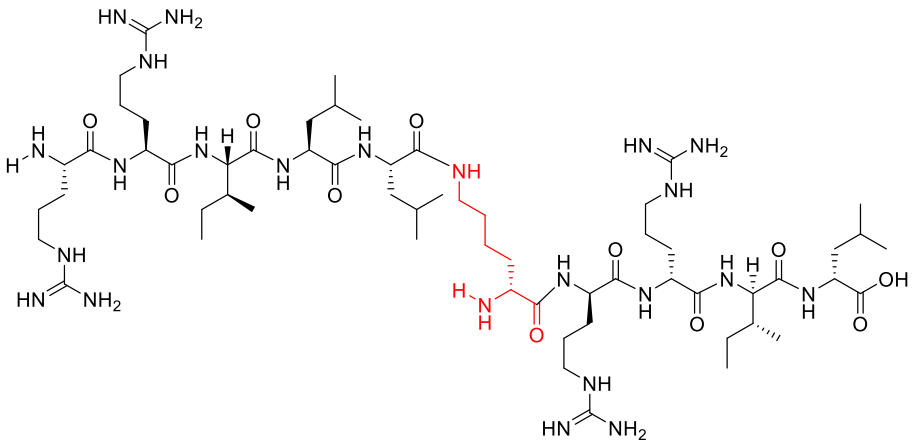

Figure 57: Structure of peptide 14 with D-Lysine as a central residue.

Figure 56 shows the chromatogram and the mass spectrum after purification of peptide 14. As can be seen, the chromatogram shows a single peak after a retention time of 15.6 minutes, indicating a pure product. This is confirmed by the mass spectrum of peptide 14 showing a charge pattern corresponding to an observed mass of 1336.2 Da, which is in good agreement with the calculated mass of 1336.7 Da.

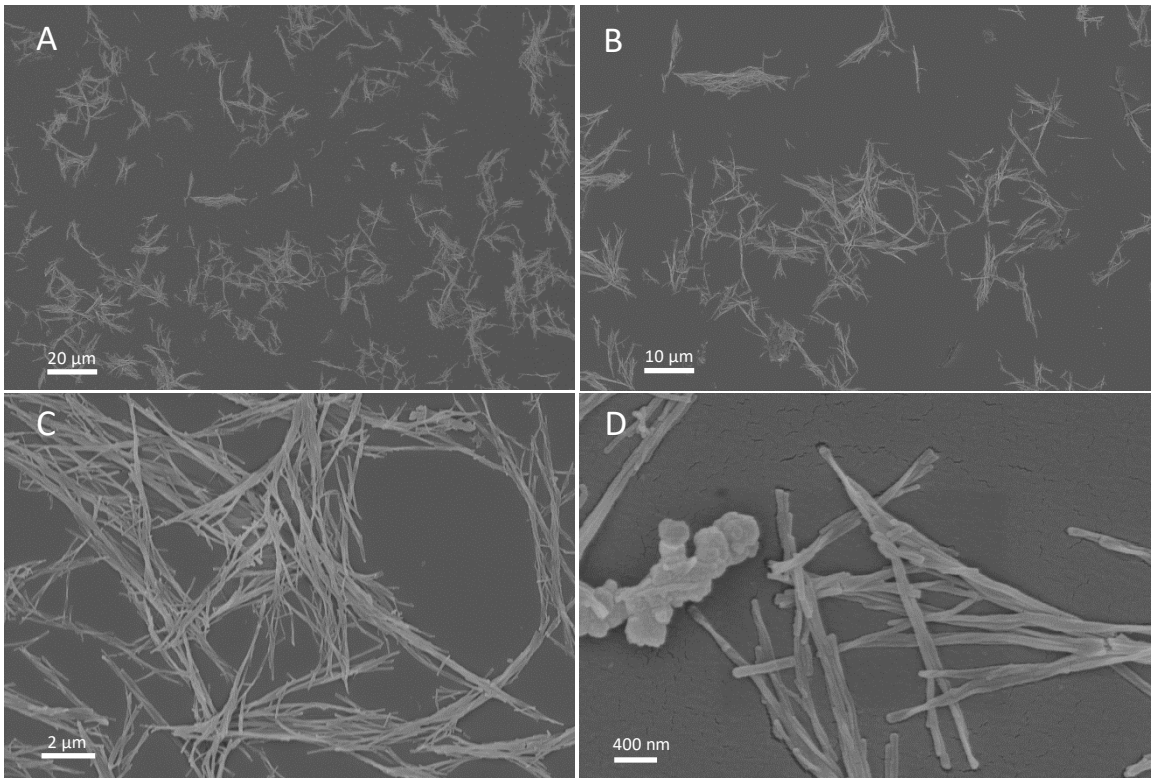

Figure 58: SEM images of particles obtained after silica precipitation according to section 2.9 with peptide 14.

Figure 58 shows the SEM microscopy images after silica precipitation with peptide 14. The particles show a rod-like morphology comparable to the particles derived from peptide 11. This was expected since peptide 11 and 14 represent a pair of enantiomers. In isolated cases, deviant structures similar to spherical particles can be seen, as shown in Figure D. Nevertheless, the vast majority of silica particles show a rod-like morphology with lengths in the range of several hundred nm to several µm, similar to peptide 11.

Similar to peptide 11, a precipitate was formed during incubation in phosphate buffer with peptide 14. As described in section 2.10.1, a sample of the precipitate was taken and examined via SEM-microscopy.

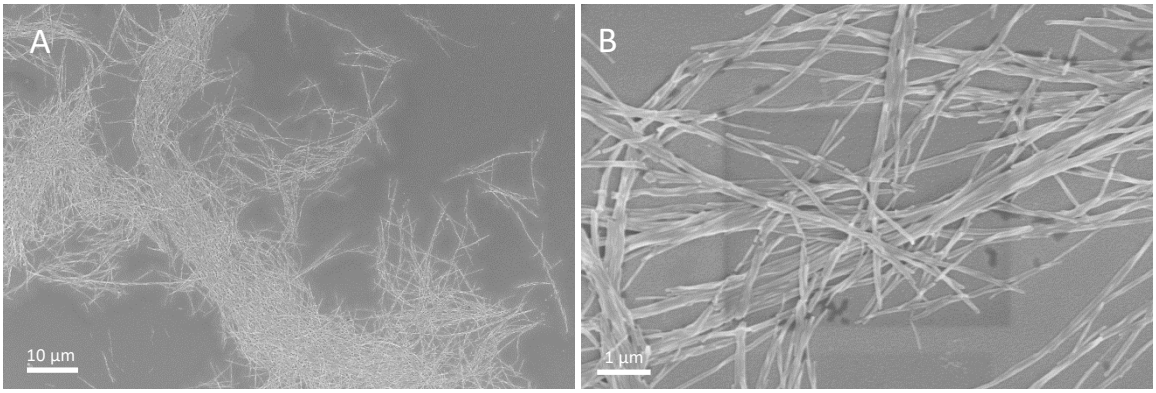

Figure 59: SEM images from the precipitate obtained during phosphate buffer incubation with peptide 14 according to section 2.9.

As expected, the peptide particles in Figure 59 show the same morphology as their silica equivalents and the peptide precipitate from section 3.1.1.11, respectively. The particles show rod like structures and the length of the sticks are in same range as their silica equivalents. This confirms the assumption that peptide 11 and 14 serve as a template for silica precipitation.

3.1.2 Functionalization of rrill-K*-RRIL with the fluorescent dye Cy5

After synthesis of RRIL peptides with different central residues, the second aim of this work consisted in the functionalization of peptide 11 with the fluorescent cyanine-5. Peptide 11 was chosen because of the outstanding rod like morphology of the resulting silica particles, which have certain advantages in potentially subsequent applications.

In order to achieve the desired goal, a test peptide with an acetylated β-alanine instead of the Cy5 modification was synthesized first. This test peptide was also used to investigate the effect of the hydrophobic Cy5 residue on the morphology of the resulting silica particles. The synthesis of the test peptide and the Cy5-functionalized peptide differed only in the second step of the synthesis route, shown in Figure 60.

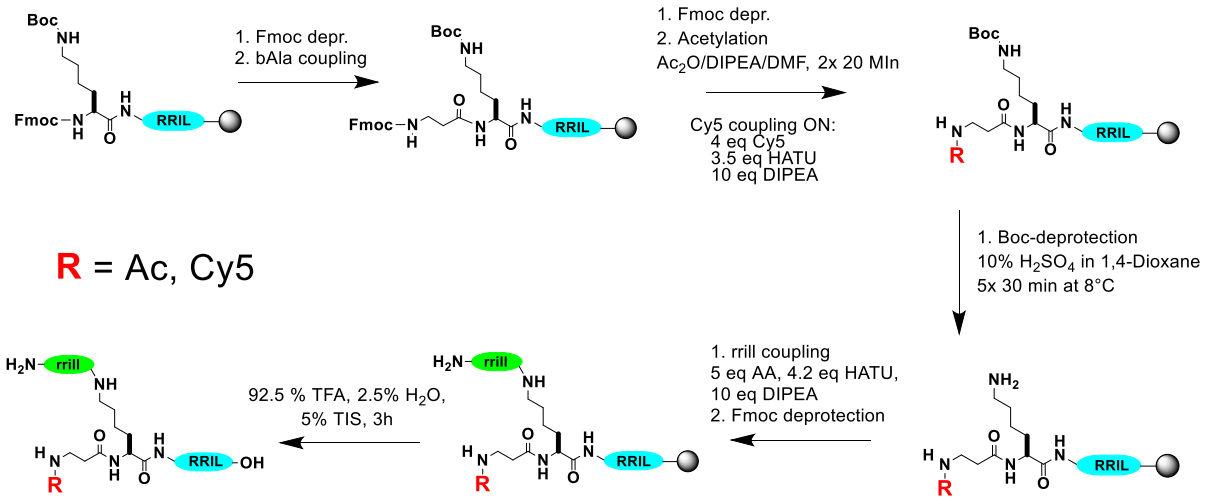

Figure 60: Synthesis scheme for the synthesis of the test peptide and the Cy5-modified construct. The only difference between the two peptides was in the second synthesis step, where the Cy5 modification was performed instead of acetylation.

In the beginning, the KRRIL sequence was synthesized via SPPS and the second linker molecule β-alanine was coupled, as described in section 2.2. In the next step the Fmoc protecting group of the beta alanine was removed, whereupon the free amine was either acetylated (see section 2.3) or the Cy5 was attached according to section 2.4. It should be highlighted again that the test peptide and the Cy5 peptide differed only in this one step, all other steps were performed in the same way. The Boc-protecting group of lysine was then removed with 10% sulfuric acid in 1,4-dioxane according to section 2.5.

Subsequently, the *N*-terminal RRILL sequence was coupled via SPPS (see section 2.2) and the peptide was cleaved from the resin as described in section 2.6. After final cleavage, purification was performed using RP-HPLC according to section 2.7. The purity of the resulting products was determined via HPLC and direct injection mass spectrometry (see section 2.8).

Finally, silica precipitation was performed with the purified product (see section 2.9) and the resulting silica particles were investigated via SEM microscopy (see section 2.10.2). In addition, the rate of peptide incorporation during silica precipitation was investigated applying the protocol from section 2.12.

3.1.2.1 Results of the synthesis, purification and silica precipitation of peptide 15

The yield of peptide 15 with the sequence *rrill-K*(βAla(Ac))-RRIL* after RP-HPLC purification was 2.8 mg (39 % of the theoretical yield of 7.25 mg for 0.005 mmol synthesis scale).

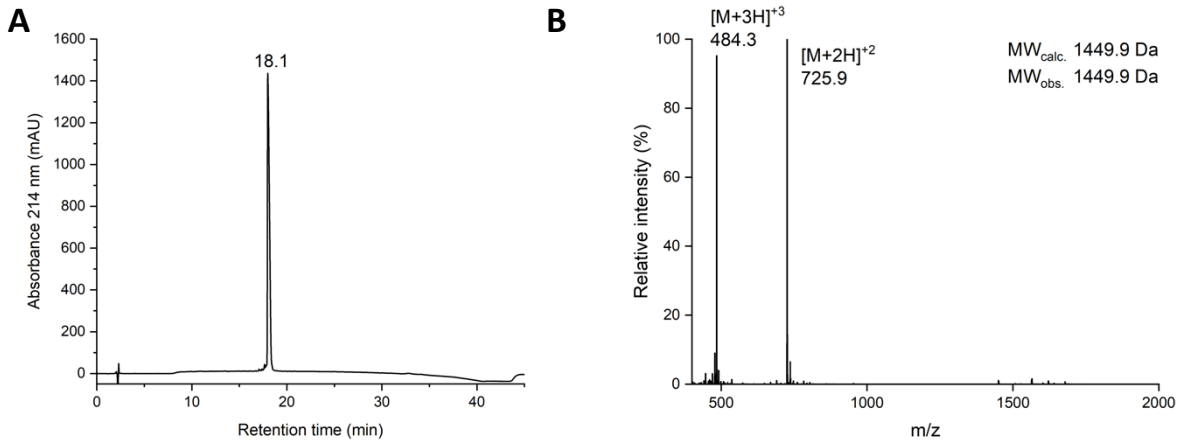

Figure 61: HPLC chromatogram of purified peptide 15. B: Mass spectrum obtained from a direct injection of purified peptide 15 on a Thermo Fisher HPLC-MS system.

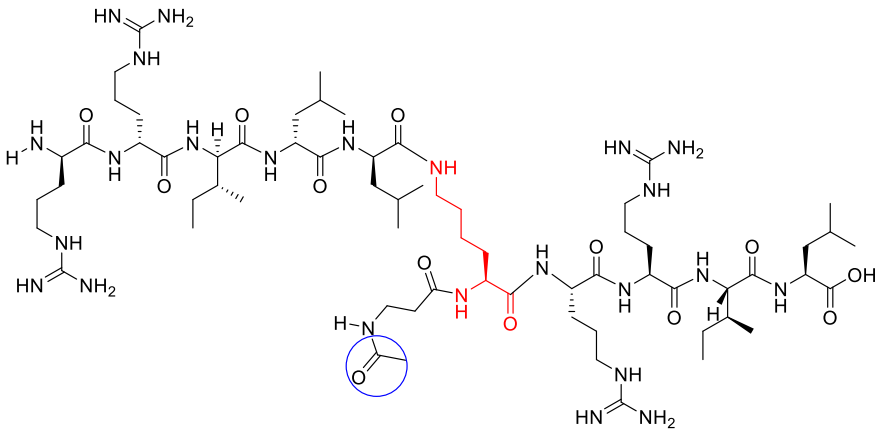

Figure 62: Structure of peptide 15 with L-Lysine as the central residue and β-alanine as the second linker molecule, the acetyl residue is highlighted in blue.

As can be seen from Figure 61 A, peptide 15 eluted after a retention time of 18.1 min. No significant additional peaks were detected, indicating successful purification. This is confirmed by the mass spectrum in Figure 61 B, which shows the expected charge pattern with an observed and calculated mass of 1449.9.

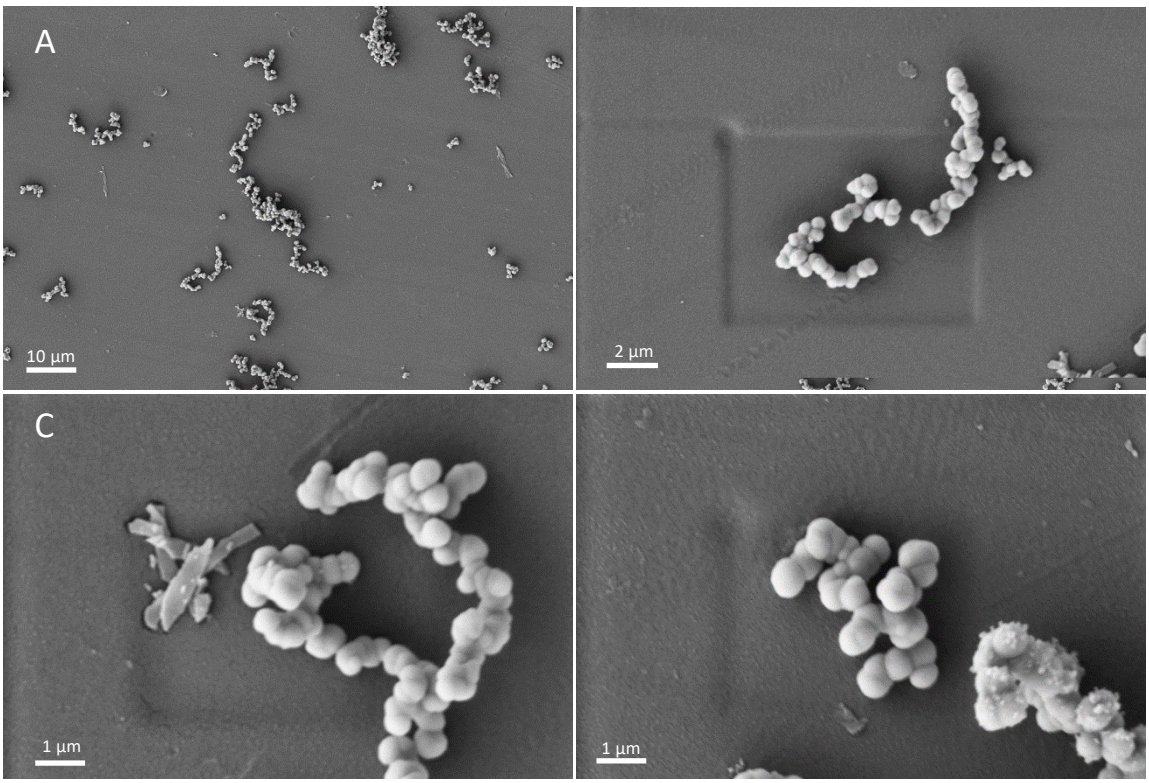

Figure 63: SEM images of particles obtained after silica precipitation according to section 2.9 with peptide 15.

Figure 63 depicts the silica particles derived from peptide 15. It can be seen that the majority of the particles show a spherical morphology. Nevertheless, some artefacts, such as the β-sheets in Figure C, can be observed. Apart from a few exceptions (e.g particles with rough surfaces in image D) the majority of the spherical particles have a smooth surface and a size in the range of 300-500 nm, similar to the spherical silica particles previous obtained. It should be highlighted that the morphology of the peptide has changed fundamentally compared to that of peptide 11 and this only due to the additional acetylated b-alanine.

Finally, the rate of incorporation of the peptide into the silica particles was also determined, according to section 2.12.

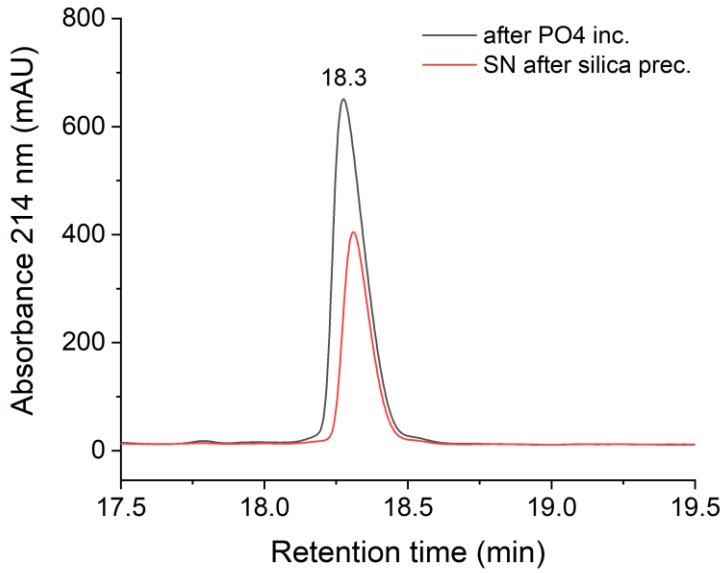

Figure 64: Determining the rate of incorporation of peptide 15 into the silica particles via HPLC analysis of the peptide solution before (black) and the supernatant after silica precipitation (red).

The overlaid chromatograms in Figure 64 show that a significant amount of peptide 15 was incorporated into the particles during silica precipitation. Taking the areas below the curves as a reference, approximately 40 % of the peptide from the initial phosphate buffer incubated peptide solution was incorporated into the particles.

3.1.2.2 Results of the synthesis, purification, silica precipitation of peptide 16, including fluorescence imaging of silica particles generated with 16

The yield of peptide 16 with the sequence *rrill-K*(βAla(Cy5))-RRIL* after RP-HPLC purification was 1.8 mg (9 % of the theoretical yield of 18.6 mg for 0.01 mmol synthesis scale).

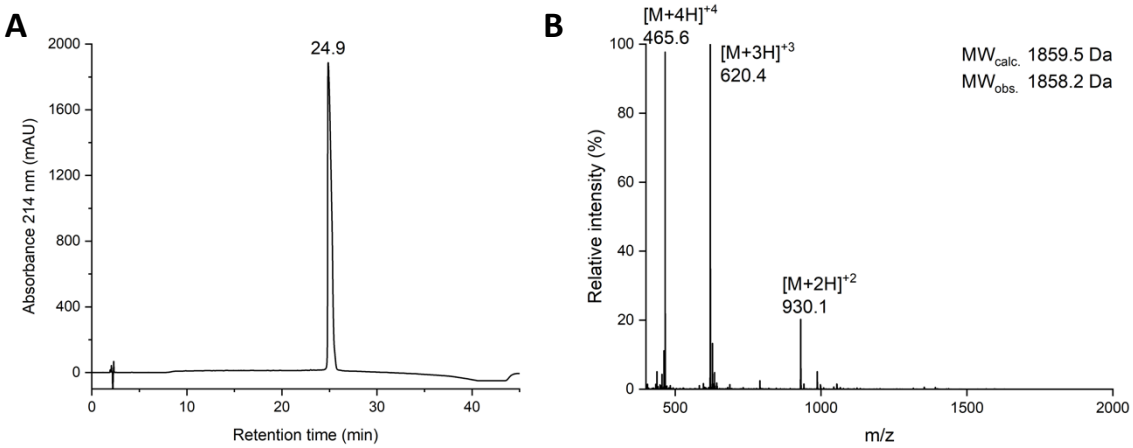

Figure 65: HPLC chromatogram of purified peptide 16. B: Mass spectrum obtained from a direct injection of purified peptide 16 on a Thermo Fisher HPLC-MS system.

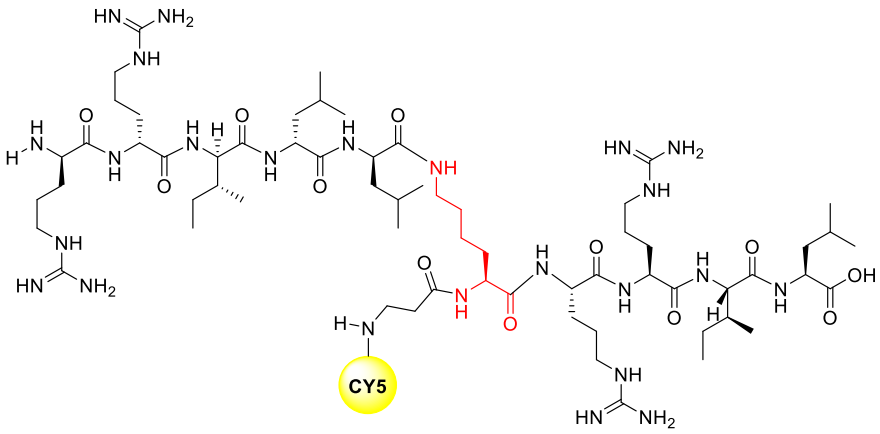

Figure 66: Structure of peptide 16 with L-Lysine as the central residue and β-alanine as second linker molecule, the Cy5 residue is highlighted in yellow.

Figure 65 A depicts the chromatogram (214 nm absorbance wavelength) from the RP-HPLC analysis of purified peptide 16 (structure shown in Figure 66). Apart from the product peak after 24.9 min, no additional peaks can be detected in the chromatogram, indicating that the purification was successful.

The corresponding mass spectrum is depicted in Figure 65 B. It shows a charge pattern corresponding to an observed mass of 1858.2 Da, which is in good agreement with the calculated mass of 1859.5 Da. Based on this data shown, it can be concluded that peptide 16 was successfully synthesized and purified. The additional peaks in the mass spectrum could not be attributed to known compounds. It may be that these are modifications of Cy5, which have been formed as a result of the harsh conditions during synthesis. Compared to peptide 15, the yield of the Cy5-modified construct was considerably lower, although the synthesis steps were almost the same. This could be due to unspecific oxidation and hydrolysis of the photolabile Cy5 molecule during Boc deprotection with sulfuric acid.

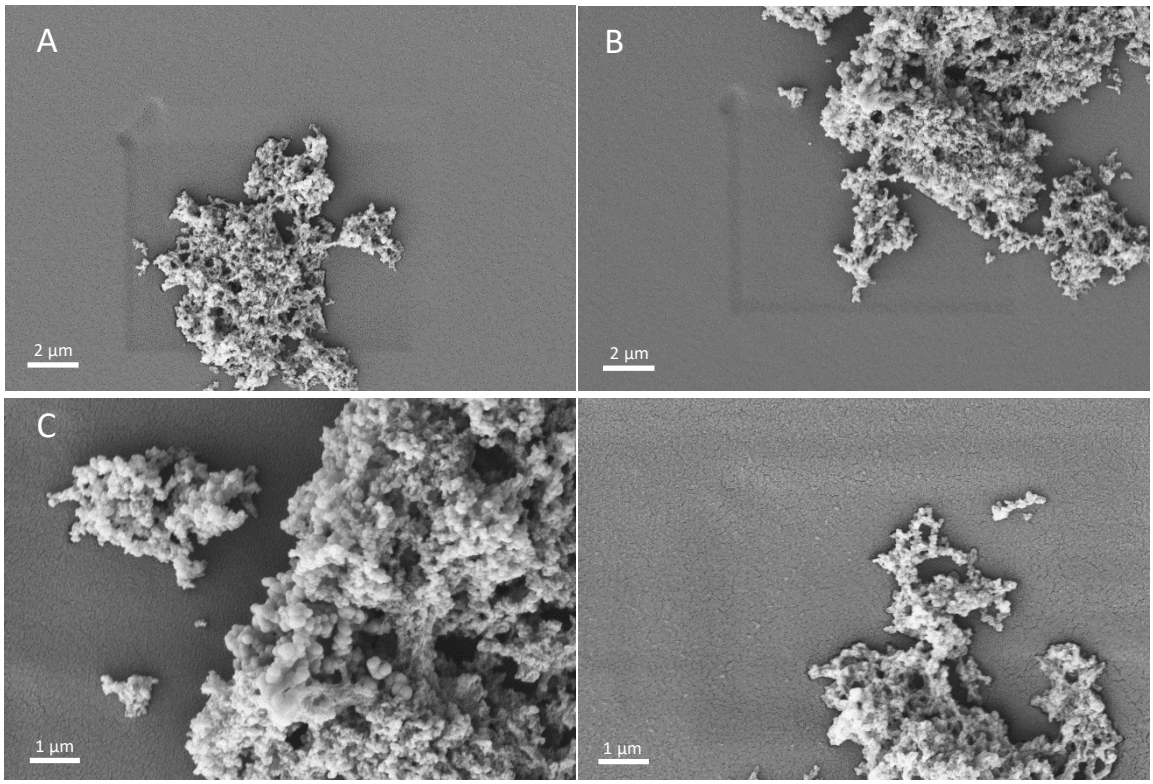

Figure 67: SEM images of particles obtained after silica precipitation according to section 2.9 with peptide 16.

Looking at the images of the silica particles in Figure 67 obtained during silica precipitation with peptide 16, it is apparent that the morphology differs significantly from all previous peptides. Instead of spherical or rod-like particles, they show an amorphous, porous and partly sponge-like structure with a size of less than a few hundred nanometers. This suggests that the process of self-assembly is strongly altered by the hydrophobic Cy5 residue.

Same as with peptide 15, the rate of incorporation or co-precipitation should be determined during the silica formation process. Therefore, the protocol of section 2.12 was applied.

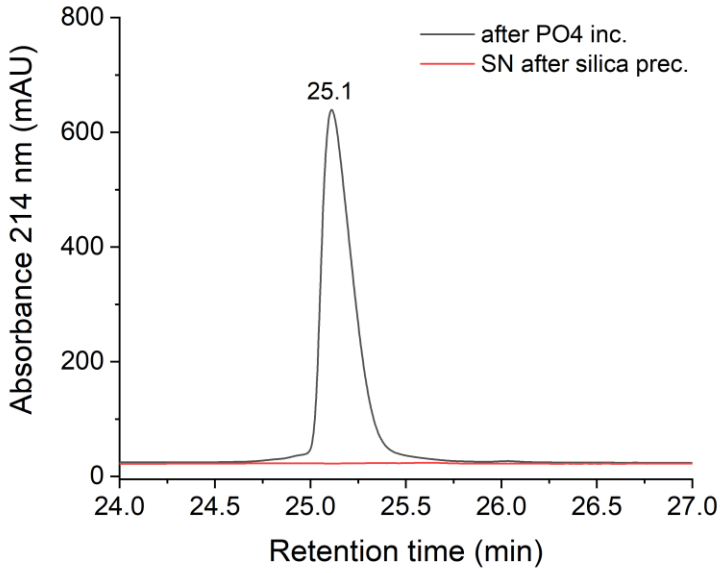

Figure 68: Determining the rate of incorporation of peptide 16 into the silica particles via HPLC analysis after incubation in phosphate buffer (black) and after silica precipitation (red).

The chromatogram in Figure 68 clearly shows that all of the peptide incorporated during silica precipitation. Unlike peptide 15, a precipitate occurred during incubation in phosphate buffer with peptide 16 (see section 2.9), which could explain the difference between the incorporation rates of the two peptides. The precipitate was also examined via SEM microscopy, in the same way as for peptide 11, whose structure was used as backbone for peptide 16.

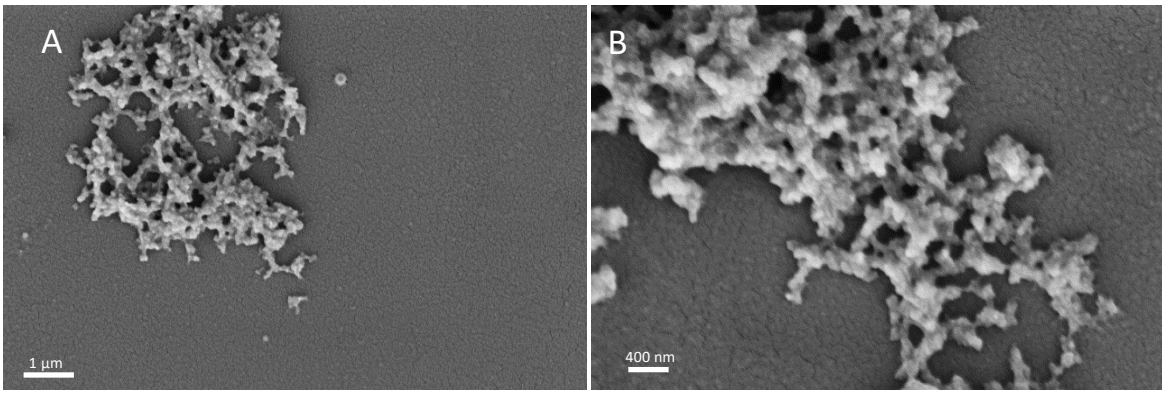

Figure 69: SEM images from the precipitate obtained during incubation in phosphate buffer with peptide 16 according to section 2.9.

Figure 69 shows the SEM images of the precipitate after incubation in phosphate buffer. By comparing the peptide precipitate with the particles after silica precipitation (Figure 67), it can be observed that the morphologies look very similar. Most of the particles in Figure 67 probably seem to consist of peptide.

Based on these results, the question arises to what extent the morphology of the silica particles would change if the supernatant was separated from the precipitate after incubation with peptide 16. The following silica precipitation was carried out with the supernatant after separation of the peptides precipitate.

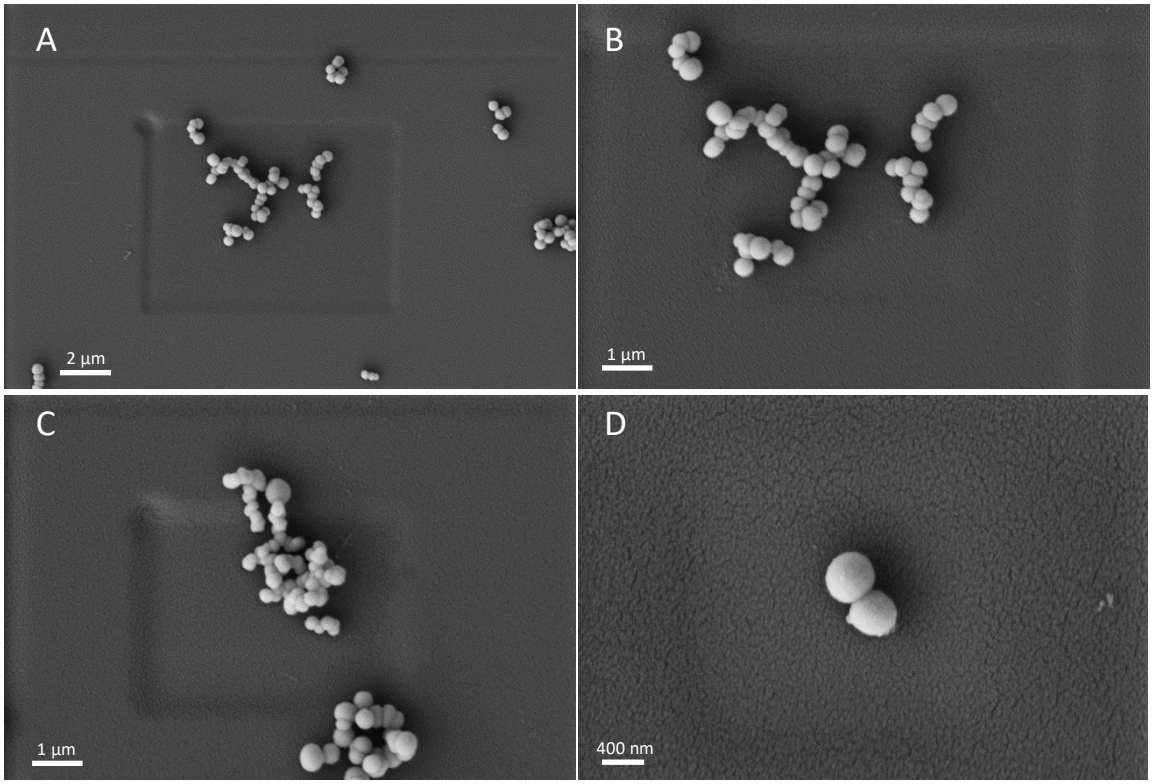

Figure 70: SEM images of particles obtained after silica precipitation using the supernatant after incubation in phosphate buffer with peptide 16 according to section 2.9.

Interestingly, the morphology changes fundamentally if the precipitate was separated and the supernatant of the peptide solution was used for silica precipitation, as presented in Figure 70. Instead of amorphous sponge-like particles, uniform spherical silica particles with a smooth surface and a diameter in the range of 300-500 nm can be observed. The morphology is comparable to the spherical particles from section 3.1.1.

After successful silica precipitation, the next step was to perform fluorescence imaging of the Cy5-modified particles. For this purpose, the particles were treated and prepared for the analysis as described in section 2.13.

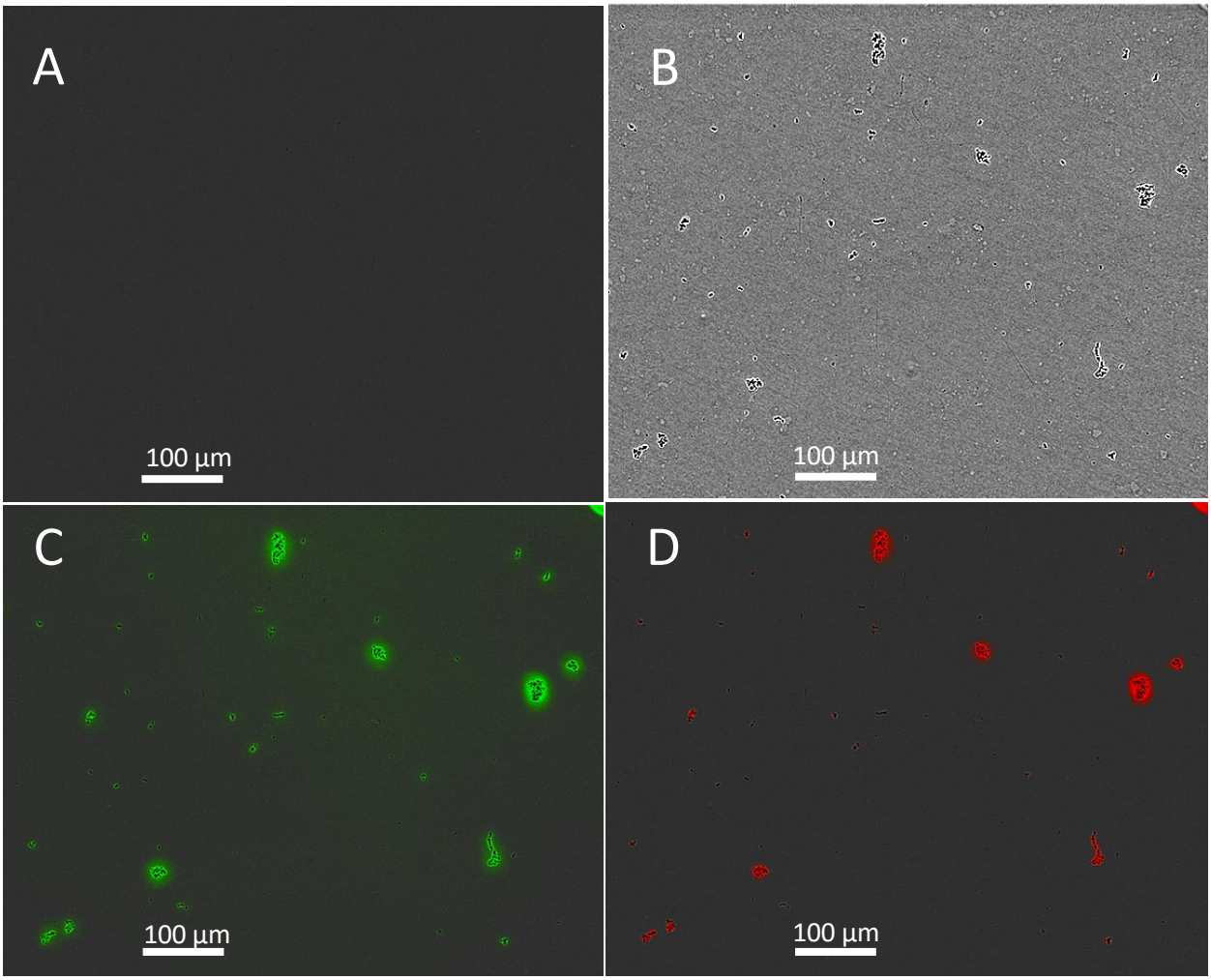

Figure 71: Fluorescence images of the silica particles derived from the Cy5-modified peptide 16.A: blank (without silica particles), B: phase contrast image, C: B + green channel with an emission range of 504-544 nm, D: B + red channel with an emission range of 625-705 nm.

Figure 71 shows the results of the fluorescence experiments with the IncuCyte® ZOOM analysis system. Image B shows the phase contrast of the Cy5-modified particles. After excitation via green (picture C) and red channels (picture D) and superposition with the phase contrast (picture B) a clear fluorescence of the sample can be seen, indicating that the Cy5-modified peptide has been incorporated into the silica particles, since the absorption spectrum of Cy5 ranges from about 500-700 nm with a maximum at 650 nm. The difference in particle size of several µm from figure 71 compared to those from the SEM images in figure 67 is most likely due to an aggregation of the particles during the sample preparation for the IncuCyte® ZOOM analysis.

4. Discussion

In order to examine the impact of different central residues, changes in stereochemistry and additional functionalization on self-assembly of the rrillK*RRIL peptide, analogues with different central residues and varying stereochemistry were synthesized. Furthermore, the silica precipitation of a RRIL-based peptide should be investigated spectroscopically. For this purpose, the dye cyanine-5 was attached to the initial peptide via a second linker as shown in section 3.1.2. Moreover, the effect of the functionalization with cyanine-5 on the morphology of the silica particles was investigated via SE-microscopy (section 4.2). Table 3 gives an overview of peptides 1-14 synthesized in this study.

Table 3: Overview of the 14 synthesized peptides including sequence, molecular weight and structure. The star at the central residue in the primary sequence indicates that the N-terminal RRILL sequence was coupled via the amine of the amino acid side chain. Lower case letters correspond to the D-version and upper case letters to the L-version of the amino acids. The yield given refers to the theoretically maximum possible yield. Dap = 2,3-Diaminopropionic acid, bAla = β-alanine, Orn = Ornithine, k/K = D/L-Lysine.

Peptide No.	Sequence	MW [g/mol]	Structure	Yield
1	rrill-LDap*-RRIL	1294.6	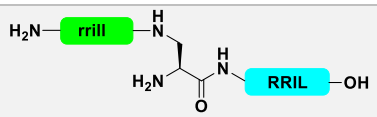	90 %
2	rrill-DDap*-RRIL		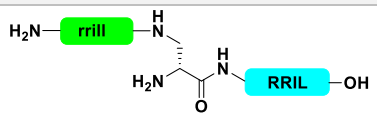	61 %
3	RRILL-LDap*-rril		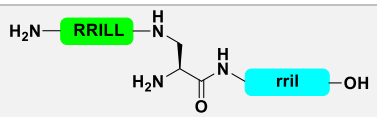	70 %
4	RRILL-DDap*-rril		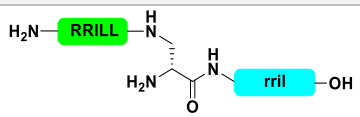	81 %
5	rrill-bAla-RRIL	1279.6	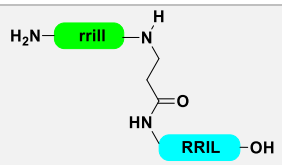	30 %
6	RRILL-bAla-rril		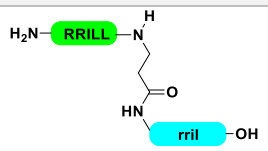	38 %

7	rrill-LOrn*-RRIL	1322.8	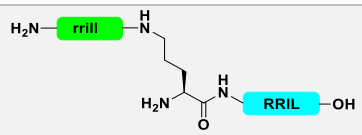	83 %
8	rrill-DOrn*-RRIL		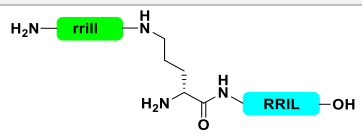	64 %
9	RRILL-LOrn*-rril		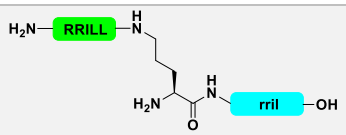	67 %
10	RRILL-DOrn*-rril		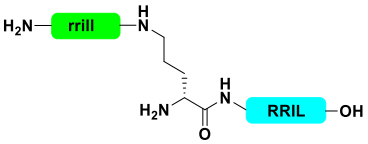	77 %
11	rrill-K*-RRIL	1336.7	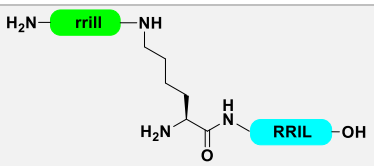	91 %
12	rrill-k*-RRIL		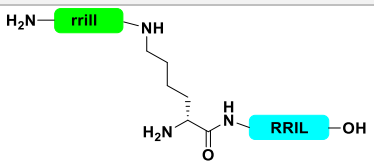	92 %
13	RRILL-K*-rril		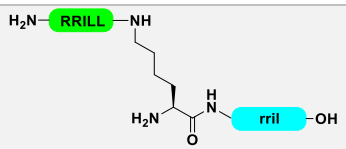	39 %
14	RRILL-k*-rril		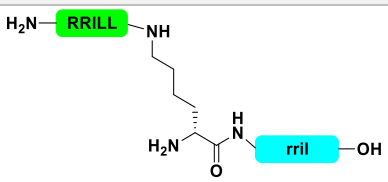	62 %

4.1 Discussing the influence of different central residues on the morphology of silica particles

In the following section, the influence of the central residue and the stereochemistry of the *N*- and *C*-terminal RRIL sequences on the morphology of the silica particles will be examined by comparing the data from section 3.1.1. The peptide groups are illustrated in Figure 72.

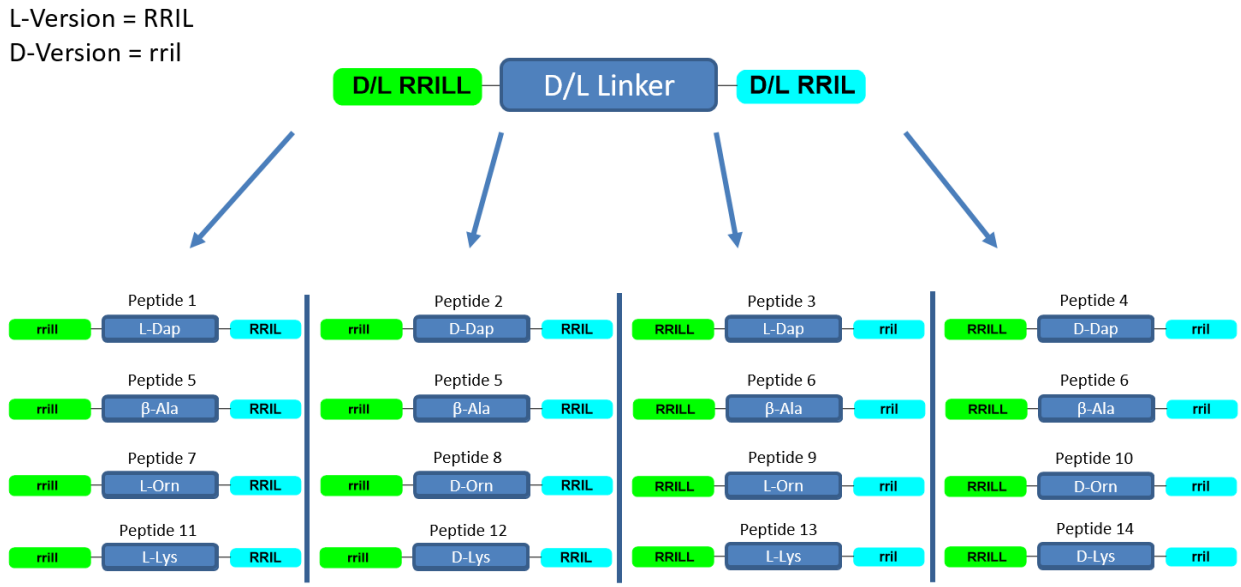

Figure 72: Organigram illustrating the following comparison of the morphologies of silica particles derived from peptides 1-14 (section 3.1.1). Dap = 2,3-Diaminopropionic acid, βAla = β-alanine, Orn = Ornithine, Lys = Lysine. Column1: peptide 1, 5, 7, 11. Column 2: peptide 2, 5, 8, 12. Column 3: peptide 3, 6, 9, 13. Column 4: peptide 4, 6, 10, 14.

As can be seen, the stereochemistry of the N-and C-terminal RRIL sequences as well as of the central residue was varied depending on the column and row where the specific peptide is located. For example, the configuration of the RRIL sequences was kept constant in the first column. The central residues were varied with each row, so that the length of the central residues increases from row 1-4. The second column is identical with the first, only that the stereochemistry of the central residues has been changed. The third and fourth columns represent the mirror peptides of the first two columns, the *N*-terminal RRIL sequence being in the L-form and the *C*-terminus in the D-form.

4.1.1 Comparison of the peptides 1, 5, 7, 11 with the core structure rrill-L-central residue-RRIL

In this section the silica particles obtained from peptide 1, 5, 7, 11 are compared with one another, represented by the first column in Fig. 72.

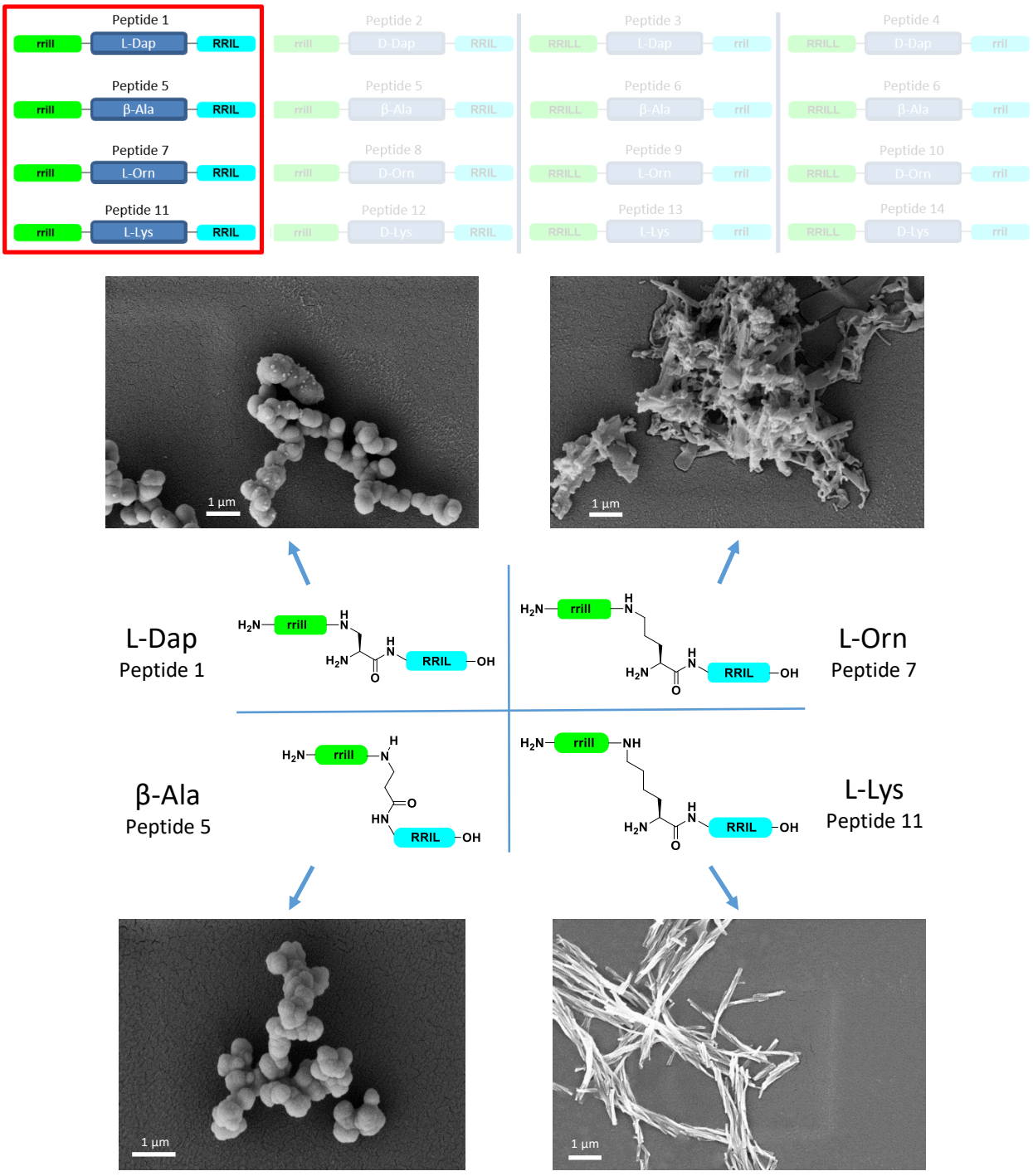

Figure 73: Comparison of the peptides (peptide 1, 5, 7, 11) from column 1 (Fig. 72). The N-terminal rrill as well as the C-terminal RRIL sequence and the stereochemistry of the central residue were kept constant, whereas the length of the central residue was varied. Dap = 2,3-diaminopropionic acid, β-Ala = β-alanine, Orn = ornithine, Lys = Lysine.

As can be seen in Fig. 73, the distance between the two RRIL sequences has a strong influence on the morphology of the resulting nanoparticles. For example, when comparing peptide 1 and peptide 7 particles, it is obvious that the two additional methylene groups of ornithine cause a completely different self-assembly mechanism. Even more profound is the difference compared to peptide 11 (lysine) derived particles, where 4 methylene groups between the RRIL-sequences result in rod like sticks. This is consistent with previous experiments by Becker and co-workers [52]. It is noteworthy that the silica particles derived from peptide 7 represent a kind of intermediate stage in the transformation from spherical L-Dap- and β-Ala-particles to rod-like particles derived from peptide 11. The peptides with L-ornithine and L-lysine as central residues differed in a further point compared to L-Dap and β-Ala. Both showed precipitations after incubation in phosphate buffer. This could be due to an increased exposure of hydrophobic residues to the aqueous environment, indicating a completely different self-assembly mechanism. Especially for peptide 11, the peptide precipitate showed fibrillar structures very similar to the morphology of the silica particles. This supports the previously postulated template theory [52].

On the other hand, the influence of the free amine group of the central residue seems to be negligible compared to the length of the central residue, as can be assumed from the comparison of the β-Ala- and the Dap- particles. This is contrary to the previously assumed acid-base catalyzed condensation reaction of silicic acid via free amine residues [35].

4.1.2 Comparison of the peptides 2, 5, 8, 12 with the core structure rrill-D-central residue-RRIL

In this section, silica particles obtained from peptide 2, 5, 8, 12 are compared with one another, represented by column 2 in Figure 72. Unlike before, the D-version of the central residues is used.

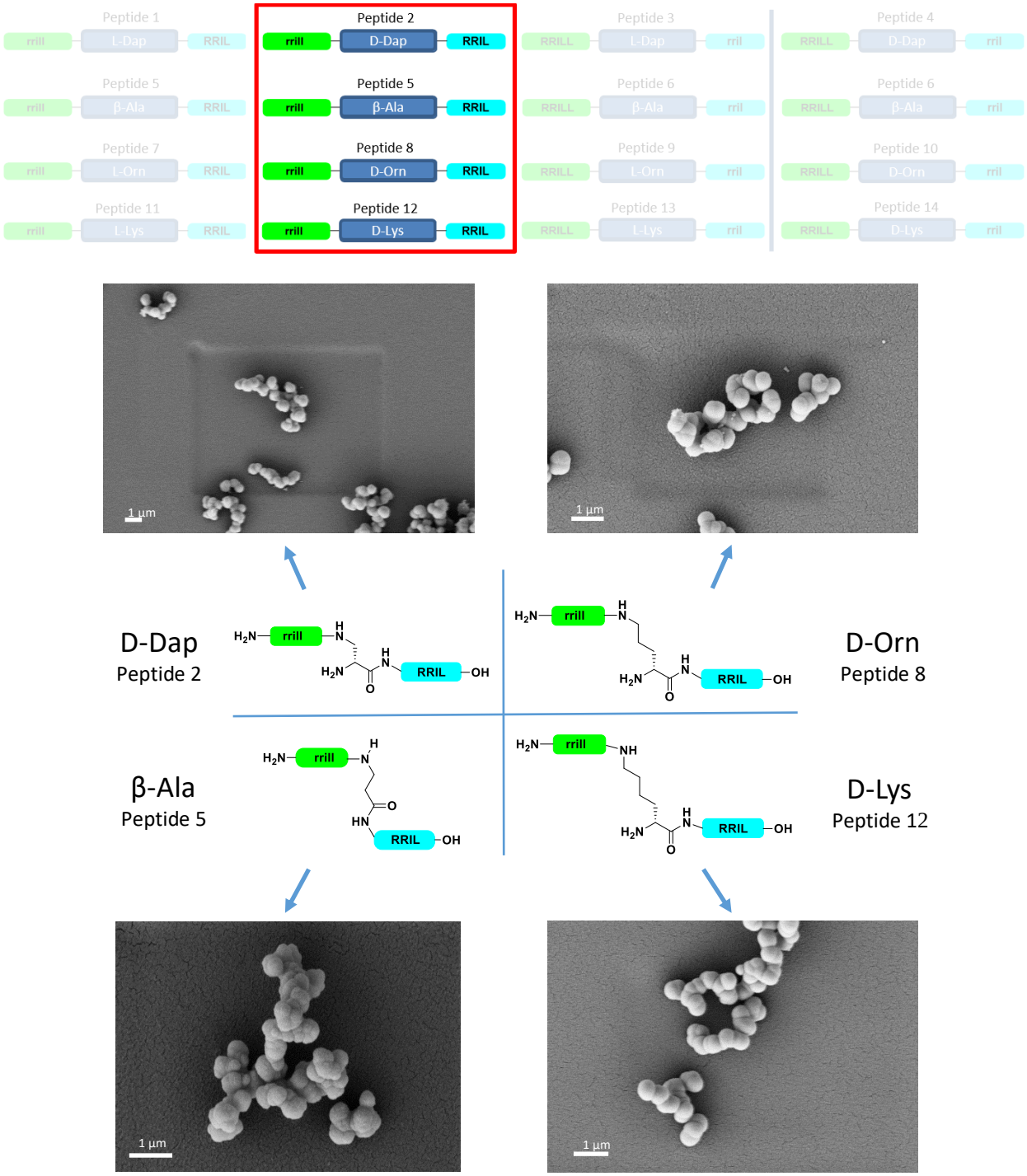

Figure 74: Comparison of the peptides (peptide 2, 5, 8, 12) from column 2 (Fig. 72). The N-terminal rrill as well as the C-terminal RRIL sequence and the stereochemistry of the central residue were kept constant, whereas the length of the central residue was varied. Dap = 2,3-diaminopropionic acid, β-Ala = β-alanine, Orn = ornithine, Lys = Lysine.

In contrast to section 4.1.1, no significant shifts of silica particle morphology can be observed in the case of Fig. 74. On the whole, the particles shape and size are similar, independent of the peptide and the respective length of the central residue. Particularly noteworthy is peptide 12 with D-lysine as a central residue. It shows no signs of rod like structures anymore. This dramatic shift in morphology is caused solely by the stereochemical modification of the central lysine residue. Recent studies have shown that the replacement of L-lysine with D-lysine can lead to a significant change in the conformational propensity of adjacent amino acids in short peptides. It is possible that this is the cause for the strongly deviating morphology [71]. In addition, the peptides with D-ornithine and D-lysine as central residues did not show any precipitation after incubation with phosphate buffer, which was the case with their L-amino acids equivalents. This also indicates a different self-assembly mechanism. Overall the comparison of particles in Fig. 74 with those from section 4.1.1 shows that the stereochemical change of the central residue has significant consequences on the morphology of the particles.

4.1.3 Comparison of the peptides 3, 6, 9, 13 with the core structure RRILL-L-central residue-rril

Unlike section 3.2.2, the L-versions of the central residues were used in this section and the stereochemistry of the RRIL sequences has been changed. Thus, the peptides from column 3 in Fig. 72 represents the mirror image of the peptides from the second column.

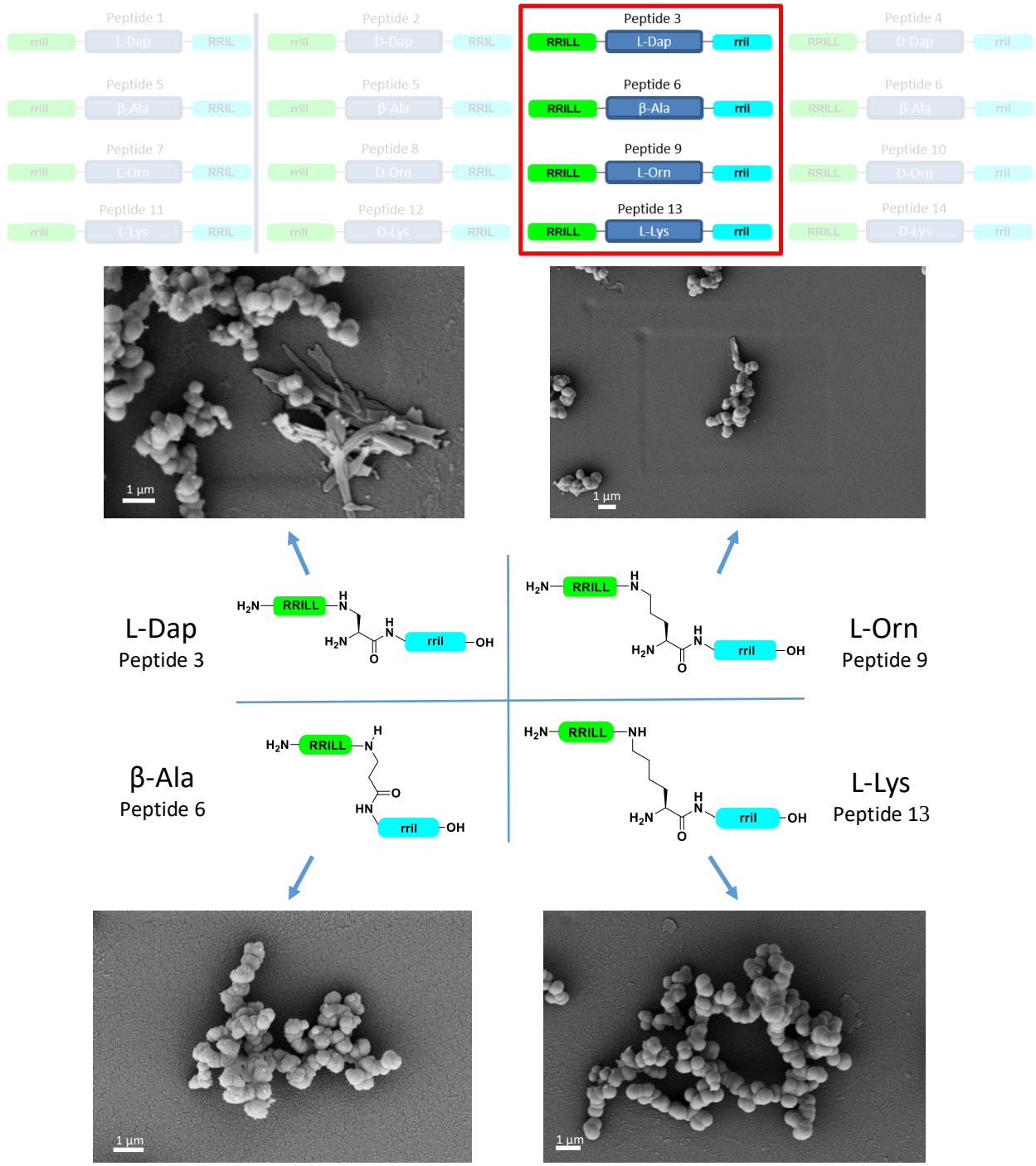

Figure 75: Comparison of the peptides (peptide 3, 6, 9, 13) from column 3 (Fig. 72). The N-terminal RRILL as well as the C-terminal rril sequence and the stereochemistry of the central residue were kept constant, whereas the length of the central residue was varied. Dap = 2,3-diaminopropionic acid, β-Ala = β-alanine, Orn = ornithine, Lys = Lysine.

Fig. 75 shows the silica particles corresponding to peptide 3, 6, 9 and 13. Since these peptides represent the mirrored peptides of the previous column (section 4.1.2), the silica particles derived from an enantiomeric pair should be almost identical in theory. In fact, the particles show the same spherical morphology indicating similar self-assembly mechanisms. It has to be considered that the β-sheet structures derived from peptide 3 are an artifact because by far the largest part was made up of spherical particles, as can be seen in section 3.1.1.3. Once again it should be emphasized that instead of rod-like particles, spherical silica particles were formed during precipitation with peptide 13. It seems that the different stereochemistry of the lysine residue from the adjacent leucine is another key factor for obtaining silica particles with a rod-like morphology. This is also confirmed by comparison with previous experiments by Kamalov *et al.* [52].

4.1.4 Comparison of the peptides 4, 6, 10, 14 with the core structure RRILL-D-central residue-rril

The peptides presented represent the mirror images of the peptides from the first column.

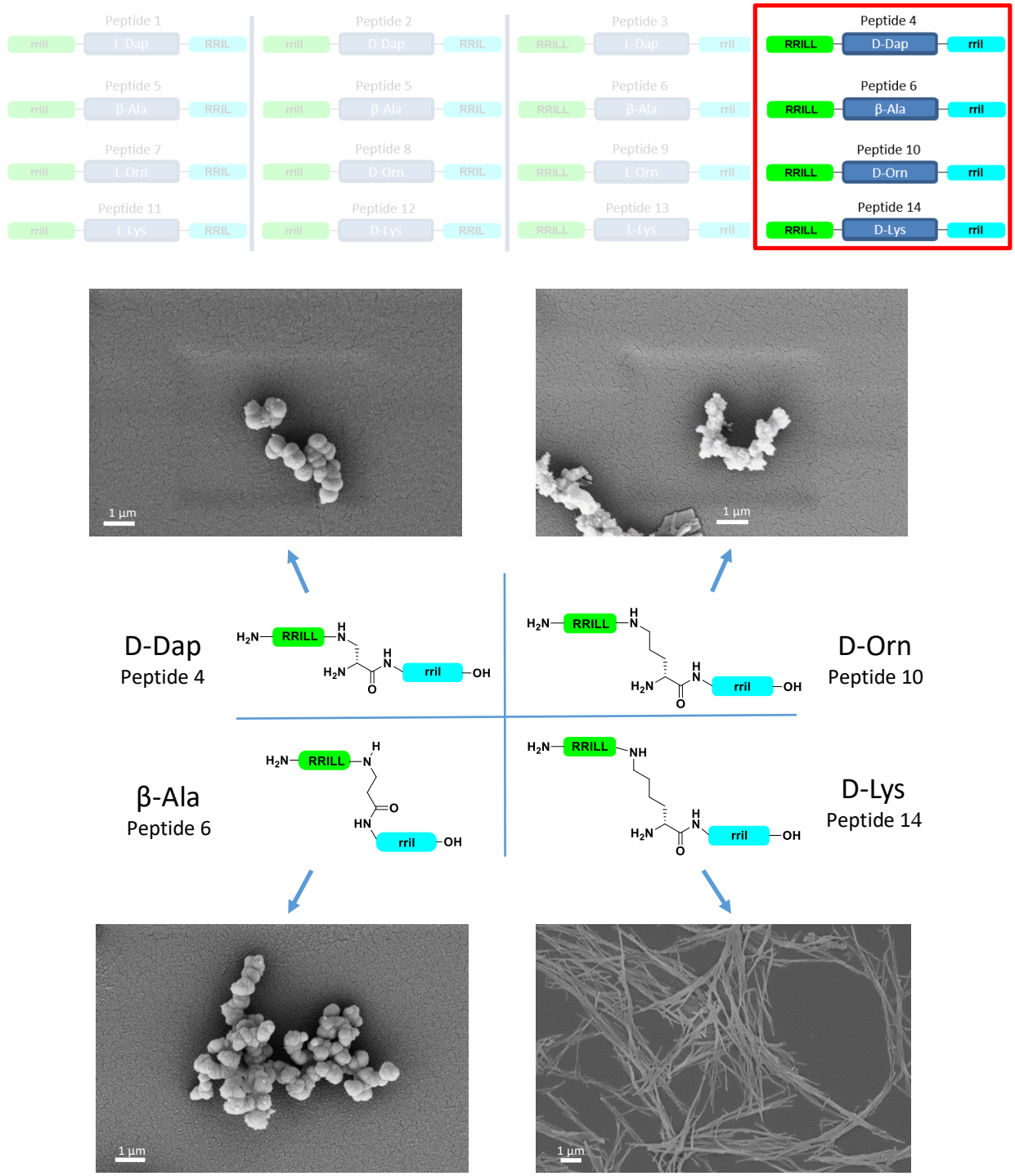

Figure 76: Comparison of the peptides (peptide 4, 6, 10, 14) from column 4 (Fig. 72). The N-terminal RRILL as well as the C-terminal rril sequence and the stereochemistry of the central residue were kept constant, whereas the length of the linker was varied. Dap = 2,3-diaminopropionic acid, β-Ala = β-alanine, Orn = ornithine, Lys = Lysine.

Figure 76 shows the silica particles deriving from peptide 4, 6, 10 and 14. Since these peptides are the mirror peptides of the first column (section 4.1.1), the silica particles are almost identical. As expected, the particles derived from L-ornithine show a strong similarity to the particles of the enantiomer equivalent from section 4.1.1. Furthermore, the rod-like sticks obtained with peptide 14 (L-lysine) are special, confirming that the stereochemistry and the length of the central residue plays a significant role in self-assembly and thus in silica formation. It should be emphasized that precipitates were formed after incubation in phosphate buffer with peptides 10 and 14. This was expected, since these results were observed for the enantiomeric peptides 7 and 11 (see section 3.1.1.7 and 3.1.1.11). Identical to peptide 11, the fibrillar peptide structures resulting from 14 served as a template for the silica precipitation process.

4.1.5 Comparison of the Lysine-containing peptides 11-14

Due to the unique rod-like morphology of the lysine peptides 11-14, they should be compared in this section, representing the last row in the organigram in Fig. 72.

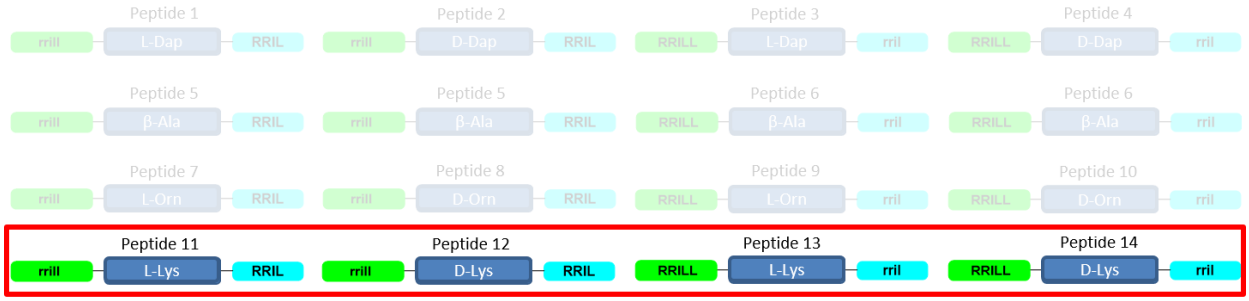

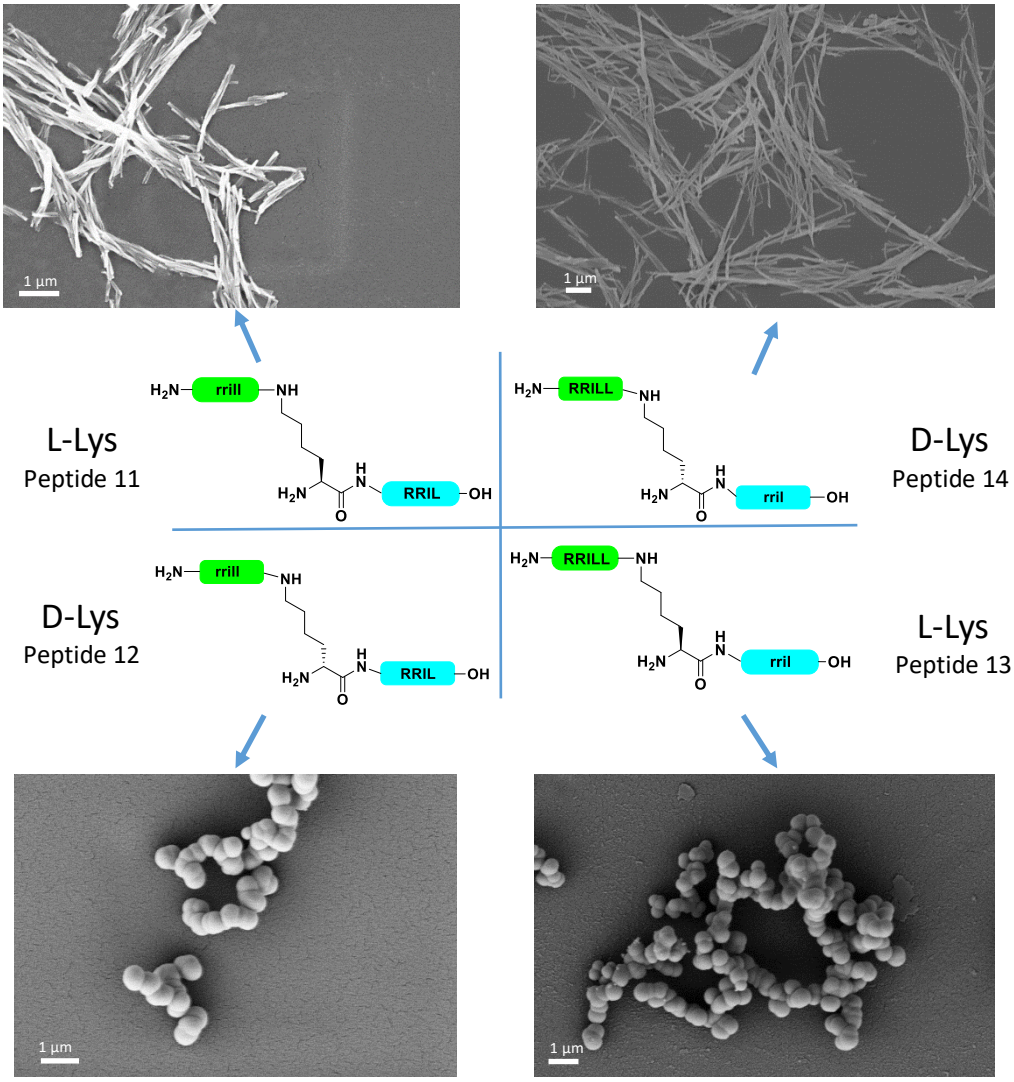

Figure 77: Comparison of Lysine-peptides (peptide 11-14) from row 4 (Fig. 72). The central residue was kept constant, whereas the stereochemistry of the RRILL(L) sequences was varied., Lys = Lysine.

Figure 77 highlights the influence of stereochemical modifications of the central residue on the morphology of silica particles. While peptide 11 and its mirror equivalent peptide 14 produced rod like particles, peptide 12 and its mirror image peptide 13 led to spherical particles. As indicated before, even the slightest shifts in the molecular structure of peptides lead to drastic changes in the mechanism of self-assembly. It is difficult to predict self-assembly behavior and the resulting supramolecular structure of heterochiral peptides. Even with much less complex and shorter heterochiral peptides, no general conclusions could be drawn regarding the effect of the primary sequence on self-assembly [55]. Nevertheless, certain rules regarding the supramolecular structure of peptides can be derived on a case by case basis. Based on previous experiments and the results of this work, two conditions in addition to those given in the introduction (see section 1.4) are necessary to obtain silica particles with rod-like morphology: the length of the central residue must be at least in the order of lysine and the stereochemical configuration of the central residue has to be identical to that of the *N*-terminal RRILL sequence. Further investigations are necessary to clarify whether a central residue with more than 4 methylene groups in side chain length also lead to rod-like sticks. In order to elucidate the differences between the self-assembly mechanisms of different RRIL-based peptides, extensive conformational studies via NMR and Cryo-electron microscopy will be necessary in future experimental set-ups.

4.2 Discussing the influence of the second linker and functionalization with Cy5 on the morphology of silica particles

In this section the influence of an additional β-alanine linker as well as the functionalization with Cy5 on the properties of the silica precipitation process are investigated. For this purpose, results of the unmodified peptide (peptide 11) will be compared with those of the peptides 15 and 16. Table 3 gives an overview about the characteristics of peptide 15 and 16.

Table 4: Characteristics of peptides 15 and 16 including primary sequence, molecular weight and structure. The star at the central residues in the primary sequence means that the N-terminal rrill sequence was coupled via the amine of the lysine side chain. Lower case letters correspond to the D-version and upper case letters to the L-version of the amino acids. The yield given refers to the theoretically maximum possible yield.

Peptide No.	Sequence	MW [g/mol]	Structure	Yield
15	rrill-K*(βAla(Ac))-RRIL	1449.9	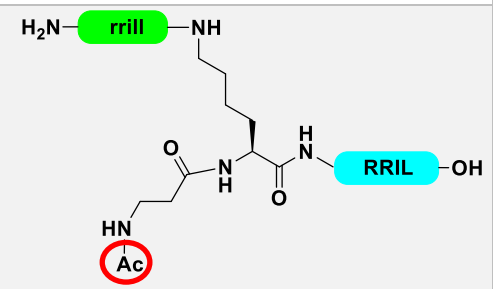	39 %
16	rrill-K*(βAla(Cy5))-RRIL	1859.5	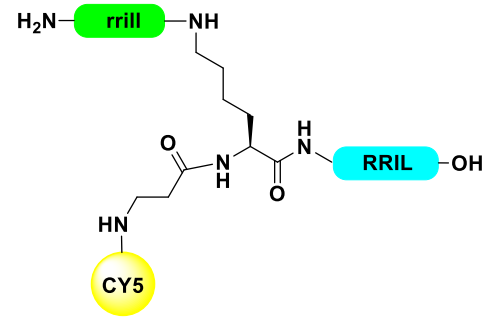	9 %

4.2.1 Elucidating the influence of an additional acetylated β-alanine linker on silica particle formation by comparison of peptides 11 and 15

One of the objectives of this work was to elucidate the effect of an additional acetylated linker molecule on self-assembly. For this purpose, the data of peptide 15 and peptide 11 (unmodified peptide) are compared in order to estimate the influence of the additional acetylated beta-alanine linker.

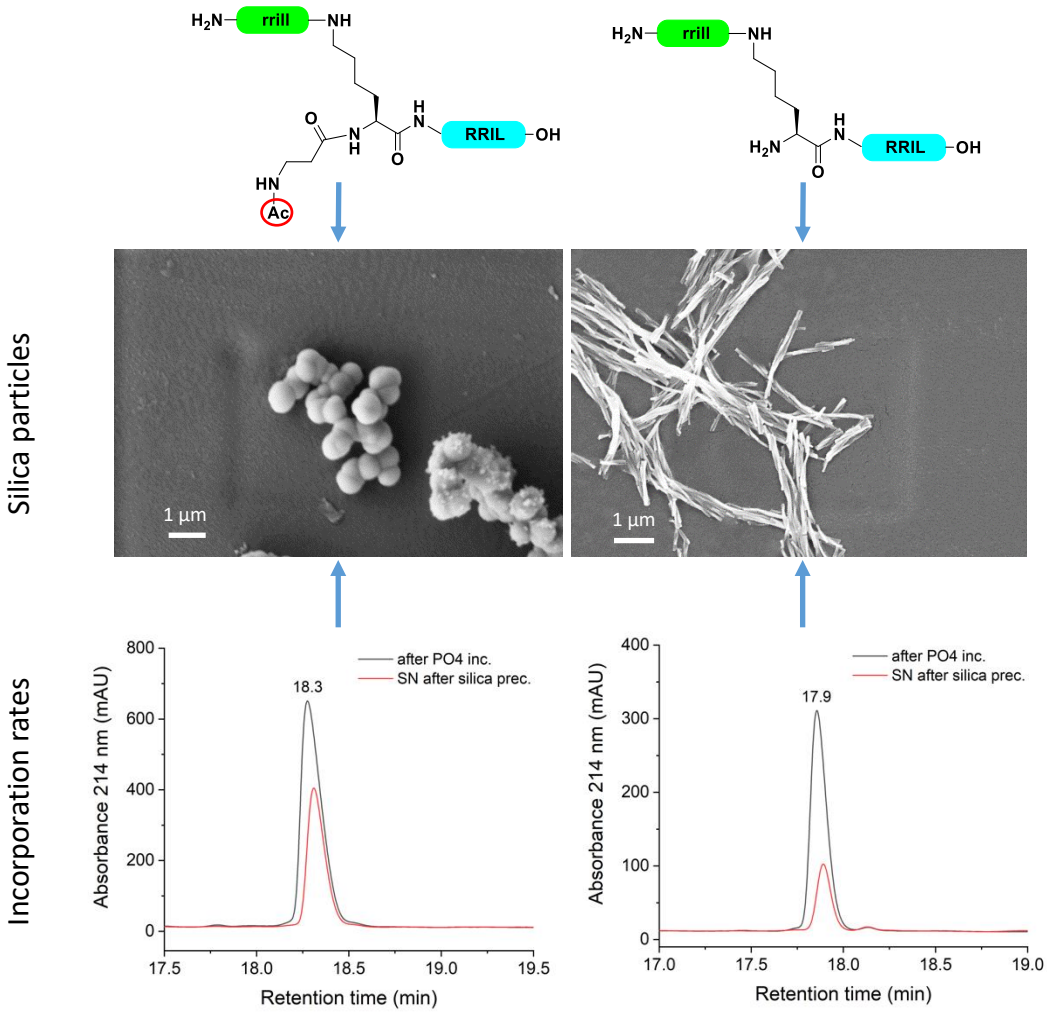

Figure 78: Comparison of the morphology of the silica particles and the peptide incorporation rate of peptide 15 (left) and peptide 11 (right). The chromatograms represent the HPLC runs after incubation in phosphate buffer and the supernatant after silica precipitation (see section 2.9).

As can be seen from Figure 78, the additional acetylated β-alanine residue caused spherical silica particles. Despite the similarity of the backbone structure RRILLK*rrill, the silica morphologies of peptides 11 and 15 differ fundamentally. Differences between the two peptides were already apparent during incubation in phosphate buffers. While peptide 11 showed a precipitate, the acetylated peptide remained completely

in solution. It can be assumed that the acetylated β-alanine residue strongly affects self-assembly and hence leads to an altered solubility of the peptide. Furthermore, the negative mesomeric and inductive effect of the acetyl-group affect the electronic properties of the secondary amine and could be the reason for a different silica precipitation mechanism. In addition, steric effects caused by the acetylated β-alanine residue are likely to influence the self-assembly and thus lead to an altered shape of the silica particles.

4.2.2 Elucidating the influence of an additional Cy5-beta-alanine residue on silica particle formation by comparison of peptides 11 and 16

Next, the Cy5 construct (peptide 16) is compared with the unmodified peptide 11 to investigate the influence of the Cy5-beta-alanine residue on silica particle morphology and peptide incorporation rate during silica precipitation.

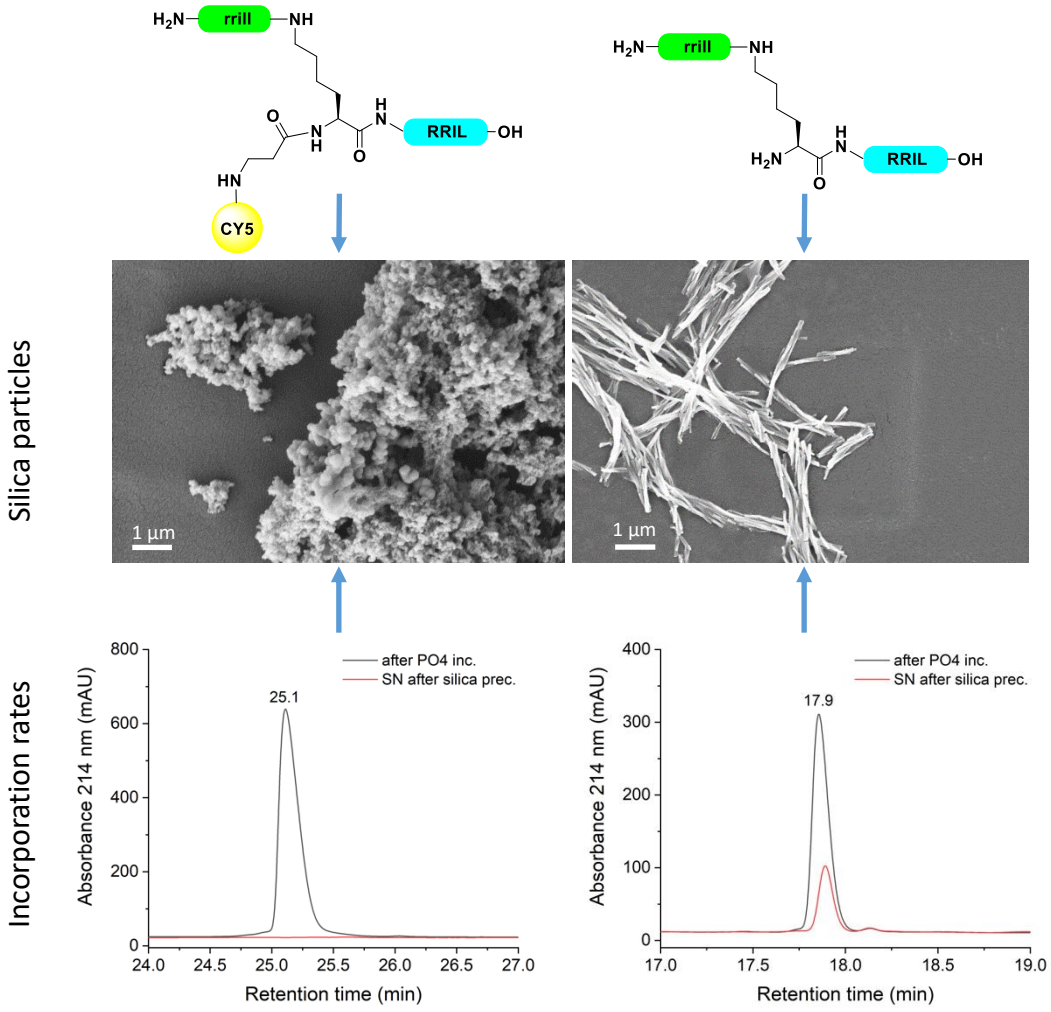

Figure 79: Comparison of the morphology of the silica particles and the peptide incorporation rate of peptide 16 (left) and peptide 11 (right). The chromatograms represent the HPLC runs after incubation in phosphate buffer and the supernatant after silica precipitation (see section 2.9).

Similar to section 4.2.1, the difference in the morphologies of the silica particles in Fig. 79 is substantial. Instead of spherical or rod-like particles, sponge-like structures can be observed when looking at the particles derived from peptide 16 (left).

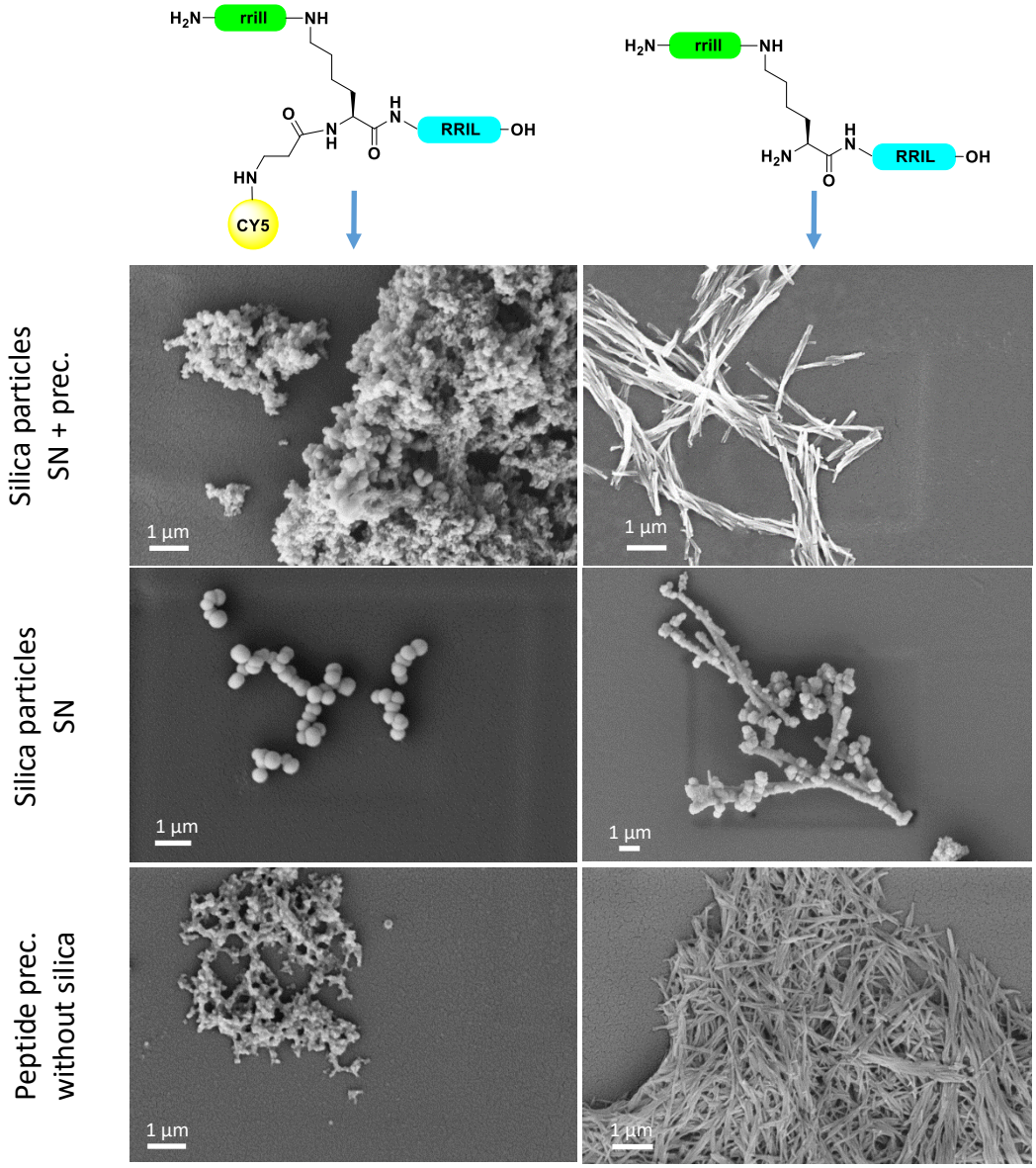

Figure 80: Comparison of the morphology of the silica particles obtained via standard silica precipitation procedure (row 1), morphology of silica particles obtained via silica precipitation using the supernatant after incubation in phosphate buffer (row 2) and the peptide precipitate after incubation in phosphate buffer (row 3) of peptide 16 (left) and peptide 11 (right).

In contrast to peptide 15, peptide 16 showed a significant amount of precipitation during incubation in phosphate buffer. As previously mentioned, an alteration of self-assembly possibly leads to a lower solubility of the peptide. This could have led to the bulk of the peptide remaining as a precipitate before,

during and after silica precipitation. The fact becomes visible by the complete absence of a chromatogram peak after silica precipitation (left). The influence of the Cy5-beta-alanine residue on self-assembly seems to be pronounced, which also explains the different morphologies of peptide 11 and 16 in Figure 79. Due to the fact that both peptides showed a precipitate after incubation in phosphate buffer, the SEM-images of the peptide precipitates are compared in Fig. 80. In addition, the silica particles resulting from the supernatant after incubation in phosphate buffer are shown.

The functionalization with Cy5 has massive effects on the physicochemical properties of the peptide, as can be seen in Fig 80 (row 1). Sponge-like spherical particles precipitated instead of rod-like sticks. Since the test peptide 15 already caused strong shifts in morphology, it would have been surprising if a hydrophobic residue as large as Cy5 would not have shown a greater effect on self-assembly. Moreover, the positive charge of the Cy5 residue could affect intra- and intermolecular electrostatic interactions and thus influence the self-assembly of the peptide. Interestingly, the attachment of Cy5 to the *N*-terminus of full length R5 variants showed no significant impact on the morphology of the silica particles in previous experiments [77]. The reason for this might be the position of the functionalization, since in this work Cy5 was attached to the central residue, whereas previously the *N*-terminus was modified. Simultaneously Cy5 has greater relative impact on the physico-chemical properties of the rrillK*RRIL peptide (10 AA, MW 1337 /mol) compared to the full length R5 (19 AA, MW 2014 g/mol).

The precipitations of both peptide 16 and 11 show a strong similarity to the morphology of the silica particles. This confirms previous assumptions that self-assembled silaffin peptides serve as template for silicification process [50]. However, it is possible that the particles of peptide 16 consist of peptide precipitates partially covered with silica. Future investigations using energy dispersive X-ray spectroscopy are needed to elucidate the elementary composition of the sponge-like structures resulting from peptide 16. Considering the silica particles resulting from silica precipitation with the supernatant after incubation in phosphate buffer, another contrast between the Cy5 modified peptide and the unmodified peptide becomes obvious. Although the supernatant particles of peptide 11 exhibit some irregularities, the rod-like structure can be well identified. However, the supernatant particles of peptide 16 differ fundamentally from the sponge-like morphology. Since the purification of peptide 16 was successful (see section 3.1.2.2), impurities can be excluded as a cause. It seems that another self-assembly mechanism, induced by a variation in concentration, led to this result.

5. Conclusions and Outlook

The aim of this thesis was to deepen the understanding of the relationship between structure and activity of silaffin-inspired peptides. Further factors with significant impact on self-assembly and silica particle morphology have been identified. Especially the clarification of the influence of the central residue and thus the distance between two RRIL(L) sequences within a RRILLKRRIL derived peptide was of great interest. For this purpose, the four amino acids lysine, β-alanine, diaminopropionic acid and ornithine, each in the D and L versions, were used as central residues between two RRIL motifs.

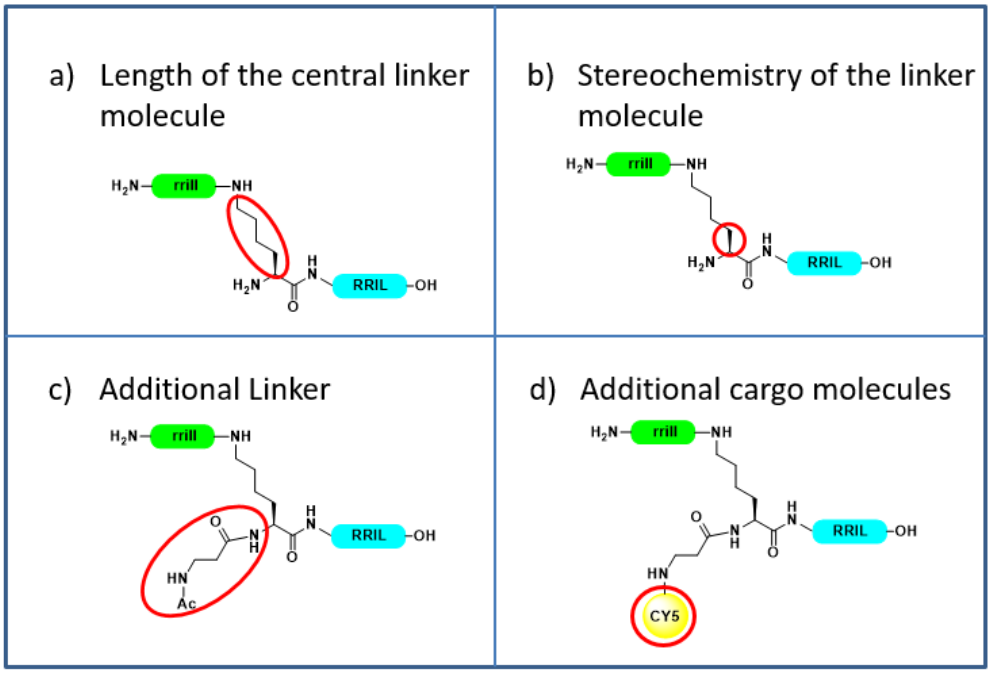

Figure 81: Different parameters whose influence on self-assembly and silica particle morphology could be elucidated in this thesis.

It turned out that as the distance between the two RRIL sequences increases, the silica particles undergo a transformation from spherical to rod-like morphology. In the case of ornithine, a transitional morphology was observed. As soon as the length of the central residue was increased from three to four methylene groups (lysine), rod-like structures known from previous studies could be observed [52]. However, this was only valid as long as the stereochemistry of the central residue was identical to the *N*-terminal RRILL-sequence. Interestingly, the length of the central residue did not affect the morphology if the stereochemistry of the *N*-terminal sequence was contrary to that of the central residue. Furthermore, it could be shown that a free amine residue within the peptide sequence is not obligatory to initiate biomineralization of silica. This became particularly evident when comparing the silica particles of

diaminopropionic acid and β-alanine, but also when considering the acetylated peptide 15. Such observations are inconsistent with the previously postulated acid-base catalyzed polycondensation reaction of silica via free amine residues [50]. Nevertheless, it is likely that the guanidine residues of the four arginines have the ability to catalyze the poly-condensation of silicic acid and could thus initiate silica precipitation alongside free amines. Further investigations are necessary to determine the importance of free amine and arginine residues for biosilicification. Finally, it became evident that the functionalization of a RRIL-based peptide has significant influence on the mechanism of self-assembly and thereby affects the morphology of the resulting silica particles. It could be shown that the incorporation of a Cy5 functionalized RRIL-peptide into a silica matrix is possible. This in turn opens up the possibility of fluorescence spectroscopic investigations, which might play a more important role in the future.

The wide range of possible applications in medical and biotechnological fields and the simple production make further investigations on silaffin-inspired peptides a promising investment for the future [35]. In order to get there, it is necessary to decode the sequence function dependency of self-assembly. This will require extensive conformational studies via NMR and Cryo-electron microscopy. Furthermore, it will be important to better understand the effect of single atom changes on self-assembly and thus the morphology of silica particles. Ideally, these efforts will lead to new avenues of creating biologically relevant nanomaterials.

6. References

1. Stephanopoulos, N., J.H. Ortony, and S.I. Stupp, *Self-assembly for the synthesis of functional biomaterials.* Acta materialia, 2013. **61**(3): p. 912-930.
2. Cui, H., M.J. Webber, and S.I. Stupp, *Self-assembly of peptide amphiphiles: From molecules to nanostructures to biomaterials.* Peptide Science: Original Research on Biomolecules, 2010. **94**(1): p. 1-18.
3. Sun, L., C. Zheng, and T.J. Webster, *Self-assembled peptide nanomaterials for biomedical applications: promises and pitfalls.* International journal of nanomedicine, 2017. **12**: p. 73.
4. Hargreaves, W.R., S.J. Mulvihill, and D.W. Deamer, *Synthesis of phospholipids and membranes in prebiotic conditions.* Nature, 1977. **266**(5597): p. 78-80.
5. Luisi, P.L., P. Walde, and T. Oberholzer, *Lipid vesicles as possible intermediates in the origin of life.* Current Opinion in Colloid & Interface Science, 1999. **4**(1): p. 33-39.
6. Whitesides, G.M. and B. Grzybowski, *Self-Assembly at All Scales.* Science, 2002. **295**(5564): p. 2418.
7. Nitschke, J.R. and J.-M. Lehn, *Self-organization by selection: Generation of a metallosupramolecular grid architecture by selection of components in a dynamic library of ligands.* Proceedings of the National Academy of Sciences, 2003. **100**(21): p. 11970-11974.
8. Mandal, D., A.N. Shirazi, and K. Parang, *Self-assembly of peptides to nanostructures.* Organic & biomolecular chemistry, 2014. **12**(22): p. 3544-3561.
9. Zelzer, M. and R.V. Ulijn, *Next-generation peptide nanomaterials: molecular networks, interfaces and supramolecular functionality.* Chemical Society Reviews, 2010. **39**(9): p. 3351-3357.
10. Choi, S.-j., et al., *Differential self-assembly behaviors of cyclic and linear peptides.* Biomacromolecules, 2012. **13**(7): p. 1991-1995.
11. Stendahl, J.C., et al., *Intermolecular forces in the self-assembly of peptide amphiphile nanofibers.* Advanced Functional Materials, 2006. **16**(4): p. 499-508.
12. Edwards-Gayle, C.J. and I.W. Hamley, *Self-assembly of bioactive peptides, peptide conjugates, and peptide mimetic materials.* Organic & biomolecular chemistry, 2017. **15**(28): p. 5867-5876.
13. Zhang, S., et al., *Spontaneous assembly of a self-complementary oligopeptide to form a stable macroscopic membrane.* Proceedings of the National Academy of Sciences, 1993. **90**(8): p. 3334-3338.
14. Löwik, D.W. and J.C. van Hest, *Peptide based amphiphiles.* Chemical Society Reviews, 2004. **33**(4): p. 234-245.
15. Vauthey, S., et al., *Molecular self-assembly of surfactant-like peptides to form nanotubes and nanovesicles.* Proceedings of the National Academy of Sciences, 2002. **99**(8): p. 5355-5360.
16. von Maltzahn, G., et al., *Positively charged surfactant-like peptides self-assemble into nanostructures.* Langmuir, 2003. **19**(10): p. 4332-4337.
17. Caplan, M.R., et al., *Control of self-assembling oligopeptide matrix formation through systematic variation of amino acid sequence.* Biomaterials, 2002. **23**(1): p. 219-227.
18. Zhao, X., et al., *Designer short peptide surfactants stabilize G protein-coupled receptor bovine rhodopsin.* Proceedings of the National Academy of Sciences, 2006. **103**(47): p. 17707-17712.
19. Zhang, S., et al., *Unusually stable β-sheet formation in an ionic self-complementary oligopeptide.* Biopolymers: Original Research on Biomolecules, 1994. **34**(5): p. 663-672.
20. Gelain, F., A. Horii, and S. Zhang, *Designer self-assembling peptide scaffolds for 3-D tissue cell cultures and regenerative medicine.* Macromolecular bioscience, 2007. **7**(5): p. 544-551.
21. Zhang, S., *Emerging biological materials through molecular self-assembly.* Biotechnology advances, 2002. **20**(5-6): p. 321-339.
22. Dehsorkhi, A., V. Castelletto, and I.W. Hamley, *Self-assembling amphiphilic peptides.* Journal of Peptide Science, 2014. **20**(7): p. 453-467.
23. Hamley, I., *Self-assembly of amphiphilic peptides.* Soft Matter, 2011. **7**(9): p. 4122-4138.
24. Sephel, G., et al., *Laminin A chain synthetic peptide which supports neurite outgrowth.* 1989. **162**(2): p. 821-829.
25. Silva, G.A., et al., *Selective differentiation of neural progenitor cells by high-epitope density nanofibers.* 2004. **303**(5662): p. 1352-1355.
26. Velichko, Y.S., S.I. Stupp, and M.O. De La Cruz, *Molecular simulation study of peptide amphiphile self-assembly.* The journal of physical chemistry B, 2008. **112**(8): p. 2326-2334.

27. Yuwono, V.M. and J.D.J.L. Hartgerink, *Peptide amphiphile nanofibers template and catalyze silica nanotube formation.* 2007. **23**(9): p. 5033-5038.
28. Chen, C.L. and N.L. Rosi, *Peptide-based methods for the preparation of nanostructured inorganic materials.* Angewandte Chemie International Edition, 2010. **49**(11): p. 1924-1942.
29. Palmer, L.C., et al., *Biomimetic systems for hydroxyapatite mineralization inspired by bone and enamel.* Chemical reviews, 2008. **108**(11): p. 4754-4783.
30. Lutolf, M. and J. Hubbell, *Synthetic biomaterials as instructive extracellular microenvironments for morphogenesis in tissue engineering.* Nature biotechnology, 2005. **23**(1): p. 47.
31. Song, R.Q. and H. Cölfen, *Mesocrystals—ordered nanoparticle superstructures.* Advanced materials, 2010. **22**(12): p. 1301-1330.
32. Lakshminarayanan, R., et al., *Formation of transient amorphous calcium carbonate precursor in quail eggshell mineralization: an in vitro study.* Biomacromolecules, 2006. **7**(11): p. 3202-3209.
33. Kröger, N., R. Deutzmann, and M. Sumper, *Silica-precipitating peptides from diatoms the chemical structure of silaffin-1A from Cylindrotheca Fusiformis.* Journal of Biological Chemistry, 2001. **276**(28): p. 26066-26070.
34. Dickerson, M.B., K.H. Sandhage, and R.R. Naik, *Protein-and peptide-directed syntheses of inorganic materials.* Chemical reviews, 2008. **108**(11): p. 4935-4978.
35. Lechner, C.C. and C.F. Becker, *Silaffins in Silica Biomineralization and Biomimetic Silica Precipitation.* Mar Drugs, 2015. **13**(8): p. 5297-5333.
36. Sumper, M. and N. Kroger, *Silica formation in diatoms: the function of long-chain polyamines and silaffins.* Journal of Materials Chemistry, 2004. **14**(14): p. 2059-2065.
37. Tréguer, P., et al., *The balance of silica in the world ocean: a re-estimate.* Science, 1995. **268**(5209): p. 375-379.
38. Martin-Jézéquel, V., M. Hildebrand, and M.A. Brzezinski, *SILICON METABOLISM IN DIATOMS: IMPLICATIONS FOR GROWTH* Journal of Phycology, 2000. **36**(5): p. 821-840.
39. Bradbury, J., *Nature's Nanotechnologists: Unveiling the Secrets of Diatoms.* PLOS Biology, 2004. **2**(10): p. e306.
40. Wetherbee, R., *The diatom glasshouse.* Science, 2002. **298**(5593): p. 547-547.
41. Kröger, N., R. Deutzmann, and M. Sumper, *Polycationic Peptides from Diatom Biosilica That Direct Silica Nanosphere Formation.* Science, 1999. **286**(5442): p. 1129.
42. Kröger, N., et al., *Self-assembly of highly phosphorylated silaffins and their function in biosilica morphogenesis.* Science, 2002. **298**(5593): p. 584-586.
43. Min, K.-H., et al., *High expression and biosilica encapsulation of alkaline-active carbonic anhydrase for CO2 sequestration system development.* Chemosphere, 2016. **143**: p. 128-134.
44. Bernecker, A., et al., *Tailored synthetic polyamines for controlled biomimetic silica formation.* Journal of the American Chemical Society, 2009. **132**(3): p. 1023-1031.
45. Cole, K.E., et al., *Peptide-and long-chain polyamine-induced synthesis of micro-and nanostructured titanium phosphate and protein encapsulation.* 2006. **18**(19): p. 4592-4599.
46. Naik, R.R., et al., *Controlled formation of biosilica structures in vitro.* 2003(2): p. 238-239.
47. Lechner, C.C. and C.F. Becker, *Modified silaffin R5 peptides enable encapsulation and release of cargo molecules from biomimetic silica particles.* Bioorganic & medicinal chemistry, 2013. **21**(12): p. 3533-3541.
48. Mody, K.T., et al., *Mesoporous silica nanoparticles as antigen carriers and adjuvants for vaccine delivery.* Nanoscale, 2013. **5**(12): p. 5167-5179.
49. Luckarift, H.R., et al., *Enzyme immobilization in a biomimetic silica support.* Nature biotechnology, 2004. **22**(2): p. 211.
50. Lechner, C.C. and C.F. Becker, *A sequence-function analysis of the silica precipitating silaffin R5 peptide.* Journal of Peptide Science, 2014. **20**(2): p. 152-158.
51. Wieneke, R., et al., *Silica precipitation with synthetic silaffin peptides.* Organic & biomolecular chemistry, 2011. **9**(15): p. 5482-5486.
52. Kamalov, M., et al., *Silaffin-Inspired Peptide Assemblies Template Silica Particles with Variable Morphologies.* ChemNanoMat, 2018. **4**(12): p. 1209-1213.
53. Basak, S., et al., *On the Role of Chirality in Guiding the Self-Assembly of Peptides.* Angewandte Chemie International Edition, 2017. **56**(43): p. 13288-13292.
54. Shamovsky, I.L., G.M. Ross, and R.J. Riopelle, *Theoretical studies on the origin of β-sheet twisting.* The Journal of Physical Chemistry B, 2000. **104**(47): p. 11296-11307.

55. Wang, M., et al., *Left or Right: How Does Amino Acid Chirality Affect the Handedness of Nanostructures Self-Assembled from Short Amphiphilic Peptides?* Journal of the American Chemical Society, 2017. **139**(11): p. 4185-4194.
56. Wadai, H., et al., *Stereospecific amyloid-like fibril formation by a peptide fragment of β2-microglobulin.* Biochemistry, 2005. **44**(1): p. 157-164.
57. Marchesan, S., et al., *Chirality effects at each amino acid position on tripeptide self-assembly into hydrogel biomaterials.* Nanoscale, 2014. **6**(10): p. 5172-5180.
58. Vargiu, A.V., et al., *Design of a hydrophobic tripeptide that self-assembles into amphiphilic superstructures forming a hydrogel biomaterial.* Chemical Communications, 2016. **52**(35): p. 5912-5915.
59. Luo, Z., S. Wang, and S. Zhang, *Fabrication of self-assembling D-form peptide nanofiber scaffold d-EAK16 for rapid hemostasis.* Biomaterials, 2011. **32**(8): p. 2013-2020.
60. Fu, Y., et al., *Terminal is important for the helicity of the self-assemblies of dipeptides derived from alanine.* Langmuir, 2013. **29**(20): p. 6013-6017.
61. Menchise, V., et al., *Insights into peptide nucleic acid (PNA) structural features: The crystal structure of a d-lysine-based chiral PNA–DNA duplex.* Proceedings of the National Academy of Sciences, 2003. **100**(21): p. 12021-12026.
62. Zhao, K., et al., *Enhanced activity of cyclic transporter sequences driven by phase behavior of peptide–lipid complexes.* Soft Matter, 2012. **8**(24): p. 6430-6433.
63. Edwards-Gayle, C.J.C., et al., *Self-Assembly, Antimicrobial Activity, and Membrane Interactions of Arginine-Capped Peptide Bola-Amphiphiles.* ACS Applied Bio Materials, 2019. **2**(5): p. 2208-2218.
64. Dehsorkhi, A., et al., *Interaction between a cationic surfactant-like peptide and lipid vesicles and its relationship to antimicrobial activity*. Langmuir, 2013. **29**(46): p. 14246-14253.
65. Castelletto, V., et al., *Restructuring of lipid membranes by an arginine-capped peptide bolaamphiphile*. Langmuir, 2018. **35**(5): p. 1302-1311.
66. Edwards-Gayle, C.J., et al., *Self-Assembly, Antimicrobial Activity, and Membrane Interactions of Arginine-Capped Peptide Bola-Amphiphiles.* ACS applied bio materials, 2019.
67. Hamley, I.W., et al., *Self-assembly of a model amphiphilic oligopeptide incorporating an arginine headgroup.* Soft Matter, 2013. **9**(19): p. 4794-4801.
68. Veiga, A.S., et al., *Arginine-rich self-assembling peptides as potent antibacterial gels.* Biomaterials, 2012. **33**(35): p. 8907-8916.
69. Ozbas, B., et al., *Semiflexible chain networks formed via self-assembly of β-hairpin molecules.* Physical review letters, 2004. **93**(26): p. 268106.
70. Decandio, C.C., et al., *Self-assembly of a designed alternating arginine/phenylalanine oligopeptide.* Langmuir, 2015. **31**(15): p. 4513-4523.
71. Zhou, P., et al., *Amino acid conformations control the morphological and chiral features of the self-assembled peptide nanostructures: Young investigators perspective*. Journal of colloid and interface science, 2019. **548**: p. 244-254.
72. Zhou, P., et al., *Interplay between Intrinsic Conformational Propensities and Intermolecular Interactions in the Self-Assembly of Short Surfactant-like Peptides Composed of Leucine/Isoleucine.* Langmuir, 2016. **32**(18): p. 4662-4672.
73. Schweitzer-Stenner, R., et al., *Disorder and order in unfolded and disordered peptides and proteins: A view derived from tripeptide conformational analysis. I. Tripeptides with long and predominantly hydrophobic side chains.* Proteins: Structure, Function, and Bioinformatics, 2013. **81**(6): p. 955-967.
74. Towse, C.-L., et al., *Nature versus design: the conformational propensities of D-amino acids and the importance of side chain chirality.* Protein Engineering, Design & Selection, 2014. **27**(11): p. 447-455.
75. Schweitzer-Stenner, R., *Conformational propensities and residual structures in unfolded peptides and proteins.* Molecular BioSystems, 2012. **8**(1): p. 122-133.
76. Hermkens, P.H., H.C. Ottenheijm, and D.C. Rees, *Solid-phase organic reactions II: A review of the literature Nov 95–Nov 96.* Tetrahedron, 1997. **53**(16): p. 5643-5678.
77. Kamalov, M., et al., *N-terminal residues of silaffin peptides impact morphology of biomimetic silica particles.* Materials Letters, 2018. **212**: p. 114-117.